AN INVESTIGATION OF BONDING MECHANISM IN METAL CLADDING BY WARM ROLLING

A Dissertation

by

WEI YANG

Submitted to the Office of Graduate Studies of
Texas A&M University
in partial fulfillment of the requirements for the degree of

DOCTOR OF PHILOSOPHY

December 2011

Major Subject: Mechanical Engineering

An Investigation of Bonding Mechanism in Metal Cladding by Warm Rolling

AN INVESTIGATION OF BONDING MECHANISM IN METAL CLADDING BY WARM ROLLING

A Dissertation

by

WEI YANG

Submitted to the Office of Graduate Studies of
Texas A&M University
in partial fulfillment of the requirements for the degree of

DOCTOR OF PHILOSOPHY

Approved by:

Chair of Committee,	Jyhwen Wang
Committee Members,	Amine Benzerga
	Karl Ted Hartwig
	Ibrahim Karaman
Head of Department,	Jerald Caton

December 2011

Major Subject: Mechanical Engineering

ABSTRACT

An Investigation of Bonding Mechanism in Metal Cladding by Warm Rolling.

(December 2011)

Wei Yang, B.S., Harbin Institute of Technology;

M.S., Harbin Institute of Technology

Chair of Advisory Committee: Dr. Jyhwen Wang

Clad metals are extensively used for their multi-functionality and their optimal combination of quality and cost. Roll bonding is an effective and economic processing approach to making clad metals. This dissertation presents an experimental investigation of the roll cladding process as well as thermo-mechanical modeling of mechanism for roll bonding of clad metals. The objectives of this research are to investigate the bonding mechanism of dissimilar metals in a warm rolling process and to advance the knowledge of the roll cladding process.

To accomplish the objectives, aluminum 1100 sheet (Al 1100) and stainless steel 304 sheet (SST 304) are bonded by warm rolling under controlled conditions. The 180^{o} peel test is used to determine the bonding property of those clad metals. The experimental results show that the rolling thickness reduction and the entry temperature are two major factors of bonding strength. Minimum thickness reduction at a particular entry temperature is required to bond Al 1100 and SST 304. Increasing of either thickness reduction or entry temperature significantly improves the bonding strength between the two metals. X-ray microanalysis is also performed to characterize the

diffusion state at the bonding interface. The diffusion coefficients of aluminum and iron are estimated through experimental method.

A thermo-mechanical model was developed to describe the rolling plastic deformation of component metal sheets and the diffusion evolution during a roll bonding process of dissimilar metals. The effect of various rolling conditions on the contact area ratio was quantitatively discussed. Finite element simulation of 2-D diffusion under the rolling created boundary conditions was performed. The peel strength during the diffusion evolution was predicted by the integrated roll bonding model. The modeling predictions correspond to the experimental results well. The correspondence validates the effectiveness of the thermo-mechanical roll bonding model.

Based on experimental observation, this research presents a bonding mechanism for the roll cladding process of dissimilar metals. The roll bonding model can help optimize rolling parameters for varying bonding strength depending on the demands of the application. It can also provide insights into design and analysis of rolling bonding process of other groups of dissimilar metal sheets.

DEDICATION

This dissertation is dedicated to my mother Fuxia Liu, my father Benhua Yang and my wife Juan Yin. Thank you for all your love and support.

ACKNOWLEDGEMENTS

I would like to thank my committee chair, Dr. Jyhwen Wang, and my committee members, Dr. Hartwig, Dr. Karaman and Dr. Benzerga, for their professional and insightful guidance and support throughout the course of this research. Thanks go to Dr. Price for providing a furnace and a roll mill, as well as professional experiment training for this research.

Thanks also go to my friends and colleagues, and the department faculty and staff, for making my time at Texas A&M University a great experience. I also want to extend my gratitude to the National Science Foundation, which provided financial support for this research.

Finally, thanks to my mother and father for their encouragement, and to my wife for her patience and love.

TABLE OF CONTENTS

CHAPTER Page

LIST OF FIGURES

FIGURE Page

FIGURE Page

FIGURE Page

FIGURE Page

LIST OF TABLES

CHAPTER I

INTRODUCTION

1.1 Background

In modern industrial applications, composite materials are extensively used for their multi-functionality and for optimal combination of quality and cost. Clad metals are layered composites that can be manufactured in various forms such as plate, sheet, foil, tube, rod, wire etc. Functionalities from different clad metals can be integrated into structural, thermal expansion management, thermo-mechanical control, electrical, magnetic, corrosion resistant, joining and cosmetic applications [1]. For example, in large scale, clad materials can be used in lightweight cladding applications to satisfy the thermal, fire and acoustic requirements of roofs and walls (Figure 1.1), and stainless steel clad aluminum is used as bumpers in automotives to fulfill the requirement of both strength and corrosion resistance (Figure 1.2); in small scale, clad metals can be used as bipolar plates of proton exchange membrane (PEM) fuel cell to lower the cost and improve the durability of PEM fuel cell stacks (Figure 1.3) by reducing the material and manufacturing costs for potential use in transportation applications. To integrate the advantages and avoid the disadvantages of two or more groups of materials (especially alloys), numerous research works on clad metals and cladding techniques have been conducted in both academia and industry.

This dissertation follows the style of Journal of Manufacturing Science and Engineering.

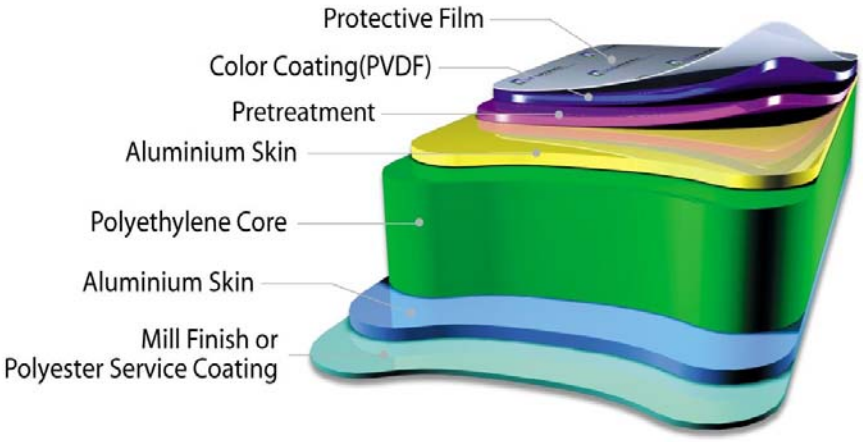

Figure 1.1 Alcopanel/ FR - Aluminum composite panel fire resistant [2]

Rolling is one of the most commonly used manufacturing methods in metal industry, particularly for plate processing. It is always preferred in bonding dissimilar metal sheets with large area. Roll cladding (bonding) is a solid welding technique to join dissimilar metals which is widely used as a cost-effective manufacturing technology. This technique passes a stack of dissimilar metal sheets, plates or strips through a pair of rollers to achieve proper deformation that promotes a solid state bonding between the metal pieces. The roll cladding metals provide many advantages including: 1) the large area welding on the plate plane can be achieved cost-effectively; 2) roll cladding provides high production rate; 3) the multi-layer structure can be fabricated; 4) the bonding interface has a smooth continuity of material properties such as conductivity, stiffness and thermal expansion coefficient.

Therefore, clad metals and the roll cladding process have been active research areas in the community of materials manufacturing and processing. The present research

is to investigate how the rolling initiates the metal bonding and how the bonding state is driven by thermal loading. The objective of the research is to investigate the bonding mechanism of dissimilar metals in a warm rolling process.

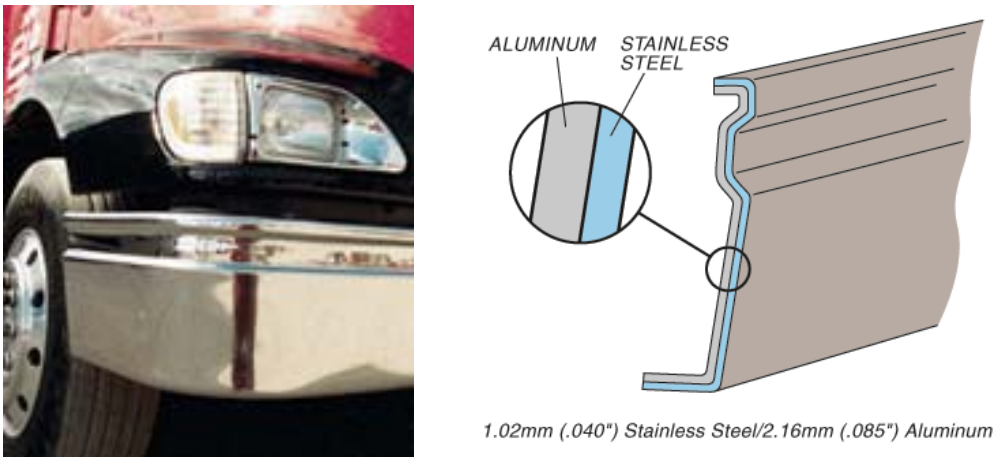

Figure 1.2 Truck bumpers made of cladding metals [3]

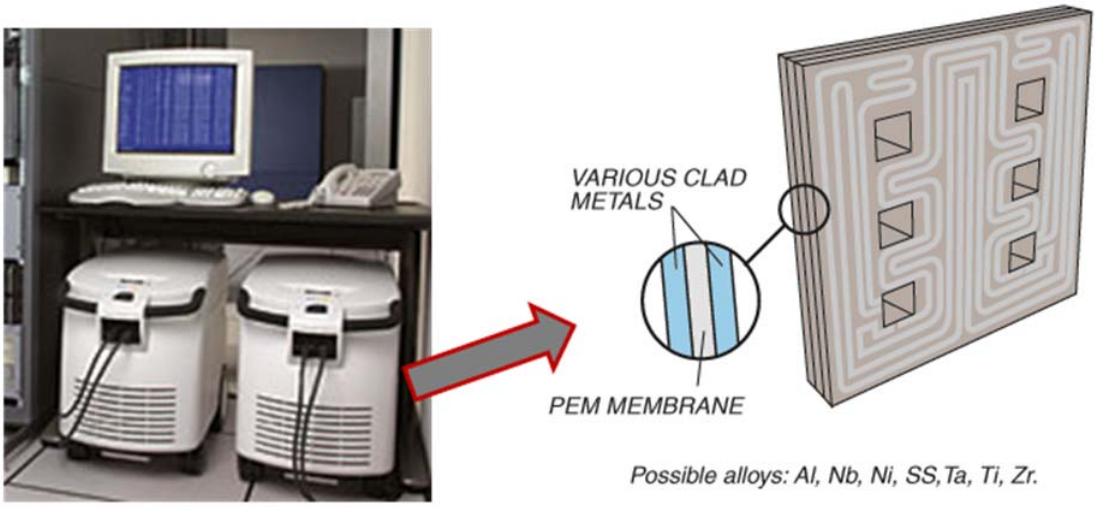

Figure 1.3 PEM fuel cell plates made of cladding metals [4]

1.2 Problem Description

The major physical mechanism of roll bonding of metals in air ambient is solid-state diffusion involving in the plastic deformation of metal substrate and the fracture of surface oxide film. Theoretically, the diffusion is determined by the thermal loading (*i.e.*, temperature) and the loading time. In practice, the intimate contact condition needs to be achieved for bonding component metals through mechanical loading. In order to make diffusion components contact each other such that the atoms of the component metals are close enough to activate the atomic bond, the oxide film needs to be broken by sufficient plastic deformation and a normal force is necessary to extrude the exposed metal through the oxide crack and to push the atoms of the diffusion components sufficiently close. Therefore, the diffusion bonding of dissimilar metals requires both thermal loading and mechanical loading.

1.2.1 Roll bonding processes

In the rolling industrial, roll is generally divided in three categories [5]:

- *Cold rolling*: performing temperature $<$ half of melting temperature in Kelvin
- *Hot rolling*: performing temperature $>$ half of melting temperature in Kelvin
- *Warm rolling*: performing temperature beginning below and ending above half of melting temperature in Kelvin

Warm rolling can provide an effective and economic combination of thermal loading and mechanical loading for metal diffusion bonding. Reheating treatment after warm rolling can make further diffusion and consolidate diffusion bonding.

Many investigations on roll regimes for metal bonding have been conducted during the last 20 years [6-11], but most of those regimes require crucial working environment of vacuum or approximate vacuum and the relationship between rolling regime parameters (such as reduction ratio, rolling temperature, rolling speed and roller's size) and the effect of roll bonding process on the bonding property is not clarified yet. To establish the relationship between rolling parameters and roll bonding property, the roll bonding process of dissimilar metal sheets with controlled rolling parameters needs to be carefully developed.

1.2.2 Bonding property characterization

The property of the bonding interface is very important for the application of layered metals. The bonding interface formed in roll bonding process is a type of graded material with thickness in micron scale, and the mechanical property of the graded interface is determined by its chemical composition. The test of mechanical property of the graded interface in micron scale is challenging, while the overall bonding strength can be measured by conventional material tests such as peel test, shear test or tensile test. On the other hand, the chemical composition characterization of the bonding interface of clad metals is also challenging because of the non-homogeneity and the micron scale of bonding interface in thickness. The test of the distribution of each element's concentration in a diffusion zone involves in the quantitative analysis of chemical composition in submicron to few microns. The quantitative X-ray micro-analysis is an appropriate method to analyze chemical composition of elements with resolution of few microns. Up to date, the X-ray micro-analysis has been working on homogeneous

materials on its resolution scale [12]. The effect of interaction of incident electrons with the target specimen needs to be addressed when X-ray microanalysis technique is used to characterize the graded bonding interface.

1.2.3 Bonding mechanism

The bonding mechanism is very important for the design and analysis of clad metals and for the development and optimization of a roll cladding process. In a roll bonding process, the superficial atoms of dissimilar metal sheets are forced into intimate contact by rolling pressure such that the atomic bond can be achieved. There are several possible bonding mechanisms that can explain the creation of the intimate contact of metal atoms, and many attempts have been made to explain how the bonding is improved after the atomic bond is achieved. Those proposed mechanisms involve film theory, energy barrier theory, diffusion theory and re-crystallization and so forth. Most of those bonding mechanism were proposed qualitatively. The quantitative description of roll bonding mechanism requires plenty of experiment observation and input data collection. It also needs advanced mathematical modeling and the corresponding solving techniques. Thus, few quantitative models of roll bonding process were reported. The quantitative description of roll bonding mechanism is still very challenging.

1.3 Research Objectives

The primary thrust of this research is to improve our understanding of the bonding mechanism for dissimilar metals in a warm rolling process. This study will enhance our capability in designing and analyzing the roll bonding process for multifunctional clad

metals. This dissertation will comprehensively investigate the roll bonding mechanism of dissimilar metals through experiments, analytical modeling and finite element simulations. The specific objectives are to

1) bond aluminum 1100-O and stainless steel 304 sheets by warm rolling through a laboratory rolling mill and a furnace,
2) evaluate the bonding strength of the bonded metal sheets under controlled processing parameters,
3) develop a roll bonding model, considering the oxide film fracture and the exposed metal extrusion in a rolling process, to analyze the effect of these rolling parameters on the roll bonding process.
4) obtain the diffusivity of the target materials for the diffusion bonding in a roll bonding process,
5) establish the quantitative relationship between the processing parameters and the bonding state of the dissimilar metals to bond for the prediction of the bonding strength of clad metals in a roll bonding process.

This research will improve the fundamental understanding of the bonding mechanism of dissimilar metals in a roll bonding process. These investigations will provide insights and guidance for the development of clad metals and the associated roll bonding process.

CHAPTER II

LITERATURE REVIEW

Clad metals and the roll cladding process have been extensively studied recently. Various roll bonding processes have been developed to make clad metals. The engineering properties of clad metals are characterized by different testing methods such as hardness test, lap tensile shearing test, peel test and so forth. Several bonding mechanisms have been put forward to analyze the bonding properties of clad metals. The state-of-the-art of the roll cladding processes, of the roll bonding property characterization and of the roll bonding mechanism is summarized in the following three sections.

2.1 Roll Cladding Processes

Rolling at a designed temperature and thickness reduction ratio can readily provide both thermal and mechanical loadings which are required by diffusion bonding. According to Fick's law, high temperature increases the diffusion coefficient and thus makes diffusion bonding occur in an acceptable time. The reduction ratio in rolling not only drives the bonding component materials into an inter-atomic distance but also breaks the oxidation and contamination film by sufficient plastic deformation. Therefore, many researchers have been focusing on developing roll bonding techniques to weld metals. The bonding targets involve a wide range of alloys including both identical and different ones.

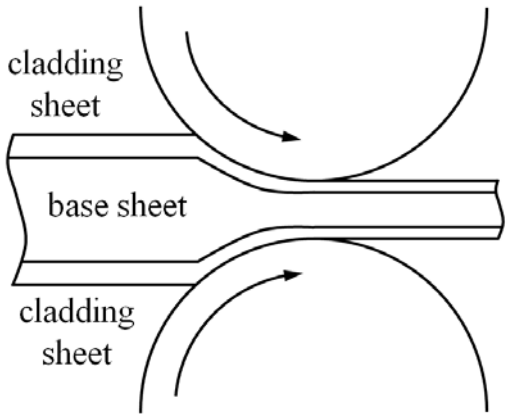

Figure 2.1 A typical roll cladding process

Up to date, a lot of metals and alloys have been successfully bonded by rolling process [13, 14]. For example, aluminum, copper and stainless steel were bonded by continuously rolling [15, 16]. The overlay clad is commonly used in roll cladding process. The cladding materials could be either single layer or multiple layers [17]. Based on the application of clad metals, the clad style could also be various inlays [18-20]. For some hard-to-weld materials, the interlayer or intermediate layer is used to facilitate the roll bonding [21-25], such as the application of the nickel interlayer for the roll bonding of titanium alloy and stainless steel [25]. The roll cladding processes were developed successfully not only for flat sheets but also for wires, rods [26-29], bars [30] and tubes [31-34]. On the other hand, the rolling technique for metal bonding can be either symmetric (as shown in Figure 2.1) or asymmetric rolling such as cross shear rolling [8]. Even though various styles of stacking components and rolling techniques have been developed to bond dissimilar metal components, the underlying principle of

the roll bonding is the same. Generally, the basic roll cladding process in industry includes several sections as shown in Figure 2.2. From those roll bonding processes, it can be seen that, before roll bonding, the metal sheets need to be properly cleaned, such as abrasive grinding [15], and sometime need to be preheated to certain temperature. After roll bonding, the clad metals may need annealing to increase either the bonding quality or the formability [35].

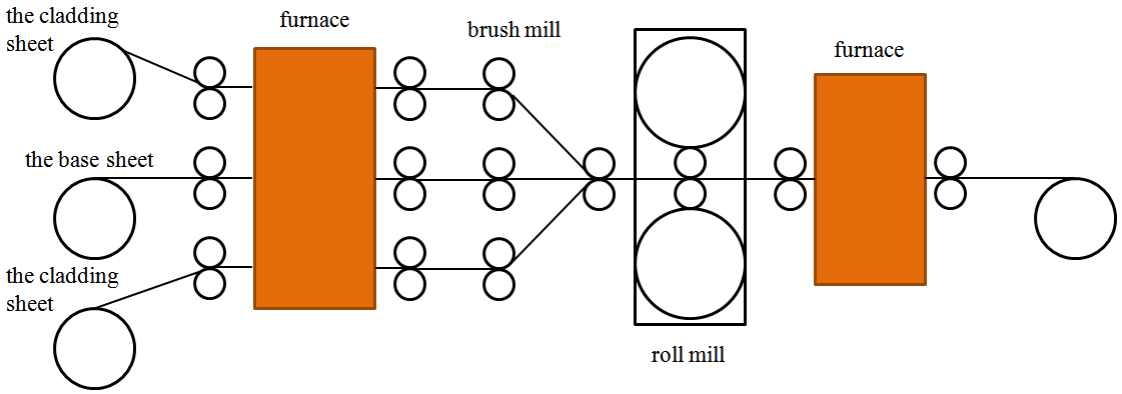

Figure 2.2 The schematic illustration of industrial roll bonding process line

2.2 Evaluation of Bonding Property

Experimental evaluation of the bonding property of clad metals is of significant importance for the development of clad metals and of the roll bonding process. In the perspective of investigating the roll bonding mechanism, the mechanical property and the chemical composition of the bonding interface are the fundamental basics which have been extensively studied recently.

2.2.1 Mechanical bonding property

The mechanical property of the bonding interface in roll bonding structures needs to be characterized accurately if one wants to use roll bonding materials in crucial engineering applications. A lot of works have been done on the evaluation of the bonding strength and the formability of roll bonding materials. Most of them were performed through peeling test, shearing test, tensile test, nano-indentation and so on.

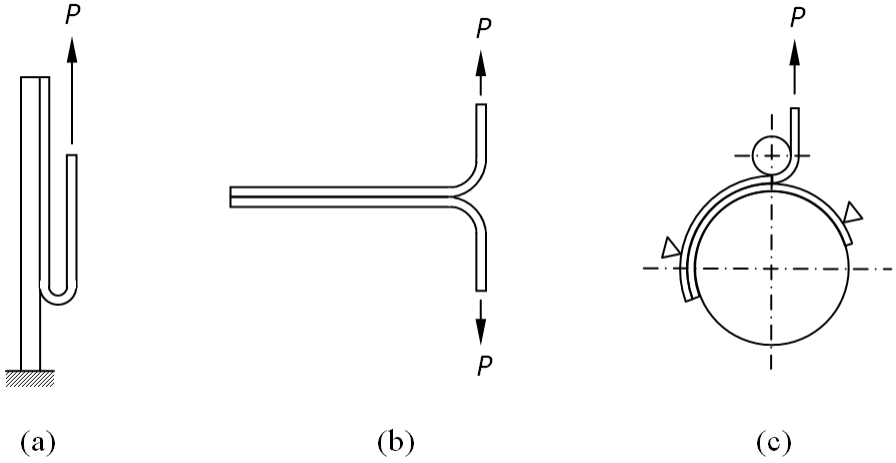

Figure 2.3 Schematic illustration of various peel tests: (a) 180^o peel test; (b) T-peel test; (c) wheel peel test

Peel test is one of the commonly used testing methods for bonding property of clad metals. The schematic illustration of various peel tests are provided in Figure 2.3. The 180^o peel test is applicable to evaluate the bonding strength of dissimilar metal sheets with a hard substrate. The T-peel test is suitable for the peel test of bonding between the same materials with high flexibility. The wheel peel test can be used to measure the peel strength of curved specimens. Using a 180^o peel test based on ASTM-D903 [36],

Eizadjou *et al.* [37, 38] evaluated the roll bonding between aluminum alloy strips by peel strength. Through T-peel test [39], Manesh and Haheri [35] investigated the mechanical properties of aluminum clad steel sheet. Pan et al [8] measured the bonding strength of cold roll clad sheets and cross-shear cold roll clad strips by wheel peel test (similar to ASTM-D3167 [40] and ASTM D1781 [41]).

Actually, in ASTM standards, those peel tests are initially designed for the evaluation of the adhesive strength wherein the peeled layer is considered to be sufficiently flexible and thin such that the deformation dissipation of the peeled layer can be ignored. When the peel test is applied to evaluate the bonding property between metal sheets, the plastic dissipation plays an important role in the total peeling work [42-51]. Therefore, the apparent peel strength measured in peel test does not accurately identify the true peel strength. A peeling mechanics analysis is required to characterize the peel strength measurement in a peel test for bonded metal sheets.

In nuclear industry, the shear test by pressing, as shown in Figure 2.4, is extensively used to examine the bonding property of clad steel plates for boilers and pressure vessels. The pressing shear test is a standard test method for shear bonding strength of stainless Chromium steel-clad plate [52], stainless Chromium-Nickel steel-clad plate [53], Nickel and Nickel-base alloy-clad plate [54], Copper and Copper alloy clad steel plate [55], and reactive and refractory metal clad plate [56], and so on. This test method is also preferred to evaluate the bonding property of clad bars and tubes. For example, Nakasuji et al [30] evaluated the shear strength of a clad bar by rotary rolling

through a shear test by pressing. The cladding thickness for this shear testing is required to be more than 1.9mm [52-56]. For thinner cladding metal sheets, other testing methods are needed.

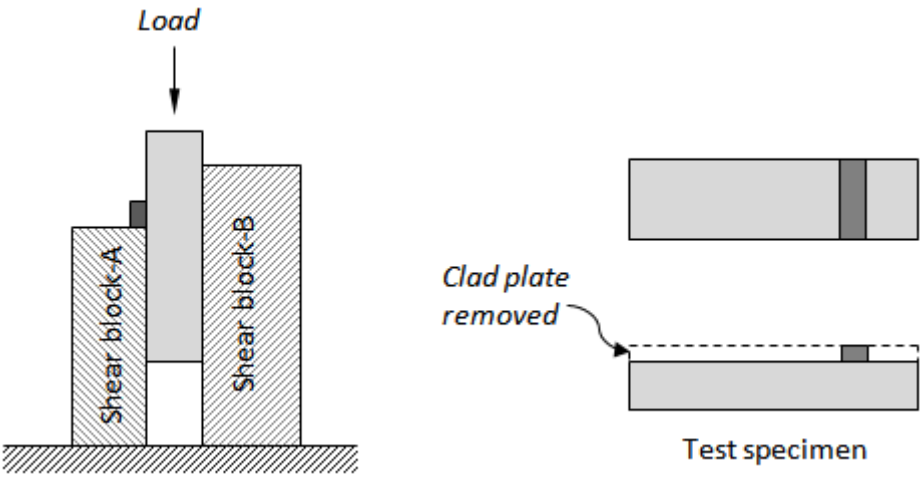

Figure 2.4 Test specimen and method of making shear test of clad plate (Shear blocks shall be bolted firmly together against filler piece)

The shear test by tension loading was also used to measure the roll bonding strength between aluminum and steel sheets [57]. The schematic illustration of the tensile shearing test and test specimen is provided in Figure 2.5. According to ASTM standards [58-60], the reported shear strength of adhesives is considered as apparent shear strength due to the edge effect [61]. Mechanical analysis of a particular tensile shearing test is required to achieve accurate shear strength of bonding. Another major problem of the tensile shearing test is that the thickness-t and the tensile strength-σ_u of the weaker layer as well as the length-L and shear strength-τ_b of target bonding section have to satisfy the condition: $\sigma_u\ t > \tau_b\ L$. Otherwise, the weaker metal sheet will break

before the bonding fails. Due to the two drawbacks, the tensile shearing test is usually not preferred for the evaluation of the bonding quality of clad metals.

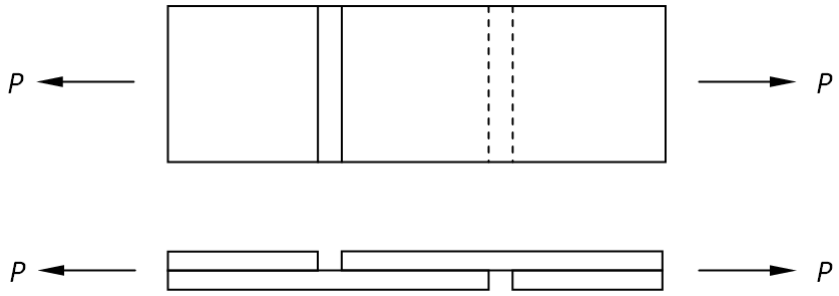

Figure 2.5 Shear test of bonding strength by tension loading

If the component layers of clad metals are sufficiently thick to make a tensile test coupon, the tensile test of bonding strength can be conducted directly. For example, Yan et al [25] used tensile test to directly evaluate the roll bonding of titanium alloy and stainless steel using nickel interlayer; Kundu and Chatterjee [62] examined the diffusion bonding between commercially pure titanium and micro-duplex stainless steel by this test method. In the tensile test of bonding property, the bonding interface is usually positioned in the center of the gauge length of a test coupon.

The previously mentioned tests are bulk test method which is capable of evaluating the overall bonding properties of roll clad metals. If one wants to investigate the detail of the mechanical properties in bonding interface, microscopic or even nano scale test method is required. Nano-indentation is a methodology to measure the mechanical properties of materials by monitoring the indenter's continuous response

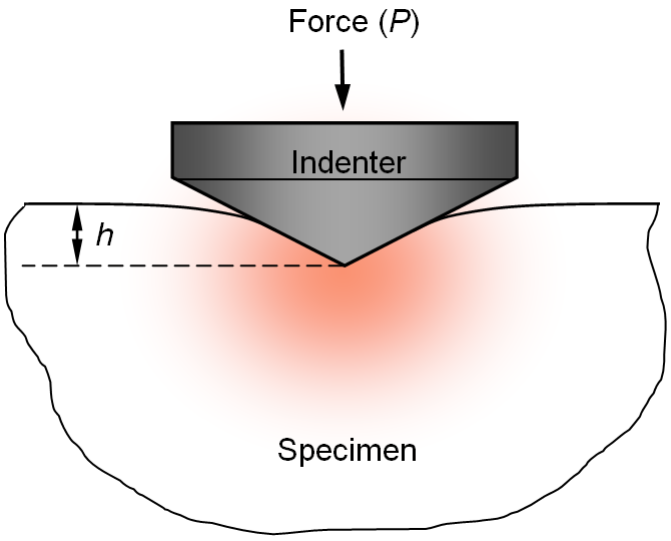

Figure 2.6 Schematic illustration of nano-indentation

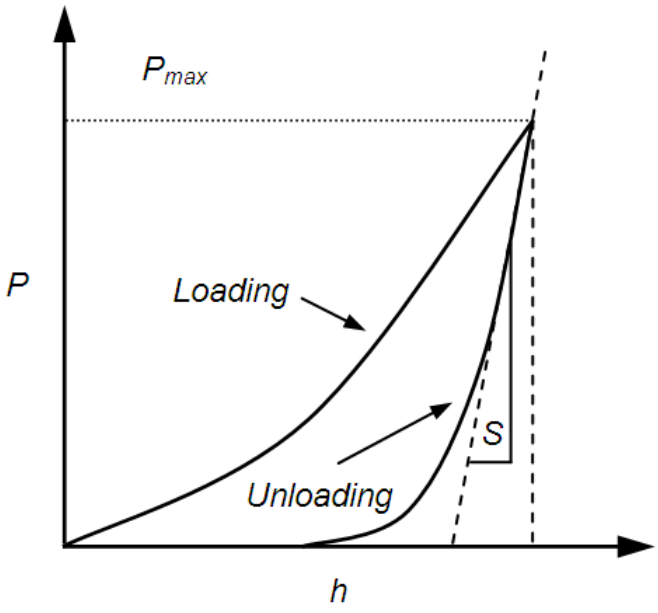

Figure 2.7 A typical force-displacement curve of nano-indentation (P_{max}-the peak indentation force; S-initial unloading stiffness)

when an indentation on the surface of a specimen is applied and the loading is released [63, 64]. The schematic illustration of a nano-indentation is provided in Figure 2.6. The typical loading-displacement curve is shown in Figure 2.7. The typical measurements provide hardness, reduced modulus, and indentation work [65]. Micro-hardness test was applied to examine the bonding interface property of clad metals [11, 62]. But the hardness does not provide sufficient evaluation of the bonding property for engineering application of clad metals. For a better resolution of mechanical property measurement of graded bonding interface, nano-indentation is a possible approach. However, the theoretical framework for extraction of elasto-plastic properties of materials from nano-indentation on the cross section of graded materials is lacking. On the other hand, the bonding interface of clad metals could be as thin as a submicron. Considering the dimension of the strain field around indentation is larger than the indentation dimension, the nano-indentation test of the detailed properties of the graded bonding interface requires nano scale indentation probe.

Those material testing methods can provide the measurement of the overall bonding strength of clad metals. A particular test method is chose based on diversified cladding structural properties such as the thickness ratio of component layers or bonding strength. The tensile shearing test could measure the shear strength of the bonding directly, but this test requires that the component layer is sufficiently strong to hold the loading to break the bonding, and the test coupon is difficult to prepare if component layers are very thin. If one of the component layers is flexible or the thickness is relatively small, a peel test is preferred to evaluate the bonding strength. Even though

peel test is not able to test very high bonding strength, it is commonly used to test the bonding or adhesive strength because it is relatively easy to make such a test coupon and to control the testing operation.

2.2.2 Chemical composition analysis of roll bonding interface

The experimental techniques for studying chemical composition in microscopic material region include secondary ion mass spectrometry (SIMS), X-ray microanalysis, auger electron spectroscopy (AES), Rutherford backscattering (RBS), nuclear reaction analysis (NRA) and nuclear magnetic relaxation (NMR) [66]. Among these methods, X-ray microanalysis is commonly used to investigate the bonding interface of clad metals [1, 10, 11, 25, 62, 67]. The technique can be combined with a scanning electron microscope (SEM), and the investigation can be facilitated by line-scanning function in the system.

The wavelength dispersive spectroscopy (WDS) is one of the X-ray microanalysis methods. The analysis technique can provides fundamental quantitative compositional information for various solid materials. Energy dispersive X-ray spectrometry (EDS or EDX) [68, 69] is another X-ray microanalysis method generally used for qualitative analysis of chemical composition [70]. Although EDS has a low energy resolution that results in a lower accuracy compared to WDS [12], it has also been used for quantitative analysis. Despite the ease of using these automated systems, it is critical to realize that careful interpretation of the results is still required [71]. To investigate the chemical composition distribution across a graded interface, such as the diffusion zone of clad

metals, EDS or WDS line scanning is frequently employed [1, 10, 11, 25, 62, 67]. The electron and X-ray interaction with the target samples, however, has not been addressed in these studies. Specifically, the X-ray absorption and fluorescence effect could lead to misinterpretation of diffusion state. As the accuracy of X-ray microanalysis also depends on the working condition of electron beam such as the beam voltage and current, the electron beam setting also need to be carefully specified. As such, it may not be appropriate to consider the X-ray intensity data as the quantitative chemical composition as suggested in some earlier work [10, 11, 25, 62, 67]. In X-ray microanalysis, matrix correction is required to convert X-ray intensity data to chemical composition. For non-homogeneous materials such as a graded bonding interface, matrix correction needs to consider the electron-specimen interaction effect [72, 73].

2.3 Roll Bonding Mechanism

As mentioned previously, clad metals have been extensively developed and applied in industry. However, the general mechanism for the roll bonding process of clad metals is still unclear. Many qualitative bonding mechanisms were proposed to explain the bonding of roll clad metals, but very few quantitative physical models can be found in either academia or industry. It is still challenging to estimate the bonding property using rigorous models, especially for bonding dissimilar metals.

Through the experimental observations of the roll bonding of identical metal sheets (Al, Cu, Pb, Sn, and Zn), Vaidyanath *et al.* [74, 75] proposed a roll bonding model in terms of shear strength:

$$\frac{\tau_B}{\tau_m} = R\left(2 - R\right) \tag{2-1}$$

where τ_B is the bonding shear strength, τ_m is the metal shear strength and R is the thickness reduction in the composite. This model considers the intimate contact of exposed metals between oxide film fragments and takes account of the triaxiality of stressing. It assumes that the faying oxide films stick to each other and thereby break up as one in rolling process, as their experiment observation suggests in Figure 2.8.

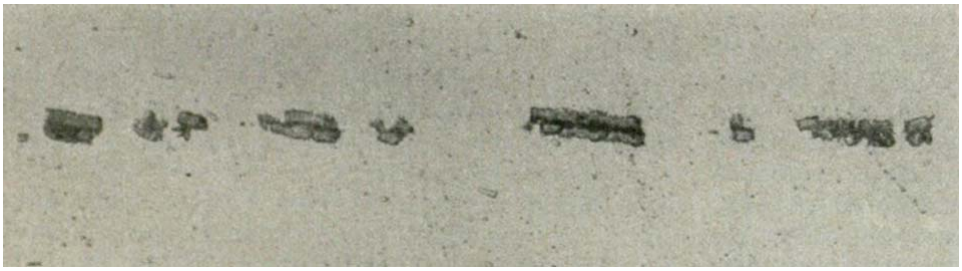

Figure 2.8 Interface of a bond between two anodized aluminum surfaces [75]

Nevertheless, Mohamed and Washburn [76] proposed another model for solid state pressure welding based on the assumption that the oxide films from the two surfaces fracture independently. As shown in Eq. (2-2), they introduced a proportionality constant C related to surface roughness.

$$\frac{\sigma_B}{\sigma_m} = CR^2 \tag{2-2}$$

where σ_B and σ_m are the tensile strength of the bond and the base metal respectively. Through the investigation of the pressure welding in polycrystalline aluminum, copper, silver and gold, the role of the oxide film was studied and it was found that no metal to oxide bonding attributes to the strength of the weld. They also suggested that the different weldability of different metals results from differences in stacking fault energy, relative hardness of the metal and its oxide film, and plastic properties of the oxide.

Based on Vaidyanath's model, Wright [77] considered contaminant barriers besides the brittle scratch-up layers. The bond area ratio thus can be reformulated as:

$$R = 1 - \left(\frac{1 - R_f}{1 - R_t} \right) \tag{2-3}$$

where R_t is the threshold thickness reduction for bonding and R_f is the final thickness reduction. On the other hand, considering the fact that the bond strength of aluminum is higher than that of the solid metal when the deformation is above 60% and that the bond strength of zinc is higher than that of the solid metal when the deformation is above 70% [74], Wright also introduced an empirical hardening factor H. Then Vaidyanath's model was extended to:

$$\frac{\tau_B}{\tau_m} = H \left(1 - \left(\frac{1 - R_f}{1 - R_t} \right)^2 \right) \tag{2-4}$$

In the previously mentioned models, the bonding strength of local bonded areas is assumed to be the strength of the base metal. According to Conrad's experimental

investigation [78], the cohesive strength of fcc metals (Ag, Al, Cu and Ni) by cold welding increases with the compressive load, not necessarily equal to the strength of the metal. The cohesive strength is directly proportional to the fracture stress of the metal and the cohesion coefficients ranged from 0.62 to 1.15. Based on Conrad's results, Bay [79] assumed that the stress necessary to break the bonds is equal to the maximum applied compressive stress p_A on the virgin metal surface. Bay [80-84] also considered the surface of metals consists of the brittle cover layer formed in scratch-brushing and the contaminant film of oxides and water vapor. Then he proposed a combined theory for the weld strength:

$$\frac{\sigma_B}{\sigma_m} = \left(1-\psi_F{}^2\right) Y \frac{p-p_E}{\sigma_m} + \psi_F{}^2 \frac{Y-Y'}{1-Y'} \frac{p}{\sigma_m} \tag{2-5}$$

where ψ_F is the fraction of film layer to total area; Y is surface exposure of weld interface surface; Y' is threshold surface exposure for contaminant film; p is the normal pressure at base metal surfaces; p_E is the extrusion pressure required to extrude the expose metals through the oxide crack to contact each other.

Based on the cold pressure welding model, Bay used slab method to calculate the pressure distribution in roll gap and developed a cold roll bonding model [85] by applying the pressure distribution in Eq.(2-5). In this model, Bay *et al* also considered the strain hardening and the friction between component layers. It is the first time that the pressure distribution in roll gap is introduced in a roll bonding mechanism. But the extrusion pressure and the threshold surface exposure for contaminant film still needs to

be determined through experiments. Thereafter, Zhang and Bay [86-88] performed extrusion analysis of exposed metals and calculated the extrusion pressure. They also analyzed the pressure distribution in roll gap for dissimilar metals rolling by slab method and extended the previous model to a roll bonding model of dissimilar metals, although this model was not able to include the strength of the harder metal.

Recently, Yan and Lenard [89] studied the warm and cold roll bonding of an aluminum alloy and found that the shear strength of the bonds increases as the temperature and the interfacial pressure are increased. They proposed that an activation energy Q_b is required for bond formation and the dependence of the bonding strength on entry temperature follows an Arrhenius type relation:

$$\frac{\tau_B}{\tau_m} = \exp\left(-\frac{Q_b}{RT}\right) \tag{2-6}$$

where R is the universal gas constant and T is the entry temperature in K.

Through those bonding models, it can be seen that the roll bonding mechanism involves many factors in the surface preparation, the rolling process and the post heat treatment. For cold roll bonding of identical metals, the cover layer fracture and the exposed metal extrusion are the widely accepted bonding mechanism and the corresponding theoretical models were developed without consideration of the temperature effect. In most of those models, the brittle cover layers on the opposing surfaces were considered to stick together and break up as one, as shown in Figure 2.9.

This postulation does not necessarily apply to the roll bonding of dissimilar metal sheets. As discussed in previous section, the roll bonding of dissimilar metals usually requires the facilitation of thermal loading. The temperature effect on the roll bonding of metal sheets is not well understood yet. The roll bonding of dissimilar metal sheets at certain temperature also involves the bonding state evolution after the intimate contact of the extruded metals. Considering those factors, the roll bonding mechanism for dissimilar metal sheets was still not clearly defined.

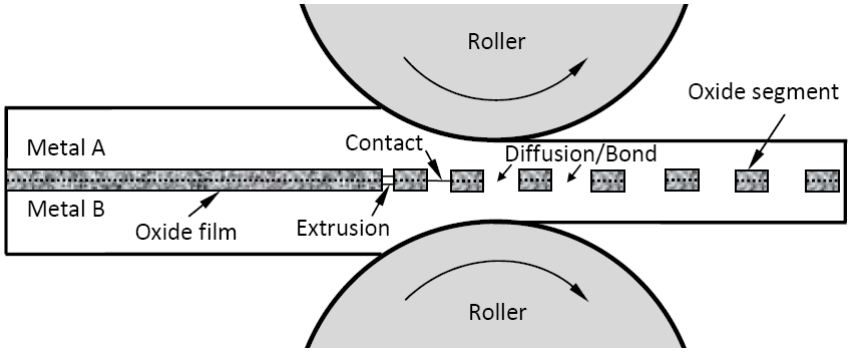

Figure 2.9 Schematic illustration of the fracture of the brittle cover layers and the extrusion of the exposed metals during roll bonding process

CHAPTER III

ROLL BONDING OF DISSIMILAR METALS AND EVALUATION OF BONDING PROPERTY

3.1 Introduction

In this chapter, design of experiment is conducted for roll bonding of dissimilar metal sheets and the warm roll bonding of aluminum 1100-O and stainless steel 304 is performed according to the design matrix. The bond strength of roll bonded metal sheets under varying rolling conditions is determined by 180^{o} peel test. The plastic dissipation of peeled metal sheet is considered for characterizing the peel strength. The improved evaluation of the bonding strength by peel test is obtained. Based on the experimental results, the effects of rolling conditions including the rolling thickness reduction, the entry temperature and the reheating treatment are discussed.

3.2 Experiments and Materials

Three layers of metal sheets are bonded by warm rolling through a laboratory rolling mill. The top and bottom layers are Aluminum 1100-O and the middle layer is stainless steel 304. Aluminum 1100-O sheet is abbreviated by Al 1100 in this context and stainless steel 304 sheet by SST 304. The melting temperature and the chemical composition are provided in Table 3.1 [90, 91]. The thickness of Al 1100 is 1.60 ± 0.08 mm (0.063 ± 0.003 inch) and that of SST 304 is 1.52 ± 0.18 mm (0.060 ± 0.007 inch). The top Al 1100 sheet and the SST 304 sheet are cut into 76mm×20mm (3 in×0.8 in)

and the bottom Al 1100 is cut into 152mm×20mm. The surface condition of one side of SST 304 is #8 Mirror-like Finish and the surface condition of the other side is as-rolled. The #8 Finish surface of SST 304 faces the bottom Al sheet when the three layers of sheets are stacked.

Table 3.1 Melting temperature and chemical composition of SST 304 and Al 1100

Alloy	**Melting Point: ℃**	**Composition: wt %**						
		Fe	**Cr**	**Ni**	**Al**	**Cu**	**Mn**	**Others**
SST 304	1400-1455	65-75	18-20	8-11	-	-	<2	BAL
Al 1100	643-657	-	-	-	>99	0.05-0.2	<0.05	BAL

The flow chart of the roll bonding process is demonstrated in Figure 3.1. The surface of Al 1100 was grinded by 400 grit aluminum oxide cloth sanding sheet, and both of the Al 1100 sheet and SST 304 are cleaned by ethanol and dried in air before they are put into furnace. The cleaned Al 1100 and SST 304 are stacked in the order of Al-SST-Al and then preheated in furnace at the designed temperature for 30 minutes. The stacked Al-SST-Al is rolled right after it is taken out of the furnace such that the difference between the preheated temperature and the entry temperature is insignificant. After the stacked Al-SST-Al specimens are bonded by warm rolling, some of the specimens are reheated in furnace at certain temperature for certain time to investigate the effect of reheating treatment.

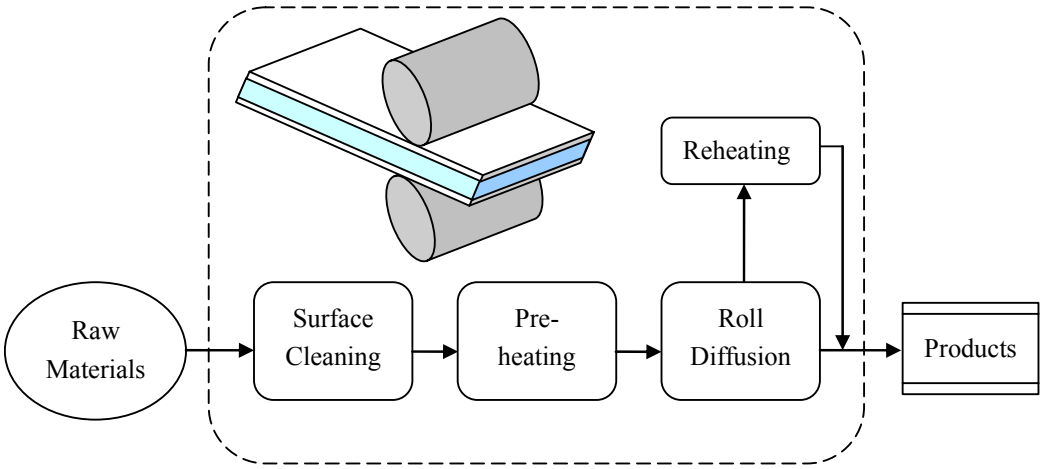

Figure 3.1 The flow chart of roll bonding process of sandwich sheet

Among roll bonding conditions, the entry temperature, the thickness reduction, the reheat temperature, and the reheat time are controlled at various values through the experiment design approach [92, 93]. The entry temperature and reheat temperature are set to be the same. The angular speed of rolls is fixed at $\omega=\pi/5$ rad/s and the radius of rolls is 41mm. Therefore, the factors in design of experiment are temperature, thickness reduction ratio, and reheating time. The factors and levels are provided in Table 3.2. Peel testing is performed on each of those roll bonded sandwich sheets Al-SST-Al by controlled roll bonding conditions. The bonding property of sandwich sheet is characterized by peel strength (or peel surface energy release rate G). According to the factors and their levels, there are 27 runs in the design of experiment. The designed replication number of each run is four. The design matrix is illustrated in Table 3.3.

Table 3.2 Factors and levels

Factor	**Level**		
	0	1	2
A. Temperature (℃)	240	280	320
B. Thickness Reduction	r_0	r_0+10%	r_0+20%
C. Reheating Time (minute)	0	t_0	2 t_0

Table 3.3 Design matrix

Run	Factor		
	A	B	C
1	0	0	0
2	0	0	1
3	0	0	2
4	0	1	0
5	0	1	1
6	0	1	2
7	0	2	0
8	0	2	1
9	0	2	2
10	1	0	0
11	1	0	1
12	1	0	2
13	1	1	0
14	1	1	1
15	1	1	2
16	1	2	0
17	1	2	1
18	1	2	2
19	2	0	0
20	2	0	1
21	2	0	2
22	2	1	0
23	2	1	1
24	2	1	2
25	2	2	0
26	2	2	1
27	2	2	2

(a) Picture of an ongoing peel test

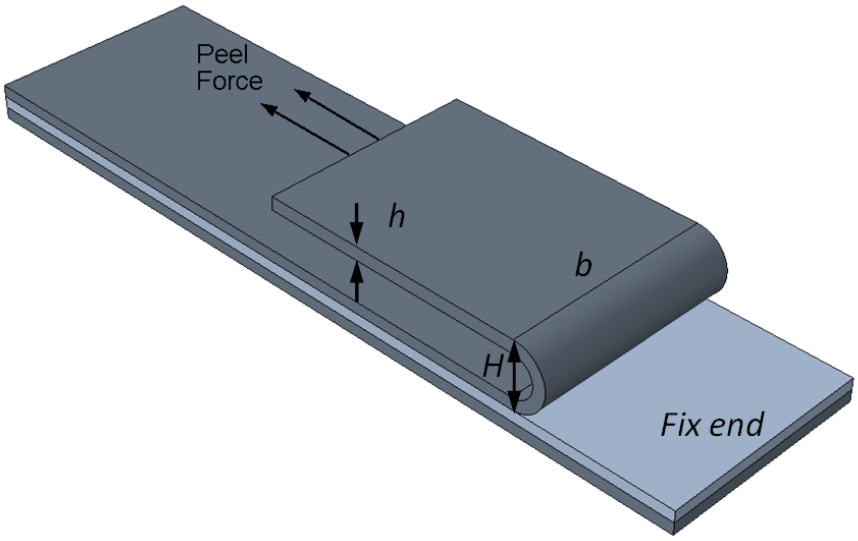

(b) The folded section of peeled metal sheet in 180^{o} peel test.

Figure 3.2 A 180^{o} peel test of roll bonded metal sheet

The test method is developed according to the standard test method ASTM D903 [36] and the work by Eizadjou *et al* [37, 38, 94]. The peel strength and the folding curvature are determined in peel testing. The peel strength is defined by the average load per unit width of the bond line required to separate progressively one member (Al 1100) from the other (SST 304) over the bonded surface at a separation angle of approximate 180^{o}. The cross head moving speed is set to be 2 inch/min. Since the stiffness of SST 304 is very high (the elastic modulus of SST 304 is 193GPa), SST 304 and the bottom layer of Al 1100 work as a backing material and no extra backing material is applied. All the peel tests are performed on tensile testing machine from Tinius Olson Material Testing Machine Company. A testing of roll bonded sandwich sheet and the peel test configuration are illustrated in Figure 3.2. In order to obtain measurable peel strength by peel test, the thickness reduction r_0 is set to be 10% for roll bonding at temperature 320℃ (*i.e.*, the three levels of the thickness reduction are 10%, 20% and 30%), 20% for roll bonding temperature 280℃, and 30% for roll bonding temperature 240℃. Similarly, at the lower temperature 240℃, the reheating time is set to be t_0=60 min, while at the higher temperatures 280℃ and 320℃, the reheating time is set to be t_0=15min.

3.3 Peeling Mechanics Modeling and Analysis

Peel test is usually used to measure the adhesive strength of thin tape on a substrate. ASTM D903 [36] is designed to determine the comparative peel or stripping characteristics of adhesive bonds by 180^o peel test. Since the adhered tape is relatively thin to the substrate and it is very compliant, the effect of the thickness of tape on peel strength is ignored in peel test. Recently the 180^o peel test is applied to characterize the bond strength between metal sheets [37, 38, 94]. In this case, the thickness of the metal sheet is much thicker and thus the plastic deformation dissipation of peeled metal sheet plays important role in the total peeling energy. The conventional peel strength in ASTM D903 cannot accurately represent the bonding property. In our experiment, it is found that the peeled metal sheets have different curvature with respect to different metal sheet thickness and different bonds. Therefore, the curvature and thickness of peeled metal sheet should be reported and the effect of metal sheet's property should be considered in a peel test for metal sheets with certain thickness.

Considering the energy conservation law during the peeling test, the following equation is derived:

$$W=E+K+S \tag{3.1}$$

where W is the work performed by the applied load, E is change of the internal energy and K is the change of kinetic energy of the body, and S is the energy used for separating the bonded metal sheets.

The internal energy change E is composed of elastic strain energy U_e and plastic work U_p, thus

$$E=U_e+U_p \tag{3.2}$$

The surface energy release rate during the metal sheet peeling is

$$G=\frac{\partial S}{\partial A} \tag{3.3}$$

where A is the released surface area.

In the peel test, the velocity of the loading end is 2 in/min (the peeling speed is 1 in/min). The velocity is so low that the kinetic energy of peeling test is insignificant. It is approximated by:

$$K\approx 0 \tag{3.4}$$

The 180^o peel test for the metal sheet bonding is shown in Figure 3.2-(a). The folding section of peeled metal sheet is illustrated in Figure 3.2-(b). When the peeling goes to steady state, the peel force tends to be a constant value. So the external work is

$$W=2Pvt \tag{3.5}$$

where P is the peeling force, v is the peeling speed (note that the velocity of the loading end with the peeling force P is $2v$ in a 180^o peel test.) and t is the loading time.

Then the Eq. (3.3) becomes

$$G = \frac{\partial(W - E)}{\partial A} = \frac{\partial(P \cdot 2v \cdot t)}{2\partial(bvt)} - \frac{\partial E}{\partial A} = \frac{P}{b} - \frac{\partial E}{\partial A} \tag{3.6}$$

where b is the width of the bonded metal sheets.

Next, the equations are developed to describe how the internal energy changes with respect to the peeling area in the peeling process.

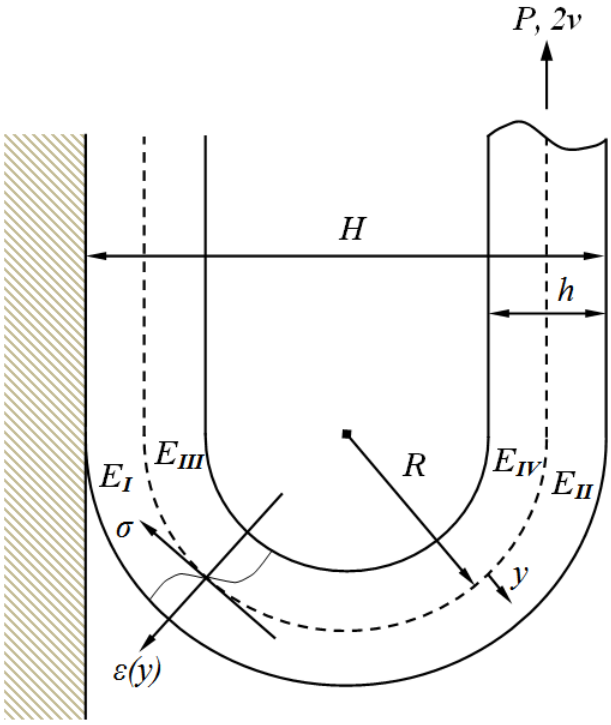

Figure 3.3 Schematic diagram of peeling test of bonded metal sheet.

The schematic illustration of the folding section in a 180^{o} peel test is provided in Figure 3.3. We define the material coordinate (x, y, z) with x in the longitudinal direction and y in the thickness direction. The dash line shows the neutral axis of the metal sheet.

To simplify without loss of generality, it is assumed that the folding section has a constant radius of curvature R. Accordingly, the following relationship is obtained:

$$2R=H-h \tag{3.7}$$

At the neighborhood (with the length dx) of the peeling edge, the flat peeling sheet is bended to a curve with a radius of curvature R when the peeling is happening. The internal energy increase through the plastic deformation dissipation is E_I+E_{III}, as shown in Figure 3.3. At the same time, the top arc (with the arc length dx) of the folding section is straightened from a curve with the radius of curvature R to a flat sheet. The internal energy increase is $E_{II}+E_{IV}$, as shown in Figure 3.3. The total internal energy change E for generating the peeled sheet dx in this peeling process is equal to the work used to bend the same sheet dx to a curvature $\kappa=1/R$ and then to bend it back to flat shape, as show in Figure 3.4. The internal energy density change components, e_I, e_{II}, e_{III}, and e_{IV}, are illustrated by the stress-strain curves in Figure 3.5.

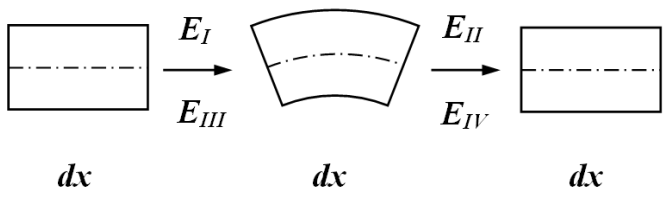

Figure 3.4 Schematic illustration of equivalent internal energy change of peeling test of bonded metal sheets

The internal energy change component E_I can be derived by integrating the plastic deformation dissipation through the corresponding deformed material:

$$E_I = b\int_0^{vt}\left\{\int_0^{h/2}\left[\int_0^{\varepsilon(y)}\sigma_I(\varepsilon)d\varepsilon - \frac{1}{2C}\left[\sigma_I\left(\varepsilon(y)\right)\right]^2\right]dy\right\}dx \qquad (3.8)$$

Then the corresponding energy change rate with respect to the released area is:

$$\frac{\partial E_I}{\partial A} = \frac{\partial E_I}{2b\partial x} = \frac{1}{2}\int_0^{h/2}\left[\int_0^{\varepsilon(y)}\sigma_I(\varepsilon)d\varepsilon - \frac{1}{2C}\left[\sigma_I\left(\varepsilon(y)\right)\right]^2\right]dy \qquad (3.9)$$

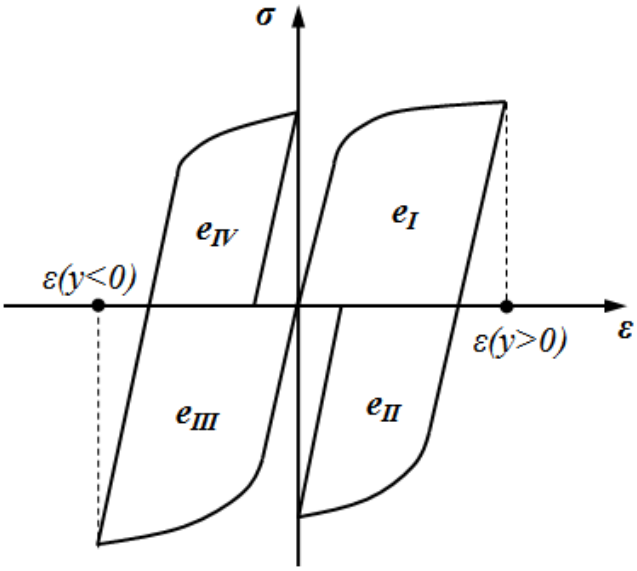

Figure 3.5 The schematic illustration of internal energy change of peeling test of metal sheet via stress-strain curve

where C is Young's modulus and σ_i is flow stress in corresponding region (i=*I, II, III, IV*). Similarly

$$\frac{\partial E_{II}}{\partial A} = \frac{1}{2}\int_0^{h/2}\left[\int_{\varepsilon(y)}^{0}\sigma_{II}(\varepsilon)d\varepsilon - \frac{1}{2C}\left[\sigma_{II}\left(\varepsilon(y)\right)\right]^2\right]dy \qquad (3.10)$$

$$\frac{\partial E_{III}}{\partial A}=\frac{1}{2}\int_0^{-h/2}\left[\int_0^{\varepsilon(y)}\sigma_{III}\left(\varepsilon\right)d\varepsilon-\frac{1}{2C}\left[\sigma_{III}\left(\varepsilon\left(y\right)\right)\right]^2\right]dy \tag{3.11}$$

$$\frac{\partial E_{IV}}{\partial A}=\frac{1}{2}\int_0^{-h/2}\left[\int_{\varepsilon(y)}^{0}\sigma_{IV}\left(\varepsilon\right)d\varepsilon-\frac{1}{2C}\left[\sigma_{IV}\left(\varepsilon\left(y\right)\right)\right]^2\right]dy \tag{3.12}$$

Then, the total internal energy change rate can be derived in the following:

$$\begin{aligned}2\frac{\partial E}{\partial A}=&\int_0^{h/2}\left[\int_0^{\varepsilon(y)}\sigma_{I}\left(\varepsilon\right)d\varepsilon-\frac{1}{2C}\left[\sigma_{I}\left(\varepsilon\left(y\right)\right)\right]^2\right]dy\\&+\int_0^{h/2}\left[\int_{\varepsilon(y)}^{0}\sigma_{II}\left(\varepsilon\right)d\varepsilon-\frac{1}{2C}\left[\sigma_{II}\left(\varepsilon\left(y\right)\right)\right]^2\right]dy\\&+\int_0^{-h/2}\left[\int_0^{\varepsilon(y)}\sigma_{III}\left(\varepsilon\right)d\varepsilon-\frac{1}{2C}\left[\sigma_{III}\left(\varepsilon\left(y\right)\right)\right]^2\right]dy\\&+\int_0^{-h/2}\left[\int_{\varepsilon(y)}^{0}\sigma_{IV}\left(\varepsilon\right)d\varepsilon-\frac{1}{2C}\left[\sigma_{IV}\left(\varepsilon\left(y\right)\right)\right]^2\right]dy\end{aligned} \tag{3.13}$$

According to the Euler-Bernoulli beam theory, the normal strain of the peeled metal sheet due to bending is

$$\varepsilon_{xx}=\frac{y}{R}=\kappa y \tag{3.14}$$

where R is the radius of curvature and κ is the curvature of the folded section of the peeled metal sheet.

If the metal sheet is considered as an elastic-perfect plastic material with Young's modulus C and yield stress σ_Y, Eq.(3.13) can be explicitly expressed as:

$$\frac{\partial E}{\partial A}=\begin{cases}0, & \text{when} \quad \dfrac{h}{2R}\le\dfrac{\sigma_Y}{C}\\ \dfrac{1}{2}\sigma_Y\left(\dfrac{h^2}{4R}+R\varepsilon_Y{}^2-h\varepsilon_Y\right), & \text{when} \quad \dfrac{\sigma_Y}{C}\le\dfrac{h}{2R}\le 2\dfrac{\sigma_Y}{C}\\ \dfrac{1}{2}\sigma_Y\left(\dfrac{h^2}{2R}+5R\varepsilon_Y{}^2-3h\varepsilon_Y\right), & \text{when} \quad \dfrac{h}{2R}>2\dfrac{\sigma_Y}{C}\end{cases} \tag{3.15}$$

Substituting Eq.(15) into Eq. (3.6), the peel surface energy release rate G during a peel test of the metal sheet can be determined by the inputs of P, b, σ_Y, C, h, and R. Here $\varepsilon_Y = \sigma_Y/C$.

$$G=\begin{cases}\dfrac{P}{b}, & \text{when} \quad \dfrac{h}{2R}\le\dfrac{\sigma_Y}{C}\\ \dfrac{P}{b}-\dfrac{1}{2}\sigma_Y\left(\dfrac{h^2}{4R}+R\varepsilon_Y{}^2-h\varepsilon_Y\right), & \text{when} \quad \dfrac{\sigma_Y}{C}\le\dfrac{h}{2R}\le 2\dfrac{\sigma_Y}{C}\\ \dfrac{P}{b}-\dfrac{1}{2}\sigma_Y\left(\dfrac{h^2}{2R}+5R\varepsilon_Y{}^2-3h\varepsilon_Y\right), & \text{when} \quad \dfrac{h}{2R}>2\dfrac{\sigma_Y}{C}\end{cases} \tag{3.16}$$

Note that the P and R should be functions of G and the peeling speed v. Here v is set to be constant 1 in/min and R is measured for each peel test.

3.4 Results

A typical curve of peel force versus peel distance and the separated metal sheets in a peel test of the roll bonded sandwich metal sheet are illustrated in Figure 3.6. According to ASTM D903, the peel strength is determined by dividing the average stable peel force by the width of the bond line. As shown in Figure 3.6, the solid black line represents the average of the stable peel force. Since the plastic dissipation has significant contribution to the peel strength defined above, the peel strength is denoted as "nominal peel strength".

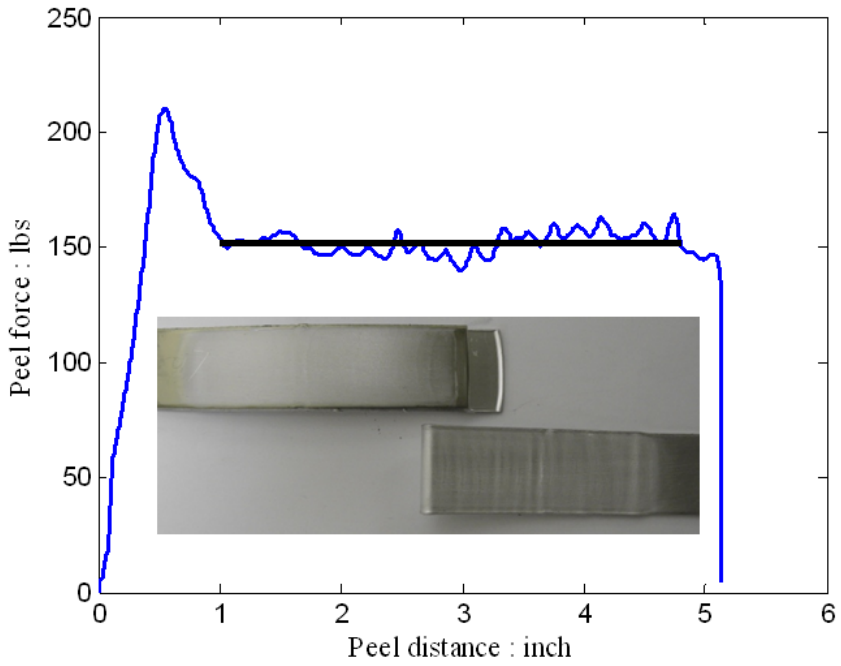

Figure 3.6 Typical curve of peel force versus peel distance

The peel surface energy release rate G characterized by the proposed model Eq. (3.16) is provided in Table 3.4. G is actually the indication of the true peel strength of

bonded metal sheets which excludes the plastic dissipation during metal sheet's peeling. The effect of the thickness reduction ratio and the entry temperature on the peel surface energy release rate G of the roll bonded sandwich sheets is demonstrated in Figure 3.7.

Table 3.4 Characterized bonding property after excluding the plastic dissipation

Run	G (× replication 4) kJ/m^2 (N/mm)				G_{avg} N/mm	s
1	1.92	2.46	-	-	2.2	0.4
2	1.19	1.26	0.89	-	1.1	0.2
3	1.51	1.01	1.98	1.65	1.5	0.4
4	5.03	5.74	5.95	4.53	5.3	0.7
5	4.71	3.92	4.74	4.04	4.4	0.4
6	5.24	7.77	6.30	6.47	6	1.0
7	19.44	20.31	21.3	-	20.4	0.9
8	15.78	11.57	17.74	-	15	3.2
9	22.80	18.32	26.53	-	23	4.0
10	4.44	3.68	4.59	4.90	4.4	0.5
11	3.42	3.85	3.66	-	3.6	0.2
12	4.45	3.74	4.08	3.73	4.0	0.3
13	7.64	10.59	8.83	-	9	1.5
14	6.53	6.35	6.67	-	6.5	0.2
15	11.09	10.11	6.83	6.68	9	2.3
16	19.99	19.89	17.5	-	19	1.4
17	15.56	15.95	13.78	-	15	1.2
18	13.07	12.89	14.73	10.30	13	1.8
19	4.81	1.90	2.83	1.68	3	1.4
20	2.68	2.06	1.60	1.78	2.0	0.5
21	8.36	11.38	14.11	8.86	11	2.6
22	10.01	8.24	9.39	9.43	9.3	0.7
23	13.99	17.87	12.96	16.34	15	2.2
24	24.07	21.35	25.51	21.40	23	2.1
25	24.08	23.08	26.82	-	25	1.9
26	19.12	21.96	20.88	18.65	20	1.5
27	33.65	22.74	25.35	22.30	26	5.3

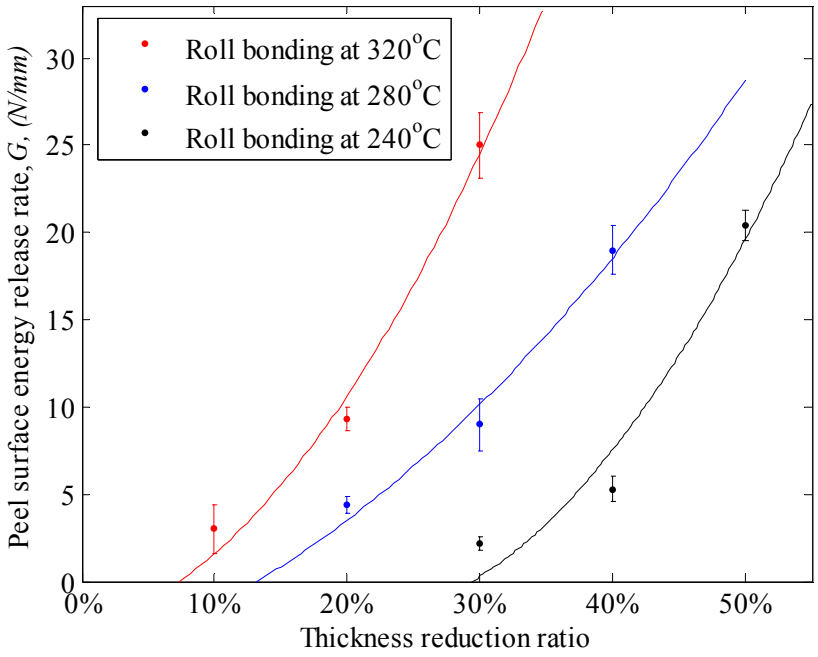

Figure 3.7 Peel strength of roll bonded sandwich sheets Al-SST-Al under various rolling conditions

It can be seen from Figure 3.7 that the bond strength by rolling increases as the entry temperature or the thickness reduction ratio increases. It can also be observed that the dependence of G on thickness reduction ratio r_t and entry temperature T is convexly non-linear. The threshold thickness reduction for roll bonding decreases as rolling temperature increases. The G curve of roll bonded Al/SST/Al at 240°C in Figure 3.7 indicates that the threshold thickness reduction ratio for roll bonding is about 30%. Similarly the minimum thickness reduction ratio for roll bonding of Al-SST-Al at 280°C is expected at about 13% and that at 320°C is expected at about 7%.

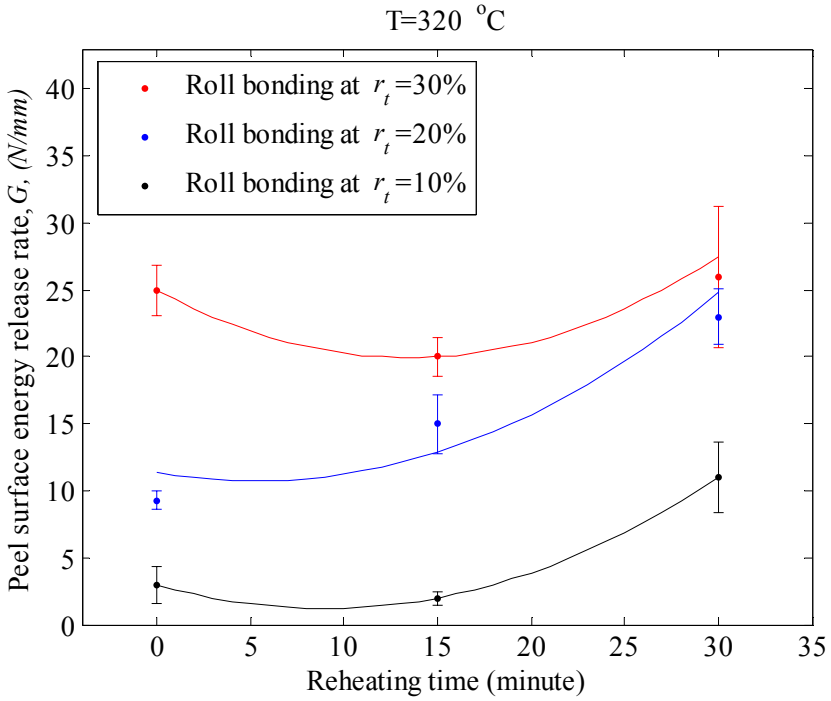

(a)

Figure 3.8 Peel strength of roll bonded sandwich sheets Al/SST/Al versus reheating time in different thickness reduction, (a) reheating temperature 320℃; (b) reheating temperature 280℃; (c) reheating temperature 240℃

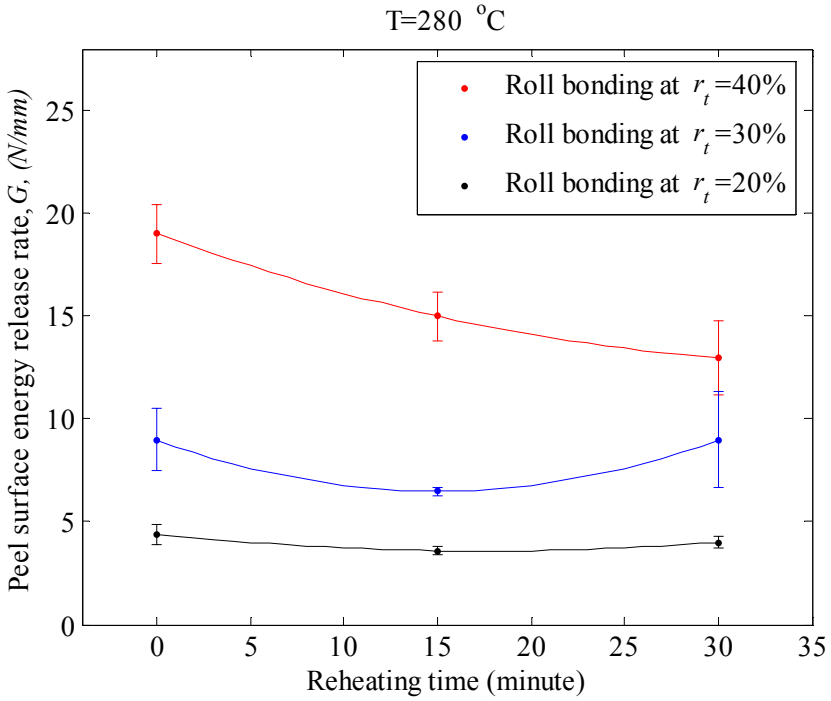

(b)

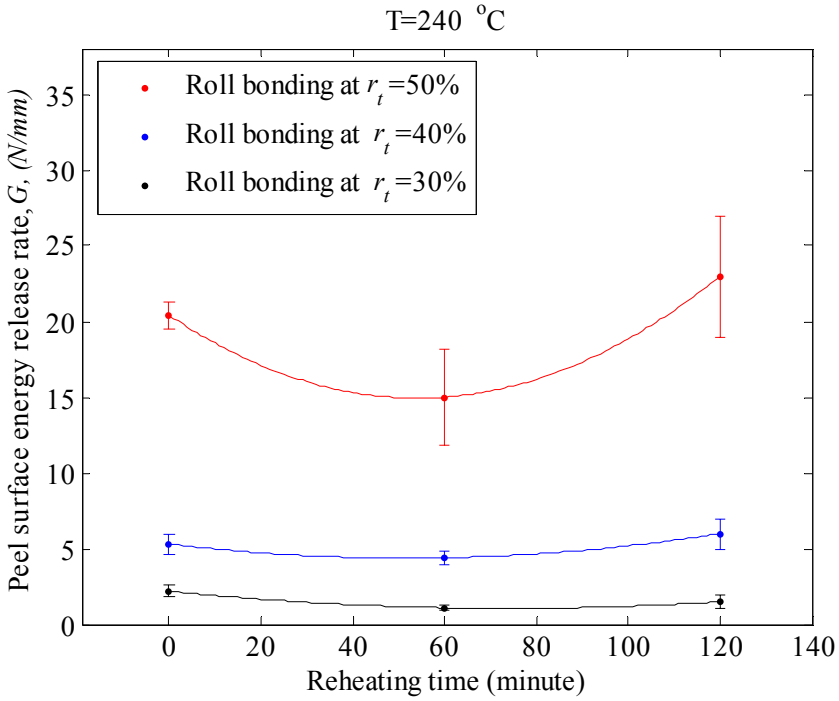

(c)

Figure 3.8 continued.

The dependence of G on the reheating time at different temperatures is illustrated in Figure 3.8. It indicates that, generally, the peel strength decreases first, and then increases in longer reheating time. The peel strength decrease-and-increase trend takes shorter time at higher temperature and lower rolling thickness reduction. For example, under 20% rolling thickness reduction, the peel strength at reheating temperature 280 °C becomes lower in 15 minutes and higher in 30 minutes, while the peel strength at reheating temperature 320 °C increases in both 15 minutes and 30 minutes which indicates that the decrease of the peel strength occurs within 15 minutes. At reheating temperature 320 °C, the peel strength under thickness reduction 30% experiences decreasing in 15 minutes and increasing in 30 minutes, while the peel strength under thickness reduction 20% experiences decreasing within 15 minutes. On the other hand, at reheating temperature 280 °C, the peel strength at rolling thickness reduction 30% experiences decreasing in 15 minutes and then increasing in 30 minutes, while the peel strength at rolling thickness reduction 40% experiences decreasing in all 30 minutes, which indicates that the peel strength increasing may occur in more than 30 minutes. In order to verify this deduction, a roll bonded metal sheet under 40% thickness reduction was reheated at 280 °C for 60 minutes and the result does show greater peel strength than that under 30 minutes reheating treatment, as shown in Figure 3.9.

It can also be noted that the final increase of peel strength is greater at low rolling thickness reduction and high temperature. As shown in Figure 3.8-(a), at heating temperature 320 °C, the peel strength is increased by 8 N/mm (267%) at r_t=10%, and by 13.7 N/mm (147%) at r_t=20%. However, the increase of peel strength is not significant

under the rolling thickness reductions 20% and 30% at the entry temperatures 280°C (see Figure 3.8-(b)) as well as under the rolling thickness reduction s 30% and 40% at the entry temperature 240°C (see Figure 3.8-(c)).

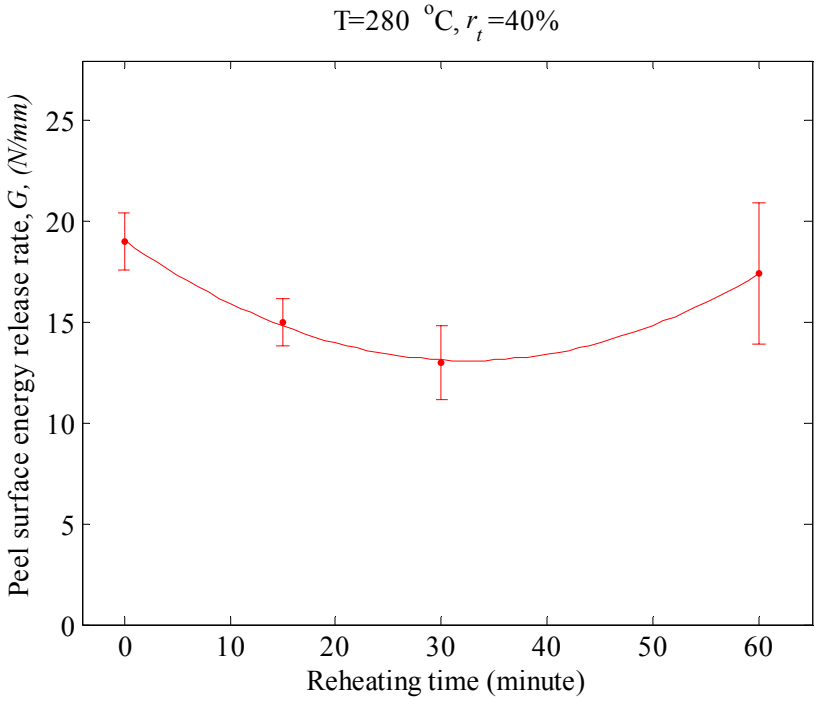

Figure 3.9 Peel strength of roll bonded sandwich sheets Al/SST/Al under different reheating treatment time (T=280°C, r_t =40%)

3.5 Discussions

3.5.1 Plastic deformation in peel test

In a peel test of metal sheet or strip with certain thickness, the plastic deformation dissipation is significant. The characterization of peel surface energy release rate in a peel test of clad metal shows that the plastic dissipation has dependence on the bonding property G, the flow stress σ_Y and the thickness of peeling sheet h. The radius of curvature R in Eq.(3.15) actually also depends on bonding property G, the flow stress σ_Y and the thickness of peeling sheet h. It can be measured in the peel test although it is not solved explicitly. The relation between $(\partial S/\partial A)$ / $(\partial W/\partial A)$ and $\partial S/\partial A$, which is the relation between G / (P/b) and G in this particular case, is depicted in Figure 3.10. It indicates that plastic dissipation depletes more of the total work-W when the bonding-G is weak. As the bonding improves, the plastic dissipation takes less part of the total work. But it is still worthy to point out that the error can still reach more than 30% even though the bonding is as high as 26 N/mm in terms of G. Therefore, not only the nominal peel strength, but also the thickness of peeling sheet and the radius of curvature of the folding section need to be recorded in a peel test of metal sheets. Peel surface energy release rate G, rather than nominal peel strength (P/b), should be reported to determine the bonding property in a peel test of metal sheet with certain thickness.

In the four replications for the experiment runs 7, 16 and 25, the failure of the Al sheet instead of the bonding interface happens among some of those peel tests. Considering the bond strength increases under higher entry temperature and greater thickness reduction ratio (as shown in Figure 3.7), more favorite roll bonding conditions

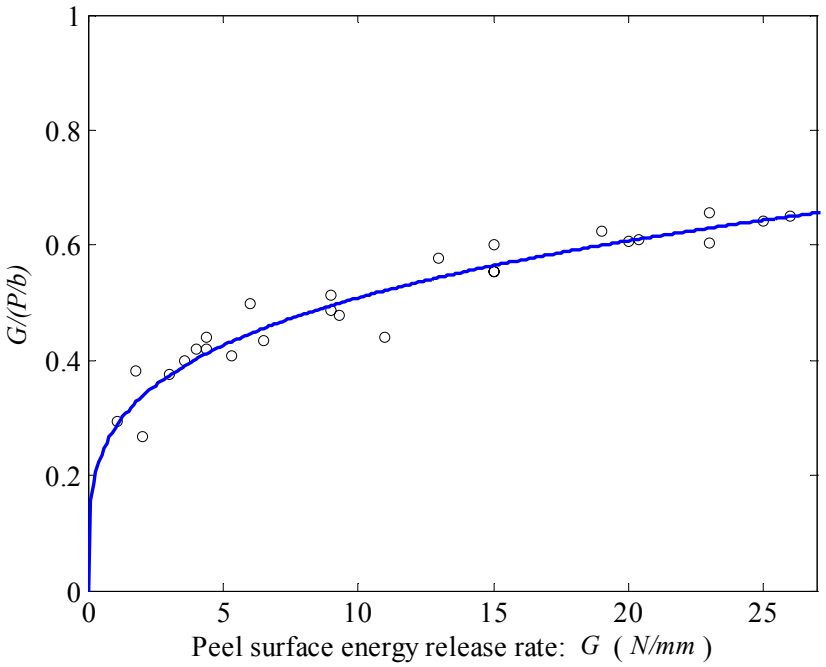

Figure 3.10 The peel surface energy release ratio w.r.t. total peel energy versus surface energy release rate G

(such as 30% thickness reduction at entry temperature 400^{o}C, 40% thickness reduction at entry temperature 320^{o}C and 50% thickness reduction at entry temperature 280^{o}C) are applied to achieve stronger bond. All the peel tests for the stronger bonds yield the failure of the Al sheets. The failure of Al sheet indicates that the bonding is too strong to be measured by the 180^{o} peel test because the bonded Al sheet would break before the peeling takes place at the bonding interface. Madaah-Hosseini and Kokabi [95] had the same observation in T-peel testing for cold roll bonding of 5754-aluminum strips.

The failure of the Al sheet has two types of modes as shown Figure 3.11. One failure mode is shown in Figure 3.11-(a) where the Al sheet fractures at the unfolding section; the other mode is shown in Figure 3.11-(b) where the Al sheet fractures at the

peeling root. From the Figure 3.11-(b), it can also be seen that the middle section of Al sheet breaks at first. It indicates that the middle part of Al sheet was bonded more strongly to SST than the edge sections. Similar phenomenon was observed for the cold roll bonding of aluminum and the cold roll bonding of copper [74, 75]. Vaidyanath *et al.* found that the threshold deformation is the same throughout the width even though the bond strength develops less readily towards the edge. They concluded that the bond strength variation across the width is because the bond development is pressure sensitive. Considering the heat convection in a warm roll bonding process, it is believed that one of the reasons could be that the center temperature is higher since the edge area loses heat faster in the rolling process. This effect can be reduced in industrial strip rolling process by using edge heater.

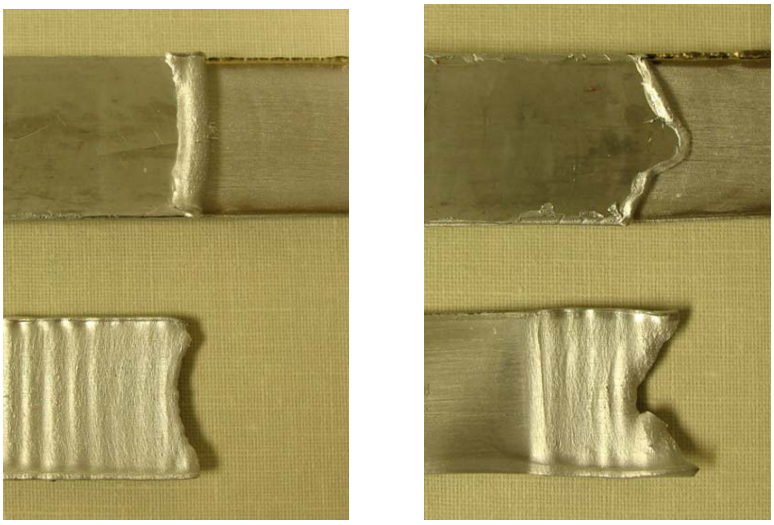

(a) (b)

Figure 3.11 The fracture modes in peel test of roll bonded metal sheets with strong bond

3.5.2 Bonding strength function as thickness reduction and entry temperature

The experimental results of peel surface energy release rate *G* show that the bonding strength is improved by increasing the thickness reduction ratio. The dependence of the bonding strength on the thickness reduction ratio, as shown in Figure 3.7, can be explained by the creation of the bond area through the oxide film fracture and the exposed metal extrusion. In the roll bonding process, the thickness reduction of metal sheets leads to serious plastic longitudinal extension. Considering the brittleness of oxide film on metal surface, it is believed that the thickness reduction breaks the oxide film and hence exposes the underlying metal. Under the rolling pressure, the underlying metals extrudes through the crevice between oxide film fragments. With the sufficient thickness reduction, the extruded metals from adjacent layers will have intimate contact with each other and the atomic metal bond will occur. In this point of view, high thickness reduction ratio makes high metal contact and bond area ratio and hence generates stronger overall bonding of clad metals. The detailed bonding mechanism in terms of the thickness reduction in the roll bonding process will be quantitatively described in Chapter IV.

The experimental results of peel surface energy release rate *G* also show that the bonding strength is improved by increasing the entry temperature. The improvement of the bonding strength, as shown in Figure 3.7, can be explained by the diffusion between the intimately contacting metals. In solid state diffusion, the different atoms will diffuse into each other once they have intimate contact. The bonding interface between different metals will be a diffusion zone with certain thickness. According to Arrhenius law, the

reaction rate increases at higher temperature. So the diffusion rate is faster at higher temperature and hence higher temperature will leads to thicker diffusion interface for intimately contacting metal sheets assuming other conditions keep the same. The dependence of peel surface energy release rate on entry temperature indicates that the bonding property of clad metal depends on the state of the interfacial diffusion. The detailed analysis of the diffusion interface between Al 1100 and SST 304 will be conducted in Chapter VI.

On the other hand, the high temperature also reduces the flow stress of base metals. The lower flow stress will facilitate the extrusion of the exposed metal through the crevice between oxide film fragments. Thus, the threshold thickness reduction required to make intimate contact of exposed metals will be reduced. This is one of the reasons why the threshold thickness reduction to bond Al 1100 and SST 304 decreases at higher temperature.

3.5.3 The effect of reheating treatment

The non-monotonic effect of the reheating treatment on roll bonding property could be explained by the combined effect of annealing and diffusion. In the reheating treatment after roll bonding, the heating will release the straining hardening effect developed by the serious plastic deformation through the previous rolling process, which is termed “annealing effect” in metallurgy. In this point of view, the reheating treatment reduces the bonding strength by release the strain hardening effect on the component materials. On the other hand, it is believed that the atomic metal bonding occurs when

the faying underlying metals contact each other after extrusion through the crevice between oxide film fragments during a rolling process, as shown in Figure 3.12. The bonding interface is created through the diffusion between Al 1100 and SST 304 after they contact each other in the rolling process. According to the mixture rule, the strength of the bonding interface decreases as the concentration of the weaker material (Al in this case) increases across the bonding interface. The lower limit is the strength of Al 1100 and the upper limit is the strength of SST 304. Therefore, the more diffusion of SST 304 into Al 1100 in reheating treatment will increase the strength of the bonding interface.

Whether the combined effect of reheating treatment increases or decreases the bonding strength depends on the softening rate and the strengthening rate. Considering the annealing temperature for Al 1100-O is 343°C (650F) and the annealing time in the furnace need not be longer than necessary to bring all parts of load to annealing temperature [96], the annealing/softening may takes effect faster than diffusion at 320°C and it completes or slows down in a short time such as no longer than 15 minutes. Then the faster annealing effect rate of the reheating treatment can explain the decrease of the peel strength within 15 minutes reheating time, as shown in Figure 3.8-(a). After the annealing effect completes or decays to certain level after certain time (such as 15 minutes), the diffusion effect starts to dominate the reheating treatment and thereafter increases the bonding strength. For both the annealing and diffusion effect, the lower reheating temperature will reduce their reaction rates and thus the effect on the bonding strength will be observed in a longer time. In this perspective, it explains the

insignificant change of the peel strength by the 280°C and 240°C reheating treatments in 30 minutes and 120 minutes respectively, as shown in Figure 3.8-(b) and (c).

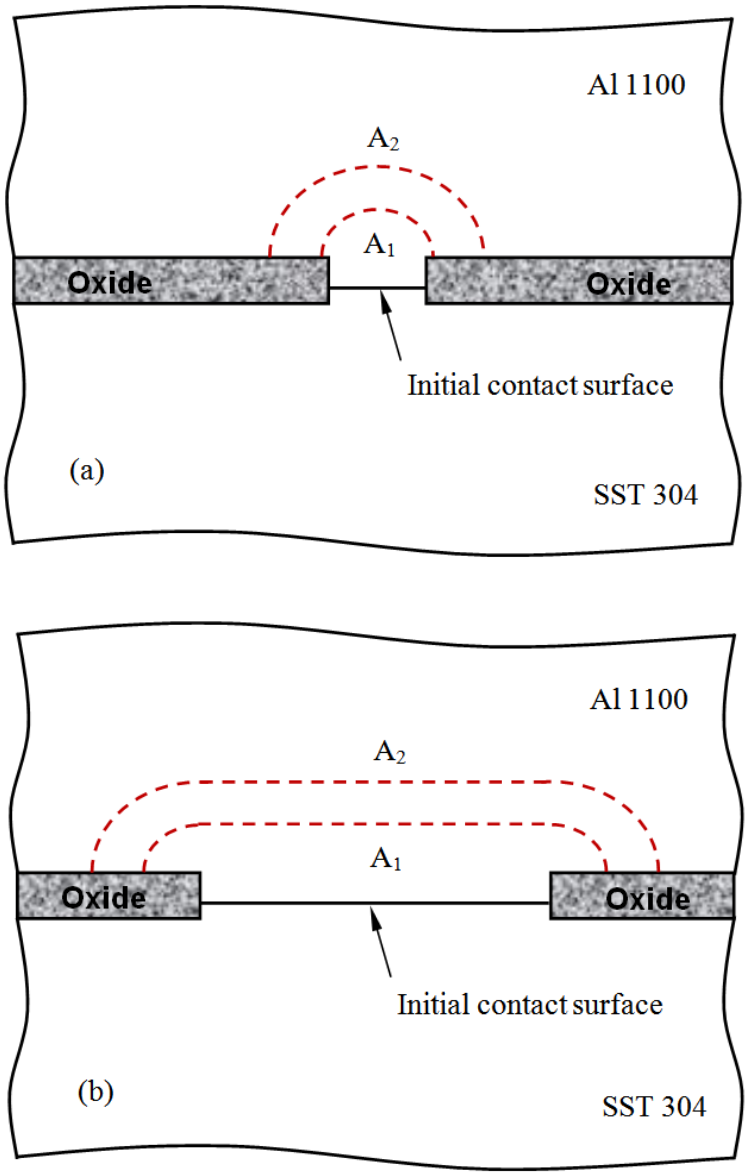

Figure 3.12 Schematic illustration of the diffusion between extruded Al 1100 and SST 304 through the crevice between oxide film fragments: (a) low bonding area ratio; (b) high bonding area ratio

Let the dash contours in Figure 3.12 represent the concentration of SST 304. The concentration along the outer contour is lower. Accordingly, the material strength along the outer contour is lower. The evidence from previous work [76] suggested that the metal to oxide fragment bond makes no contribution to the final strength of the composite metal sheets. Then it could be expected that the splitting of bonded metal sheets will propagate along one of the dash contours and the interface between the base metal and oxide fragments. The peeling will always take place in the Al rich side. This deduction can be verified by observing the surface of the SST 304 after the Al 1100 sheet is peeled off. As shown in Figure 3.13, the rich residual aluminum can be observed on the SST 304 surface after Al 1100 is peeled off. The residual aluminum is actually the rich aluminum interface covered by the red dash line in Figure 3.12 and some adherent aluminum from Al 1100.

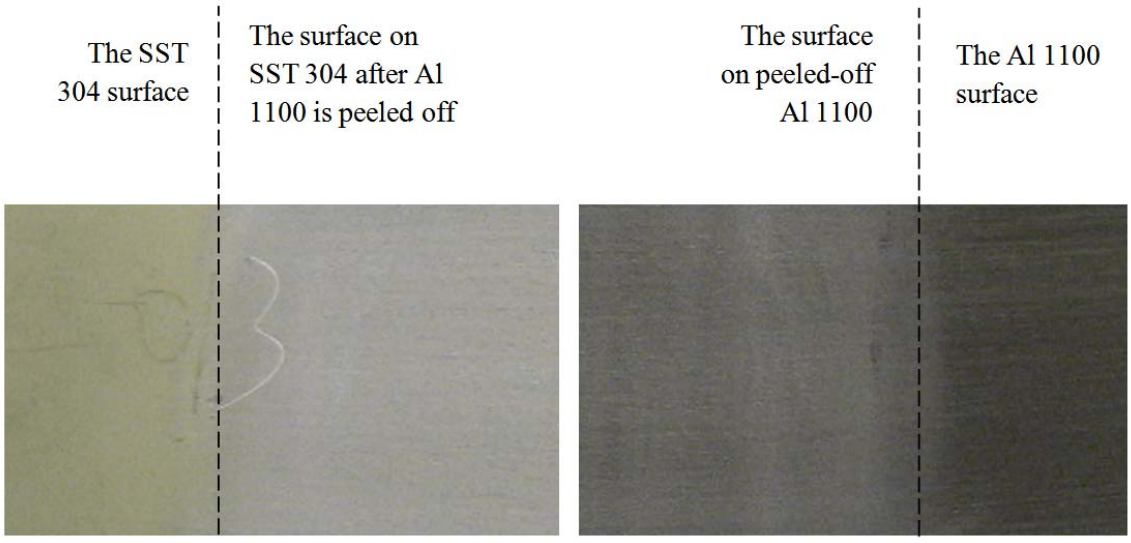

Figure 3.13 The surface of the SST 304 after the bonded Al 1100 sheet is peeled off

As shown in Figure 3.12, the contour A_2 represent the diffusion front where the theoretical concentration of SST 304 decays to zero. The adjacent diffusion front A_2 will merge with each other in a sufficient diffusion time. The contour A_2 will go farther into Al 1100 through the further diffusion and the strength under the contour will increase. At some point, the peeling failure will take place in Al 1100 instead of the diffusion interface due to the strengthening of the bonding interface. In this point of view, the lower bonding strength with lower bonding area ratio has more room to increase than that with higher bonding area ratio. Thus, the final increase of peel strength is greater at low rolling thickness reduction as shown in Figure 3.8-(a).

3.6 Summary

In this chapter, clad metals Al 1100-SST 304-Al 1100 were developed through the roll bonding process under controlled rolling conditions including rolling thickness reduction, entry temperature and reheating time. The corresponding peel strengths between Al 1100 and SST 304 were evaluated by the 180^o peel test according to design of experiments in the range of the rolling thickness reduction 10%-50% and the entry temperature 240-320^{o}C. Considering the plastic dissipation of peeled Al 1100, the peel surface energy release rate was used to obtain more accurate evaluation of the bonding strength of roll bonded metal sheets.

It is found that the bonding strength of roll clad metals highly depends on the rolling thickness reduction and entry temperature. A threshold rolling thickness reduction is required at a particular entry temperature to bond Al 1100 and SST 304. The

peel strength increases with the rolling thickness reduction or the entry temperature until the overall bonding strength exceeds the strength of Al 1100. The peeling failure would propagate in the Al 1100 once the bonding strength exceeds the strength of Al 1100. Due to the combined effect of annealing of Al 1100 near bonding interface and the diffusion at the interface, the reheating treatment decreases the bonding strength at first and then increases the bonding strength in certain time. The reheating time required to increase the bonding strength depends on the reheating temperature and the metal contact area ratio at the interface.

CHAPTER IV

ROLL BONDING MECHANICS MODELING

4.1 Introduction

The roll bonding process of clad metals involves in the fracture of the covering oxide film and the extrusion of the exposed underlying metal. The schematic illustration of the roll bonding mechanism is depicted in Figure 4.1. The plastic deformation of metals caused by rolling breaks the brittle oxide film on the metal. The broken oxide film exposes the underlying clean metal and thus allows the exposed metals to extrude through the fissures. As the materials go through the roll gap, the extruded metals from different layers will contact each other and then diffusion bonding can initiate.

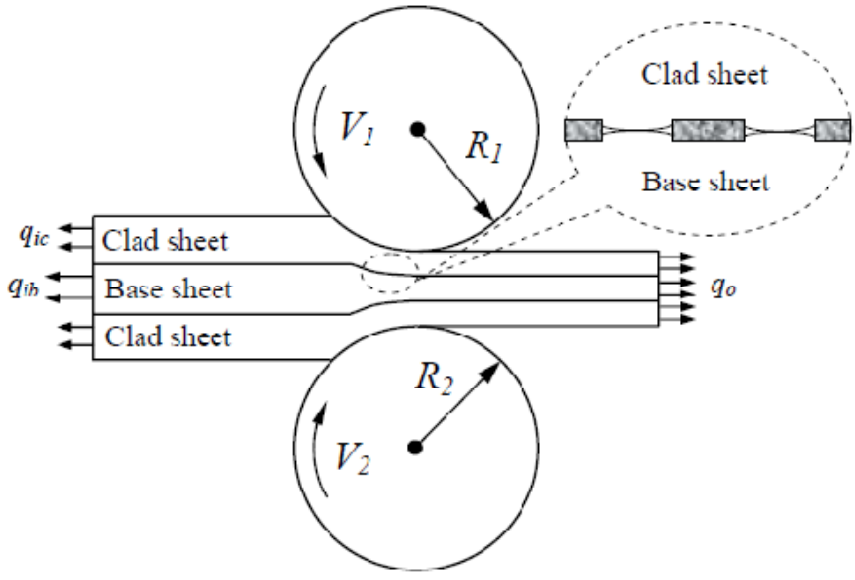

Figure 4.1 Schematic illustration of roll bonding of sandwich sheet

In this chapter, the described roll bonding mechanism is mathematically modeled and then quantitatively investigated. The roll bonding process of a three-ply metal sheet is characterized by two microscopic models (i.e. the oxide film fracture model and the metal extrusion model) and one macroscopic rolling mechanics model. In section 4.2, the oxide film fracture model is developed to predict the aspect ratio of the oxide film fragments fractured by the rolling plastic deformation of the metal sheets. Given the aspect ratio of oxide film fragments, the extrusion of the exposed metals under the rolling pressure is analyzed in section 4.3. In section 4.4, the mechanical behavior of the metals in the roll gap is analyzed by using slab method. By incorporating the oxide film fracture model and the metal extrusion model into the slab analysis, a roll bonding mechanics model is developed to evaluate the bonding state of the three-ply clad metal during the roll bonding process. In section 4.5, a finite element simulation of three-ply sandwich sheet is performed to validate the slab analysis used in section 4.4. Then the roll bonding mechanics model provides the evaluation of the bonding state of the three-ply clad metal during the roll bonding process in section 4.6. In section 4.7, the effect of various rolling condition factors (such as thickness reduction, component layers' thickness ratio, roll radius, component layers' flow stress mismatch, friction condition, and end-tension) on the stress state and the bonding state of the three-ply clad metal during the rolling process is investigated through the roll bonding mechanics model. Finally, the section 4.8 summarizes the theoretical study of the roll bonding process in this chapter.

4.2 Microscopic Oxide Film Fracture

To understand the oxide film breakage and metal extrusion process, the oxide film breakage needs to be studied first. The fracture of the oxide films between the component layers of clad metals during roll bonding is similar to the fracture of the surface oxide film during sheet rolling. Le *et al.* [97] studied the surface oxide fracture in cold aluminum rolling. The similar approach is used to analyze the fracture of oxide film between component layers of metal sheet sandwich. Since the oxide film thickness is much less than the roll radius, the oxide film is assumed to be flat. The proposed oxide film fracture mechanism during roll bonding process of metal sheet sandwich is illustrated in Figure 4.2. The cladding metal in the outer layers, i.e., on the top in Figure 4.2, is denoted as cladding sheet, while the metal sheet in the middle layer is denoted as base sheet. The bonded multi-layer metal sheet structure is named as clad metals or sandwich sheet. Relative to the surface oxide film, the metal materials are referred to as substrate. Since the oxide film is usually stiffer and more brittle than its metal substrate, the metal sheet extension during rolling reduction leads to tensile stress within oxide film in the extension direction and the tensile stress makes the brittle oxide film fracture.

As shown in Figure 4.2, the oxide fragment of the cladding sheet oxide film, with characteristic length of λ_c and thickness t_c, locates between point A and B. σ_C denotes the horizontal stress at the neutral point C of oxide fragment AB. Due to the extension of the cladding metal sheet caused by rolling thickness reduction, the shear stresses τ_A along the length L_{CA} and τ_B along the length L_{CB} are in the opposite direction. Since the oxide film is much thinner than the thickness of metal sheet, the pressure p and the longitudinal

stress through the oxide film thickness are assume to be constant. The equilibrium state in the longitudinal direction is satisfied by

$$\tau_B L_{CB} = \tau_A L_{CA} + L_{AB}\tau_\mu \tag{4.1}$$

Here, τ_μ is the friction stress between the base sheet and the cladding sheet.

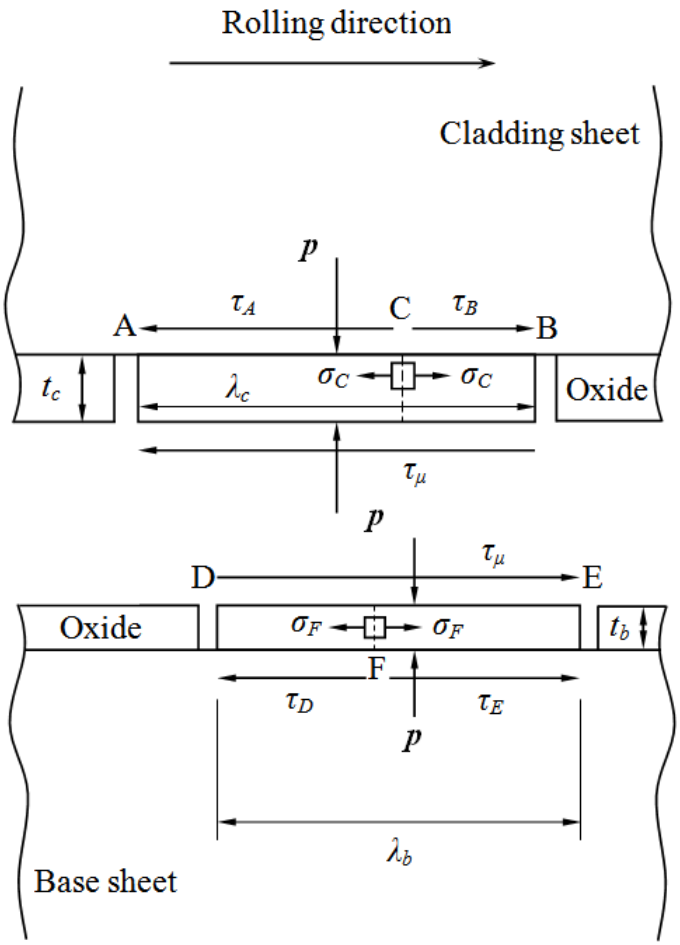

Figure 4.2 Oxide film breakage of clad and base sheets during sandwich sheet rolling

At the neutral point C, the longitudinal tensile stress σ_C within oxide film fragment reaches maximum. The equilibrium state in longitudinal direction of the section BC (part of oxide fragment AB) gives

$$\sigma_C t_c = \left(\tau_A + \tau_\mu\right) L_{CA} \tag{4.2}$$

The longitudinal tensile stress within the fragment can be solved by Eq. (4.1) and (4.2):

$$\sigma_C = \frac{\lambda_c}{t_c} \frac{\left(\tau_A + \tau_\mu\right)\left(\tau_B - \tau_\mu\right)}{\tau_A + \tau_B} \tag{4.3}$$

At point C, the shear stress can be considered as zero since the shear stress should keep the same value and in opposite direction. So the plane strain von Mises yield criterion at point C can be expressed as:

$$\sigma_C + p = 2k_{co} \tag{4.4}$$

where k_{co} is the yield shear stress of the oxide film on clad metal. Substitute Eq. (4.3) into Eq. (4.4), the maximum aspect ratio of the oxide fragment of clad sheet can be reached at

$$\left(\frac{\lambda_c}{t_c}\right)_{\max} = \frac{\left(2k_{co} - p\right)\left(\tau_A + \tau_B\right)}{\left(\tau_A + \tau_\mu\right)\left(\tau_B - \tau_\mu\right)} \tag{4.5}$$

As the metal sheets go through the roll bite, the metal sheet is compressed in thickness and extended in longitudinal direction faster than its oxide film. At certain

point, the metal substrate slides relative to its oxide film. After the sliding occurs, the friction (shear stress) between them is equal to the yield shear stress k_c of the clad sheet metal substrate, as shown in Figure 4.2:

$$\tau_A = \tau_B = k_c \tag{4.6}$$

According the mechanical behavior analysis of sandwich sheet rolling [19], the pressure near the entrance and before the bonding of component layers is essentially determined by the equivalent yield shear stress. If there is no tension on component layers at entrance, the approximation in plane strain state can be made before the bonding of component layers:

$$p = 2k_c \tag{4.7}$$

The interfacial shear stress τ_μ is defined through the friction coefficient μ between base and clad sheets (or oxide films).

$$\tau_\mu = \mu p \tag{4.8}$$

Substitute Eq. (4.6)-(4.8) into (4.5), the function of oxide film fragment aspect ratio can be derived as:

$$\left(\frac{\lambda_c}{t_c}\right)_{\max} = 4\frac{\left(\frac{k_{co}}{k_c} - 1\right)}{\left(1 - 4\mu^2\right)} \tag{4.9}$$

Similarly, for the oxide film fragment on the base sheet, the aspect ratio is:

$$\left(\frac{\lambda_b}{t_b}\right)_{\max} = 4\frac{\left(\frac{k_{bo}}{k_b}-\frac{k_c}{k_b}\right)}{\left(1-4\mu^2\left(\frac{k_c}{k_b}\right)^2\right)} \tag{4.10}$$

Here, k_b and k_{bo} denote the pure shear yield stresses of the base sheet and the oxide film of the base sheet, λ_b denotes the length of the oxide fragment of the base sheet and t_b denotes the thickness.

4.3 Microscopic Metal Extrusion through Crevice between Oxide Fragments

Le and Suctliffe [97-99] experimentally investigated the oxide film fracture on a single layer aluminum sheet under single pass rolling and developed a metal extrusion model based on Wilson and Korzekwa's [100,101] study of asperity flattening. The approach is extended to establish the metal extrusion model in roll bonding process of metal sheet sandwich. Without loss of generality, we assume the oxide fragments have the same length the length λ_0 and the same thickness t_{ox}. As shown in Figure 4.3, the spacing of the oxide fragment is λ, the extrusion depth of the exposed metal into the crevice is δ, the pressure exerting on the oxide fragment is p_{ox}, and the pressure exerting on the surface of the extruded metal in the crevice is p_{cv}. Since the toughness of oxide is much lower than that of the substrate metal, the oxide fragments is considered as an inextensible rigid body. Then the plastic strain in the longitudinal (ε_l) and the thickness (ε_t) direction can be approximately expressed by the oxide fragment spacing and the rolling thickness reduction ratio (r_t).

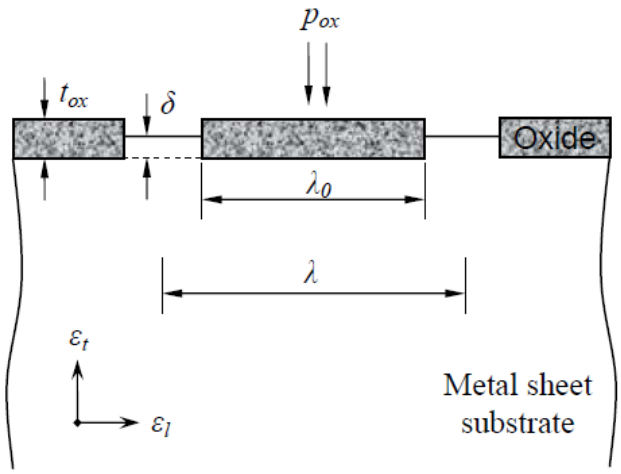

Figure 4.3 Metal extrusion through oxide fragment crevice

$$\varepsilon_l = \frac{\lambda - \lambda_0}{\lambda_0} \tag{4.11}$$

$$\varepsilon_t = -r_t \tag{4.12}$$

The metal sheets in rolling process are considered as incompressible materials, thus

$$(1+\varepsilon_l)(1+\varepsilon_t) = 1 \tag{4.13}$$

If we define the extrusion velocity v_f=dδ/dt, a non-dimensional extrusion rate R_E can be expressed in the following, as described by Sutcliffe [98, 99]:

$$R_E = \frac{2v_f}{\lambda\dot{\varepsilon}} \tag{4.14}$$

Substituting Eq. (4.11)-(4.13) into Eq. (4.14) and dividing the both side of Eq. (4.14) by the oxide film thickness, the metal extrusion ratio with respect to oxide thickness can be derived:

$$\left(\frac{\delta}{t_{ox}}\right) = \frac{\lambda_0}{2t_{ox}} \int_0^{\varepsilon_l} (1+\varepsilon) R_E d\varepsilon \tag{4.15}$$

If the oxide film fragment is considered as an indenter on the substrate, the metal extrusion can be considered as indentation of oxide fragment into metal sheet substrate, as described by Suctliffe [97]. Then the finite element simulation result of surface asperity deformation by Korzekwa [101] can be used. The numerical simulation result of R_E was fitted into a polynomial function of the oxide fragment area ratio, A_{ox}, and the difference between the normalized average pressures on the oxide fragments and on the extruded metal between the oxide fragments, $\Delta=(p_{ox}-p_{cv})/Y$ [98].

$$R_E(A_{ox}, \Delta) = A_{ox}(1-A_{ox})\left[F_0(\Delta) + F_1(\Delta) A_{ox} + F_2(\Delta) A_{ox}^{\ 2}\right] \tag{4.16}$$

where $F_0(\Delta) = 5.1206\Delta - 4.5258\Delta^2 + 3.5599\Delta^3$

$F_1(\Delta) = -9.5761\Delta + 11.3854\Delta^2 - 8.6069\Delta^3$

$F_2(\Delta) = 8.3193\Delta - 11.7954\Delta^2 + 7.6475\Delta^3$

In the metal extrusion case, there is no pressure on the extruded metal between the oxide fragments without lubrication. Therefore,

$$\Delta = \frac{p_{ox}}{Y} = \frac{p}{YA_{ox}} \tag{4.17}$$

Here, $Y = \frac{2}{\sqrt{3}}\sigma_Y$ is the plane strain yield stress of metal sheet substrate (σ_Y is the von Mises yield stress.). The p is the interfacial pressure.

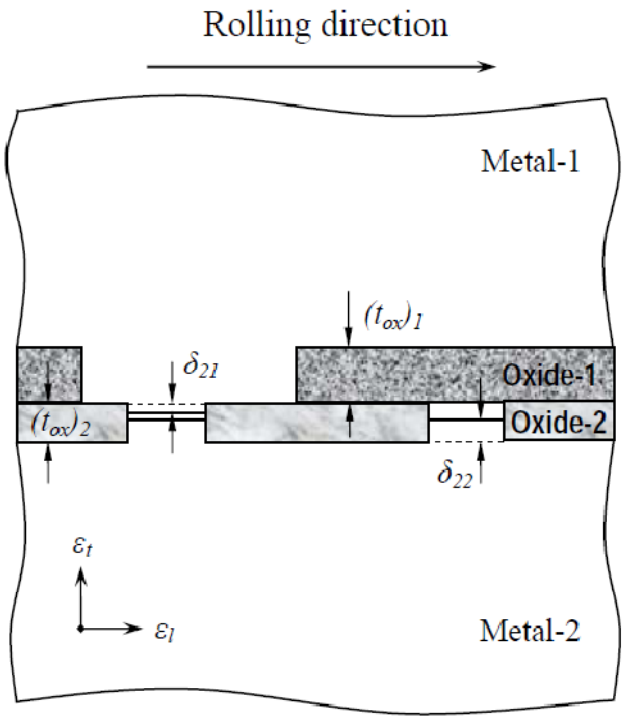

Figure 4.4 The combined metal extrusion through oxide fragment crevices

Here we use $(\delta/t_{ox})_i$ to denote the metal extrusion ratio in the crevice between the oxide fragments of metal i(i=1, 2). Since the base and cladding sheet could be different metals, it is reasonable to expect that the metal of one layer extrude through its oxide fragments, i.e., $(\delta/t_{ox})_1$=1, while the metal of adjacent layer still on the way to go through the oxide fragment crevices, i.e., $(\delta/t_{ox})_2$<1. In this case, the metal-1 will continue to extrude (but into the crevices between oxide fragments of metal-2) in the rolling process

until metal-1 and metal-2 contact each other. This combined extrusion process is illustrated in Figure 4.4, where $(\delta/t_{ox})_{2j}$ means the extrusion ratio of metal-j (j=1, 2) in the crevice between the oxide fragments of metal-2. Similarly, we use $(\varepsilon_l)_i$ to denote the longitudinal strain of metal i(i=1, 2). Assuming the $(\varepsilon_l)_1 = (\varepsilon_l)_I$ when $(\delta/t_{ox})_1$=1, the combined extrusion equation is derived as following:

$$\begin{aligned}\left(\frac{\delta}{t_{ox}}\right)_2 &= \left(\frac{\delta}{t_{ox}}\right)_{22} + \left(\frac{\delta}{t_{ox}}\right)_{21} \\ &= \frac{1}{2}\left(\frac{\lambda_0}{t_{ox}}\right)_2 \left(\int_0^{(\varepsilon_l)_2} (1+\varepsilon)(R_E)_{22}\, d\varepsilon + \int_{(\varepsilon_l)_I}^{(\varepsilon_l)_1} (1+\varepsilon)(R_E)_{21}\, d\varepsilon \right)\end{aligned} \tag{4.18}$$

It can be expected that there are a critical longitudinal strain $(\varepsilon_l)_{II,2}$ of the harder metal sheet (metal-2 as shown in Figure 4.4) and a critical longitudinal strain $(\varepsilon_l)_{II,1}$ of the harder metal sheet (metal-1 as shown in Figure 4.4) such that the extruded metals (metal-1 and metal-2 as shown in Figure 4.4) contact each other, i.e., $(\delta/t_{ox})_2$=1. Considering the flow stress mismatch of clad and base metal sheets, the critical strain is different for the cladding sheet and the base sheet, in other words, $(\varepsilon_l)_{II,2} \neq (\varepsilon_l)_{II,1}$. Nevertheless, there is an overall thickness reduction ratio $(r_t)_{II}$ corresponding to the initiation of extruded metals' contacting. Only if the total thickness reduction ratio $r_t > (r_t)_{II}$, the contact of extruded metals can make diffusion happen between the extruded metals such that diffusion bonding is achieved between the clad and the base metals.

4.4 Macroscopic Rolling Mechanics of Clad Metal Bonding

In this section, a symmetrical three-ply metal bonding through a symmetrical two-high rolling mill is considered. By using slab method, Hwang *et al.* [102] and Tzou *et al.* [103-106] studied the slab stress of two and three layers of sandwich metal sheets in a roll bonding process. The slab method is extended to model the roll bonding process of symmetrical three-ply metal sheets. The oxide film fracture analysis in section 4.2 and the exposed metal extrusion model in section 4.3 are incorporated in the slab stress analysis such that the bonding process can be modeled.

Due to the symmetry, a half plane diagram of a three-layer sandwich sheet going through roll gap is illustrated in Figure 4.5. R is the radii of rolls, ω is the angular velocity of rolls, θ_c is the contact angle, L is contact length, h_{ic} and h_{oc} are the entry and exit thickness of cladding sheets, h_{ib} and h_{ob} are half of the entry and the exit thickness of base sheet (in the middle), q_{ic} and q_{ib} are the entry end-loading (stress) on the ends of the clad and base sheets, and q_o is the exit end-loading on the end of bonded sandwich sheet. The three component layers of the sandwich sheet are stacked together without bonding before they enter the roll gap. The top and bottom layers of the sandwich sheet have the same thickness. During the rolling process, the three component layers are bonded at certain point after they enter the roll gap. According to the yielding and bonding state of component layers, the sandwich sheet in the roll gap is divided into four zones. In zone I, the soft material yields while the hard material does not. Zone II starts at point $x=x_y$, where the hard material starts to yield. In zone III, the extruded metals from component layers contact each other and the diffusion bonding of the extruded metals starts to occur

at point $x=x_b$. The sandwich sheet and rolls have the same velocity at neutral point $x=x_n$ where zone IV starts. Rolls move faster than the sheet sandwich in zone I, II and III, while the sheet sandwich moves faster in zone IV.

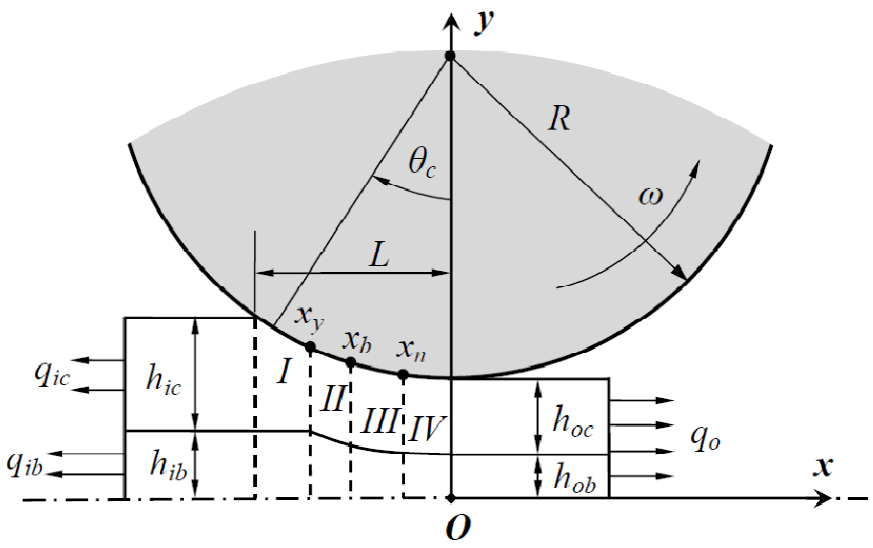

Figure 4.5 Schematic illustration of sandwich sheet during rolling

In order to simplify the complex roll bonding conditions without loss of generality, the following assumptions are made:

1. The rolls are rigid body.
2. The metal sheets are rigid perfectly plastic materials.
3. The deformation rolled sandwich sheet is in plane strain state.
4. The principal stresses are in axial directions, $(\sigma_1,\sigma_2)\approx(\sigma_{yy},\sigma_{xx})\approx(-p,q)$.
5. Materials obey von Mises yield criterion.

Based on the above assumptions, the yield criterion for each metal sheet-i (i=c means the cladding metal and i=b means the base metal) becomes:

$$p + q_i = 2k_i \tag{4.19}$$

Here, p is the vertical pressure, q_i is the horizontal tensile stress of the metal-i, and $k_i = \frac{1}{\sqrt{3}}(\sigma_Y)_i$ is yield shear stress of the metal-i. A typical slab analysis of rolled metal sheets in the roll gap is demonstrated in Figure 4.6 where h_c is the slab thickness of the cladding sheet, h_b is the half slab thickness of the base sheet, S_c is the length of the top side of the cladding sheet, S_μ is the length of the contacting sides of the cladding and base sheets, θ_μ is the tilt angle of the contacting sides of the cladding and base sheets, p_c is the pressure of the top roll on the cladding sheet, p_μ is the pressure on the contacting surfaces of the cladding and base sheets, q_c is the horizontal stress of the cladding sheet, q_b is the horizontal stress of the base sheet, τ_c is the friction stress between the top roll and the cladding sheet and τ_μ is the friction stress between the cladding and the base sheets. The equilibrium equation of the cladding sheet is derived as:

$$\frac{d(h_c q_c)}{dx} + \tau_c\left(1+\tan^2\theta_c\right) - p\left(\tan\theta_c - \tan\theta_\mu\right) - \tau_\mu\left(1+\tan^2\theta_\mu\right) = 0 \tag{4.20}$$

The equilibrium of the base sheet slab gives:

$$\frac{d(h_b q_b)}{dx} - p\tan\theta_\mu + \tau_\mu\left(1+\tan^2\theta_\mu\right) = 0 \tag{4.21}$$

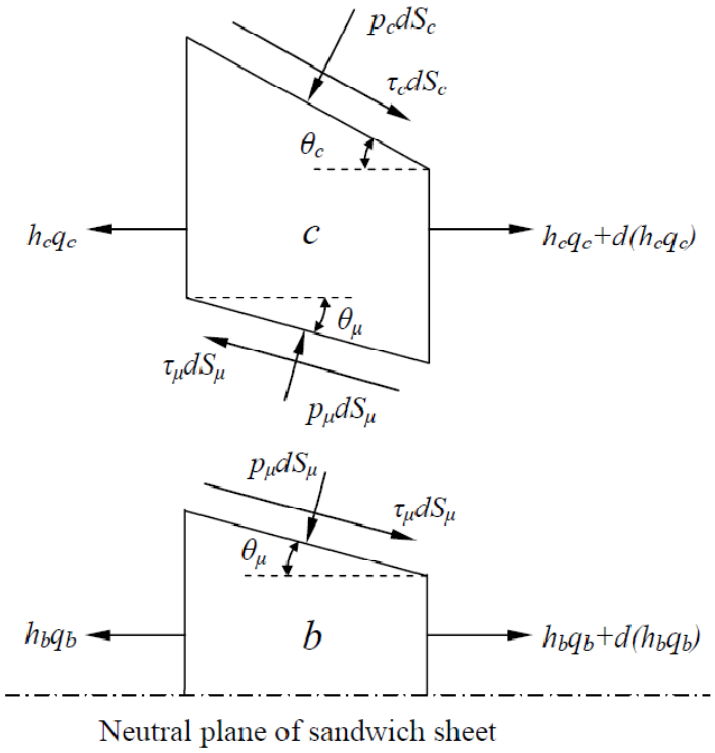

Figure 4.6 Slab stress state of rolled metal sheets in roll gap

Here, we introduce $hq = h_c q_c + h_b q_b$, where q is the equivalent horizontal tension on the sandwich sheet. Rearranging Eq. (4.20) and (4.21), we derive:

$$\frac{d(hq)}{dx} + \tau_c \left(1 + \tan^2 \theta_c\right) - p \tan \theta_c = 0 \tag{4.22}$$

Similarly, we also introduce the equivalent yield shear strength of sandwich sheet as:

$$k_e = \eta k_c + (1 - \eta) k_b \tag{4.23}$$

where $\eta = \frac{h_c}{h}$. Then the overall yield criterion of sandwich sheet can be derived as:

$$p + q = 2k_e \tag{4.24}$$

In industrial, the cladding metal (layer *c*) can be either harder or softer than the base metal (layer *b*). Here, we introduce a non-dimensional variable $s=\theta_\mu/\theta_c$. By defining the value of *s*, Eq.(4.20) and (4.21) can solve the stress of either the soft/hard/soft layered sandwich sheet or the hard/soft/hard layered sandwich sheet. When only one material yields,

$$\begin{aligned} s &= 0 \text{ if } k_b > k_c \\ s &= 1 \text{ if } k_c > k_b \end{aligned} \tag{4.25}$$

For flat rolling, usually, $|x|/R<<1$, therefore, the following approximation is applied.

$$\tan\theta_c \approx -\frac{x}{R} \tag{4.26}$$

In reality, the yield state, friction conditions and the bonding state change through the roll gap, therefore the mechanical analysis of metal deformation is performed zone by zone. As previously defined, zone I is in the domain $[-L, x_y]$, zone II is in the domain $[x_y, x_b]$, zone III is in the domain $[x_b, x_n]$, and zone IV is in the domain $[x_n, 0]$.

Zone I [$-L, x_y$]

In this zone, soft material yields first, but hard sheet doesn't yield. When the cladding sheet is softer ($s=0$) and we have

$$p + q_c = 2k_c \tag{4.27}$$

From slab's geometry, we have

$$h_c = h_o - h_{ib} + R - \sqrt{R^2 - x^2} \approx h_o - h_{ib} + \frac{x^2}{2R} \tag{4.28}$$

Since the clad sheet yields but the base sheet does not in zone I, the base sheet moves into roll gap faster than the clad sheet in this zone. Thus the direction of the shear stress τ_μ goes to the opposite of the direction as shown in Figure 4.6. Then, with Eq. (4.26), Eq. (4.27) and Eq.(4.28), Eq.(4.21) becomes

$$\frac{dp}{dx} = \frac{2\tau_c}{R} + \frac{2\tau_c\left(R - 2h_o + 2h_{ib}\right) + 2R\tau_\mu + 4k_c x}{2R\left(h_o - h_{ib}\right) + x^2} \tag{4.29}$$

Then the p in zone I can be solved by integrating Eq.(4.29).

In oxide film fracture modeling, it assumes that the oxide is inextensible. Accordingly, the friction coefficients between surfaces depend on the surface extension deformation. The average friction coefficients $\bar{\mu}_{rc}$ between the rolls and the cladding sheets and $\bar{\mu}_{bc}$ between the cladding and base sheets are defined in the following:

$$\bar{\mu}_{rc} = \mu_{rc}\left(1 - r_t\right) + \mu'_{rc} r_t \tag{4.30}$$

$$\bar{\mu}_{bc} = \mu_{bc}\left(1 - r_t\right) + \mu'_{bc} r_t \tag{4.31}$$

Here, μ'_{rc} and μ'_{bc} are the friction coefficients (between the rolls and the facing surfaces of the cladding sheets and between the cladding and base sheets) in the crevice section between oxide film fragments. r_t is the overall thickness reduction ratio that is equal to the surface extension. $r_{t,J}$ means the overall thickness reduction ratio in zone J (J=*I, II, III, IV*). When the crevice is small, the extruded metal does not contact the facing surface of the other metal sheet and thus $\mu'_{ij}=0$. Once the extruded metal go through the crevice and contact the other surface, the friction coefficient is $\mu'_{ij}=1$. Then the average friction stress becomes:

$$\tau_c=\left(\mu_{rc}+\left(\mu'_{rc}-\mu_{rc}\right)r_t\right)k_c \tag{4.32}$$

$$\tau_\mu=\left(\mu_{bc}+\left(\mu'_{bc}-\mu_{bc}\right)r_t\right)k_c \tag{4.33}$$

where $r_{t,I}\left(x\right)=1-\dfrac{2R\left(h_o-h_{ib}\right)+x^2}{2Rh_{ic}}$

Substitute Eq. (4.32) and Eq. (4.33) into Eq. (4.29), and normalize Eq. (4.29) by $2k_c$, the following equation is derived:

$$\begin{aligned}\frac{d\left(\dfrac{p}{2k_c}\right)}{dx}=&\frac{\mu'_{rc}}{R}+\frac{\mu'_{rc}\left(R-2h_o+2h_{ib}\right)+R\mu'_{bc}+2x}{2R\left(h_o-h_{ib}\right)+x^2}\\&-\left(\frac{\mu'_{rc}-\mu_{rc}}{2R^2h_{ic}}x^2+\frac{\left(\mu'_{rc}-\mu_{rc}\right)+\left(\mu'_{bc}-\mu_{bc}\right)}{2h_{ic}}\right)\end{aligned} \tag{4.34}$$

Applying the boundary condition at entry point, $p|_{x=-L}=2k_c-q_{ic}$, the normalized vertical pressure can be solved.

$$\frac{p_I}{2k_c}=\ln\frac{x^2+D^2}{L^2+D^2}+\frac{\mu'_{rc}B+\mu'_{bc}R}{D}\left(\tan^{-1}\left(\frac{x}{D}\right)+\tan^{-1}\left(\frac{L}{D}\right)\right)+\mu'_{rc}\frac{x+L}{R}+1-\frac{q_{ic}}{2k_c}$$
$$-\left(\frac{\left(\mu'_{rc}-\mu_{rc}\right)+\left(\mu'_{bc}-\mu_{bc}\right)}{2h_{ic}}\left(x+L\right)+\left(\mu'_{rc}-\mu_{rc}\right)\frac{\left(x^3+L^3\right)}{6R^2h_{ic}}\right) \tag{4.35}$$

where $H=h_o-h_{ib};\ B=R-2H;\ D=\sqrt{2RH}$.

For the equilibrium of the middle base material in zone I, the equilibrium Eq. (4.21) gives (θ_μ=0 since hard material does not yield yet.):

$$\frac{q_{Ib}}{2k_c}=\frac{\bar{\mu}_{bc}}{2}\frac{x}{h_{ib}}+c_{Ib} \tag{4.36}$$

At x=-L, the integration constant c_{Ib} can also be determined by the boundary condition $q_{Ib}|_{x=-L}=q_{ib}$. The solution Eq.(4.36) becomes:

$$\frac{q_{Ib}}{2k_c}=\frac{\mu'_{bc}}{2}\frac{x+L}{h_{ib}}+\frac{q_{ib}}{2k_c}+\frac{\mu'_{bc}-\mu_{bc}}{4Rh_{ic}}\frac{x^3+L^3}{3h_{ib}} \tag{4.37}$$

Zone II [x_y, x_b]

In this zone, both of the soft and hard materials yield. The hard material starts to yield at $x=x_y$, where the yield criterion is satisfied.

$$p+q_b=2k_b \tag{4.38}$$

Here, a location function *f(x)* is introduced:

$$f\left(x_y\right)=\frac{p+q_b}{2k_c}-\frac{k_b}{k_c} \tag{4.39}$$

Then the location $x=x_y$ where the hard material starts to yield can be determined by solving the equation $f(x_y)=0$ in the nearest neighborhood of $x=-L$.

After both of the cladding and base sheets yield, the oxide films on both sheets break and the metals extrude through the crevices among the oxide fragments. The extruded metals will contact each other at $x=x_b$, where the diffusion bonding initiates. Before this point, even though both sheets yield, they do not bond. Then the equilibrium Eq. (4.20) and Eq. (4.21) apply on the cladding and base sheets respectively. The overall equilibrium Eq. (4.22) could be expressed as:

$$\frac{dp}{dx}=\frac{2\tau_c}{R}+\frac{2\tau_c\left(R-2h_o\right)+4k_e x}{2Rh_o+x^2} \tag{4.40}$$

Substitute Eq. (4.32) into Eq. (4.40) with $r_{t,II}(x)=1-(2Rh_o+x^2)/(2Rh_i)$, the normalized equilibrium equation can be derived. Here, h_i ($=h_{ic}+h_{ib}$) is half of the total entry thickness of the sandwich sheet and h_o ($=h_{oc}+h_{ob}$) is half of the total exit thickness of the sandwich sheet.

$$\frac{d\left(\frac{p}{2k_c}\right)}{dx}=\frac{\mu'_{rc}}{R}+\frac{\mu'_{rc}\left(R-2h_o\right)+2\frac{k_e}{k_c}x}{2Rh_o+x^2}-\left(\frac{\mu'_{rc}-\mu_{rc}}{2R^2h_i}x^2+\frac{\left(\mu'_{rc}-\mu_{rc}\right)}{2h_i}\right) \tag{4.41}$$

Applying the boundary condition $p_I\big|_{x=x_y}=p_{II}\big|_{x=x_y}$, the vertical pressure p can be solved.

$$\frac{p_{II}}{2k_c}=\frac{k_e}{k_c}\ln\frac{x^2+2Rh_o}{x_y{}^2+2Rh_o}+\mu'_{rc}\frac{R-2h_o}{\sqrt{2Rh_o}}\left(\tan^{-1}\left(\frac{x}{\sqrt{2Rh_o}}\right)-\tan^{-1}\left(\frac{x_y}{\sqrt{2Rh_o}}\right)\right)$$
$$+\frac{\mu'_{rc}}{R}\left(x-x_y\right)+\frac{p_I(x_y)}{2k_c}-\left(\mu'_{rc}-\mu_{rc}\right)\left(\frac{x^3-x_y{}^3}{6R^2h_i}+\frac{x-x_y}{2h_i}\right) \tag{4.42}$$

If the thickness ratio keeps constant after all component layers yield, the relationship between θ_μ and θ_c could be expressed as following:

$$\tan\theta_\mu=\left(1-\eta\right)\tan\theta_c \tag{4.43}$$

Substituting Eq. (4.43) into Eq. (4.21), the shear stress between the cladding and base sheets can be solved.

$$\left(\tau_\mu\right)_{II}=\frac{\left(1-\eta\right)\left(\left(h_o+\frac{x^2}{2R}\right)\frac{dp}{dx}-2k_b\frac{x}{R}\right)}{1+\left(1-\eta\right)^2\left(\frac{x}{R}\right)^2} \tag{4.44}$$

Substituting Eq. (4.41) into Eq. (4.44), the normalized shear stress can be derived:

$$\frac{\left(\tau_\mu\right)_{II}}{2k_c}=\frac{\left(1-\eta\right)\left(\left(h_o+\frac{x^2}{2R}\right)\left(\frac{\mu'_{rc}}{R}+\frac{\mu'_{rc}\left(R-2h_o\right)+2\frac{k_e}{k_c}x}{2Rh_o+x^2}\right)-\frac{k_b}{k_c}\frac{x}{R}\right)}{1+\left(1-\eta\right)^2\left(\frac{x}{R}\right)^2}$$
$$-\frac{\left(1-\eta\right)\left(h_o+\frac{x^2}{2R}\right)\left(\frac{\mu'_{rc}-\mu_{rc}}{2R^2h_i}x^2+\frac{\left(\mu'_{rc}-\mu_{rc}\right)}{2h_i}\right)}{1+\left(1-\eta\right)^2\left(\frac{x}{R}\right)^2} \tag{4.45}$$

Zone III [x_b, x_n]

In zone II, the hard material yields and its oxide film on the surface fractures. Meanwhile, the exposed metal extrudes through the crevices between oxide fragments. At certain point $x=x_b$, the extension strain and the vertical pressure drive one of the extruded metals to contact the other extruded metal from the facing component layer and the adjacent layers bond. Here, a combined metal extrusion function is introduced:

$$g(x)=\frac{\delta_c}{t_{bo}}+\frac{\delta_b}{t_{bo}}-1=\left(\frac{\delta}{t_{ox}}\right)_{21}+\left(\frac{\delta}{t_{ox}}\right)_{22}-1 \tag{4.46}$$

where δ_b and δ_c are the extrusion depths of the base and cladding metals respectively into the crevice among oxide film fragments (with the thickness of t_{ob}) of the harder material in the base layer. The combined metal extrusion function $g(x)$ is defined by the metal extrusion model. The bonding point x_b can be determined by $g(x)=0$. The stress state of sandwich sheet in zone III can be solved as that in zone II.

Zone IV [x_n, 0]

In zone III, the cladding and base sheets are bonded in the form of a sandwich sheet. As the bonded sandwich sheet goes through the roll gap, the rolled sandwich sheet will translate faster than the rolling velocity of rolls at a neutral point $x=x_n$. Therefore, the shear stress on the cladding sheet by the rolls changes its direction. The zone IV is defined in the domain [x_n, 0]. The equilibrium equation of the sandwich sheet in zone IV can be derived by switching the direction of τ_c in the Eq. (4.22). At the exit $x=0$, the boundary condition as shown in Figure 4.6 gives:

$$p\big|_{x=0} + q_o = 2k_e \tag{4.47}$$

Applying the boundary condition, the pressure p can be solved:

$$\begin{aligned}\frac{p_{IV}}{2k_c} = \frac{k_e}{k_c}\ln\frac{x^2+2Rh_o}{2Rh_o} - \mu'_{rc}\frac{R-2h_o}{\sqrt{2Rh_o}}\tan^{-1}\left(\frac{x}{\sqrt{2Rh_o}}\right) - \frac{\mu'_{rc}}{R}x + \frac{2k_e - q_o}{2k_c} \\ + \left(\mu'_{rc} - \mu_{rc}\right)\left(\frac{x^3}{6R^2h_i} + \frac{x}{2h_i}\right)\end{aligned} \tag{4.48}$$

Similarly, the shear stress between the base and cladding sheets is

$$\begin{aligned}\frac{\left(\tau_\mu\right)_{IV}}{2k_c} = &\frac{(1-\eta)\left(\left(h_o + \frac{x^2}{2R}\right)\left(2\frac{k_e}{k_c}x - \mu'_{rc}\left(R-2h_o\right)}{2Rh_o + x^2} - \frac{\mu'_{rc}}{R}\right) - \frac{k_b}{k_c}\frac{x}{R}\right)}{1+(1-\eta)^2\left(\frac{x}{R}\right)^2} \\ &+ \frac{(1-\eta)\left(h_o + \frac{x^2}{2R}\right)\left(\frac{\mu'_{rc}-\mu_{rc}}{2R^2h_i}x^2 + \frac{\left(\mu'_{rc}-\mu_{rc}\right)}{2h_i}\right)}{1+(1-\eta)^2\left(\frac{x}{R}\right)^2}\end{aligned} \tag{4.49}$$

The neutral point x_n is determined by the equation $p_{III}(x_n)=p_{IV}(x_n)$ as following:

$$\begin{aligned}\frac{k_e}{k_c}\ln\frac{2Rh_o}{x_y{}^2+2Rh_o} + \mu'_{rc}\frac{R-2h_o}{\sqrt{2Rh_o}}\left(2\tan^{-1}\left(\frac{x_n}{\sqrt{2Rh_o}}\right) - \tan^{-1}\left(\frac{x_y}{\sqrt{2Rh_o}}\right)\right) \\ + \frac{\mu'_{rc}}{R}\left(2x_n - x_y\right) + \frac{p_I(x_y)}{2k_c} - \frac{2k_e - q_o}{2k_c} \\ - \left(\mu'_{rc} - \mu_{rc}\right)\left(\frac{2x_n{}^3 - x_y{}^3}{6R^2h_i} + \frac{2x_n - x_y}{2h_i}\right) = 0\end{aligned} \tag{4.50}$$

4.5 Numerical Simulation and Validation

In order to validate the slab analysis of the sandwich sheet during a rolling process, finite element analysis (FEA) of the process is performed through ABAQUS Explicit. In the FEA, the rolling of sandwich sheet is considered as a 2-D plane strain problem. The work hardening of component metal sheets is considered. For convenience, the component layers of the sandwich sheet are considered to be perfectly bonded. The material of the cladding layers is Al 1100 and the material of the base layer is SST 304. Material properties used in FEA are provided in Table 4.1 [107-110]. The element CPE4R [111] is used in this model to simulate the half of the sandwich sheet rolling due to the symmetry of this problem (as shown in Figure 4.7). Friction between the roll and the cladding Al 1100 sheet is modeled using a constant Coulomb friction coefficient μ_{rc}=0.9. The roll radius is R=41mm, the angular velocity of the rolls is w=0.628 rad/s, and the half thickness of the sandwich sheet Al-SST-Al is h_i=2.36mm with the thickness of the cladding sheet h_{ic}=1.60mm. The overall rolling thickness reduction is 30%.

Table 4.1 Material properties

Property	Modulus E (GPa)	Poisson's Ratio ν	Yield Stress σ_Y (MPa)	UTS (MPa)	Density ρ (g/cm^3)
Al 1100	68.9	0.33	103	110 (ε_p=0.12)	2.71
SST 304	193.0	0.24	290	420 (ε_p=0.40)	8.00

The stress, strain and velocity fields of the Al-SST-Al sheet sandwich solved by the FE model are illustrated in Figure 4.8. Since the oxide film is much thinner than the metal substrate, it is very difficult to incorporate the oxide film in the FE model considering the computation efficiency. Therefore, the slab analysis of the bonded Al-SST-Al specimen without oxide film in a roll gap is performed to provide the comparison between the slab analysis and the FE simulation. The comparison of stress states solved by the theoretical slab analysis and the FEA is provided in Figure 4.9. For the FEA results, the p is the average pressure through the thickness; q_c is horizontal stress extracted from the cladding metal side of the bonding interface; q_b is from the base metal side of the interface; the shear stress τ_μ is also from the interface.

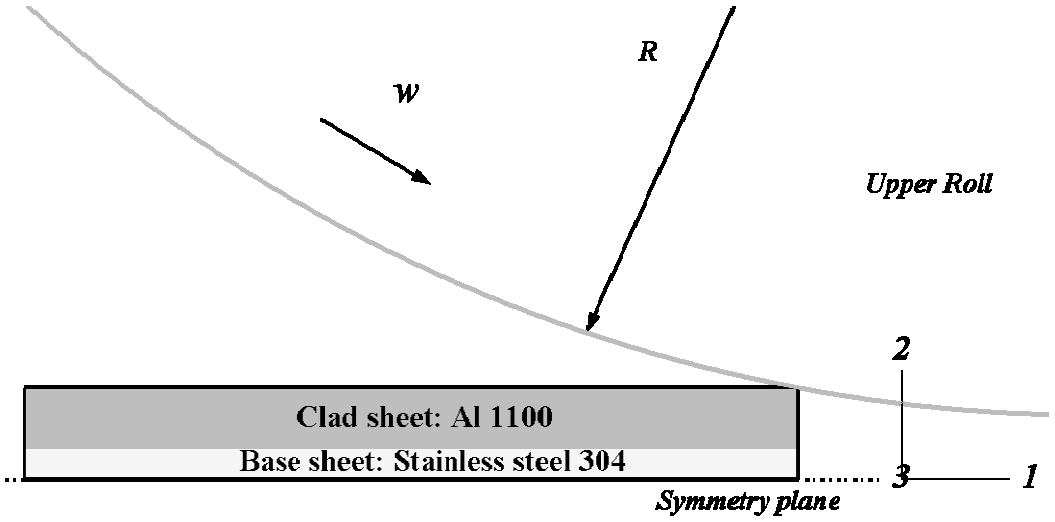

Figure 4.7 The illustration of FEA model of sandwich sheet rolling

From Figure 4.8-(a), it can be seen that the horizontal stress in the softer cladding sheet is compressive while it is tensile in the harder base sheet. The same stress state is

also predicted by the slab analysis, as shown in Figure 4.9. Figure 4.8-(a) also shows that the minimum horizontal stress of the base sheet and the cladding sheet occurs at different positions. The position of the minimum stress of the harder base sheet is slightly closer to the entrance than that of the softer cladding sheet. In the theoretical model, the minimum stresses of both the base and cladding sheets are assumed to occur at the neutral point. This assumption is one of the factors inducing inaccuracy to the slab analysis. The vertical stress by FEA, as shown in Figure 4.8-(c), indicates that the vertical stress is approximately uniform through the thickness. But the vertical stress distribution through the thickness at the entrance and the exit is slightly non-uniform. Therefore, the obvious errors of the average pressure at the entrance and the exit from the slab analysis is observed in Figure 4.9, and it can be explained the uniform pressure assumption through the thickness. However, the comparison of the stress state by the slab analysis and by the FEA shows that the analytical stress solution by the slab analysis provides reasonable agreement with the FEA results. Considering the convenience and computation efficiency of the analytical model, the slab analysis is preferred to analyze the roll bonding of metal sheets by incorporating the oxide film fracture model and the metal extrusion model.

In Figure 4.8-(b) and (d), it can also be seen that the thickness reduction and the longitudinal extension of the softer cladding sheet are slightly more than that of the harder base sheet. The same phenomenon is observed in the roll bonding experiment of Al-SST-Al sandwich sheet.

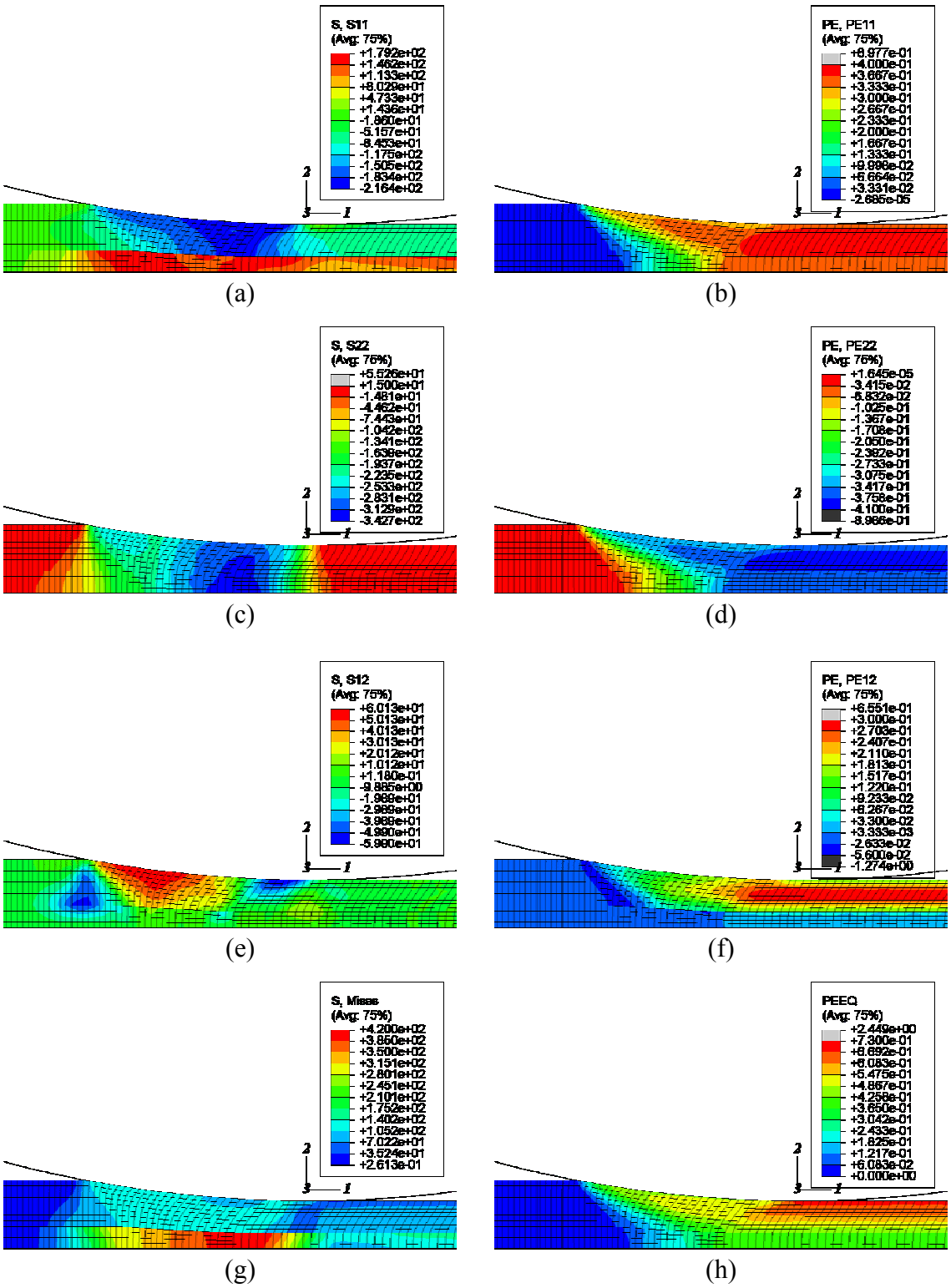

Figure 4.8 Stress, strain, and velocity fields of Al/SST/Al sheet sandwich in roll gap during rolling process

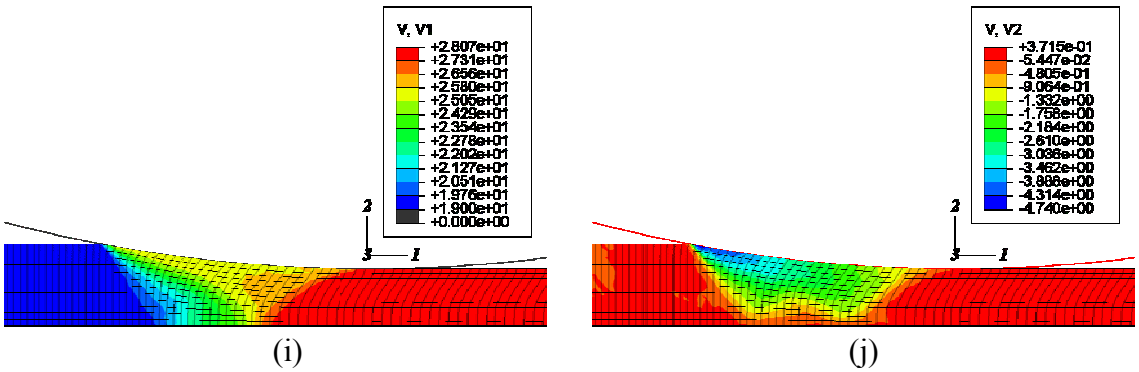

(i) (j)

Figure 4.8 continued.

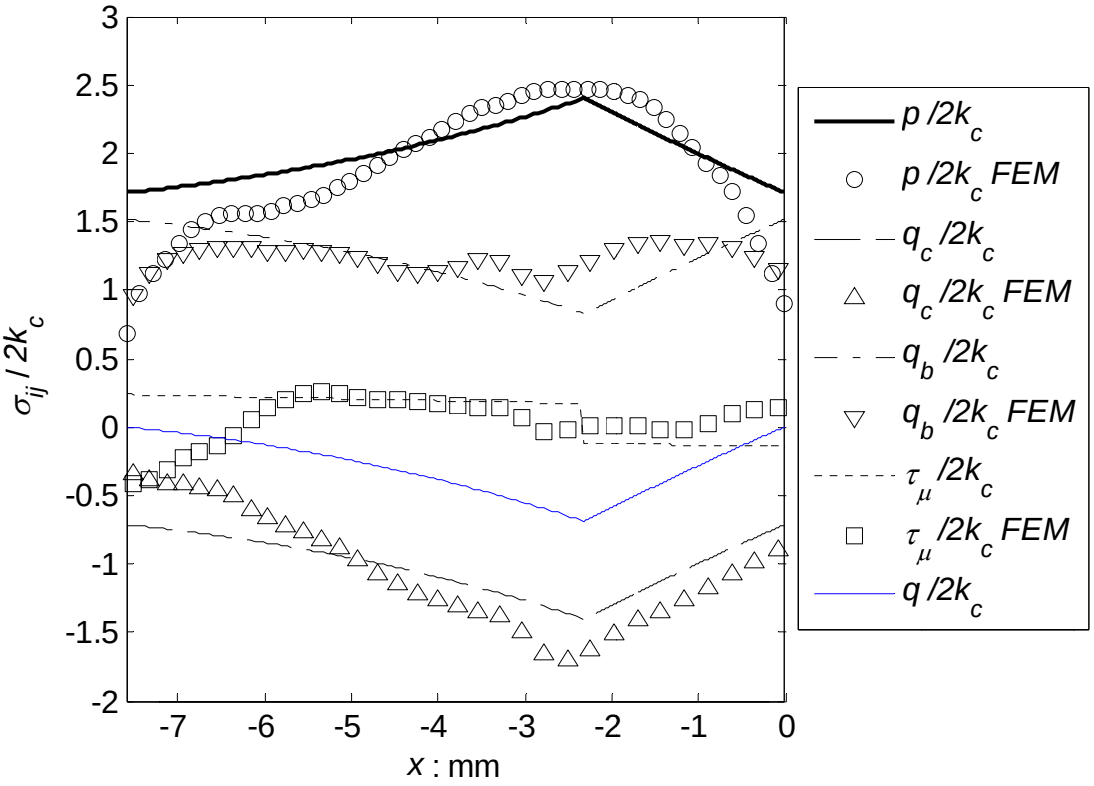

Figure 4.9 Comparison of stress state of Al/SST/Al sheet sandwich in roll gap during rolling process by slab analysis and FEA

4.6 Results

4.6.1 Aspect ratio of oxide fragments

The oxide film fracture model indicates that the aspect ratio of the oxide film fragment determined by Eq. (4.9) and (4.10) depends on the friction coefficient between contacting surfaces, the flow stress ratio of the substrate metal and its oxide film, and the flow stress ratio of the base and cladding sheets. The relevant kinetic friction coefficients provided by [112] are categorized in Table 4.2. Considering the oxide films on the Al 1100 and SST 304 sheets, the friction coefficient between the cladding and base sheets used here is 0.3. Passive oxide film can be easily formed on the surface of aluminum and stainless steel, and thus aluminum and stainless steel have good corrosion resistance. The thin oxide layer of aluminum is alumina Al_2O_3 and the passive oxide layer of stainless steel is usually composed of Fe_2O_3 in the top layer and Cr_2O_3 in the next layer contacting the metal substrate [113-116]. The flexure strength of Al_2O_3 [117] is 552MPa and the hardness is 15GPa. The accurate strength of the oxide film on metals is difficult to obtain experimentally. According to [118-120], the yield strength and hardness of most metals have linear relationship. Assuming the metal oxide follows the same correlation, the tensile strength of Cr_2O_3 and Fe_2O_3 are determined by correlating their strength and hardness. Based on the reported hardness of Cr_2O_3 film [121-123], the hardness of Cr_2O_3 film is taken as 25GPa. The hardness of Fe_2O_3 film is 18GPa [124]. So the tensile strength of Cr_2O_3 and Fe_2O_3 are determined to be 920MPa and 662MPa and the overall strength of oxide film of stainless steel takes the intermediate value 791MPa at room temperature. With those inputs, the aspect ratio of Alumina fragments

predicted by the oxide film fracture model is about 25 and that of SST oxide fragments is 10.

Table 4.2 Kinetic friction coefficient data

Material		**Kinetic friction coefficient**
Moving specimen	**Fixed specimen**	
Steel	Aluminum	0.25
Aluminum	Steel	0.38
Alumina	Aluminum	0.75
Alumina	Iron	0.45
Al_2O_3 sprayed coated surface	Stainless steel	0.13-0.3

Textor and Grauer [125] showed that the thickness of the oxide film on technically pure aluminum in air for 14 days is 2.2nm. The thickness of the oxide film on cold rolled aluminum foil is about 2.5-2.8nm while the oxide film thickness of foils annealed at 280-300^{o}C for 20-30 hours is about 4.0nm. Accordingly, the thickness of oxide film of aluminum sheet is assumed to be 2.5nm at room temperature [126]. The thickness of native oxide film on stainless steel is typically 1-3nm [127]. Nomura *et al.* [128, 129] reported that the thickness of oxide film on SST304 heated at 400^{o}C for one hour is 20nm. The thickness of the SST304 oxide film in a particular case will be interpolated from the above data.

4.6.2 Exposed metal extrusion and contact

The theoretical model integrating the oxide film fracture, the metal extrusion and the rolling of the metal sheet sandwich provides the slab stress state of the metal sheet sandwich in a bonding roll gap in Figure 4.10 and the exposed metal extrusion ratio through the crevice between the oxide fragments in Figure 4.11. In Figure 4.10, the left vertical dash line marks the position where the extruded aluminum through the oxide fragment crevice contacts the facing oxide surface of the base metal (SST 304) sheet, and the right vertical dash line marks the position where the extruded aluminum through the crevice between the oxide film fragments of stainless steel contacts the extruded stainless steel through the crevice between the oxide film fragments of stainless steel. The position marked by the right vertical dash line is actually the bonding point.

The metal extrusion versus the thickness reduction of the corresponding component sheets during the bond rolling process is illustrated in Figure 4.11. The thick solid curve shows that the aluminum extrudes through the aluminum oxide crevice and finally contacts the opposite oxide surface of the base metal SST 304 when the thickness reduction of the cladding metal sheet goes up to 7.85% (the overall thickness reduction of the sheet sandwich is 5.34% respectively). As shown in Figure 4.10, the deformation of the sheet sandwich enters zone II where the hard base metal yields and the oxide film of the base metal fractures. The dash line, the dash dot line and the thin solid line in Figure 4.11 illustrate the softer aluminum extrusion ratio, the harder stainless steel extrusion ration, and the total metal extrusion ratio through the oxide crevice of the hard

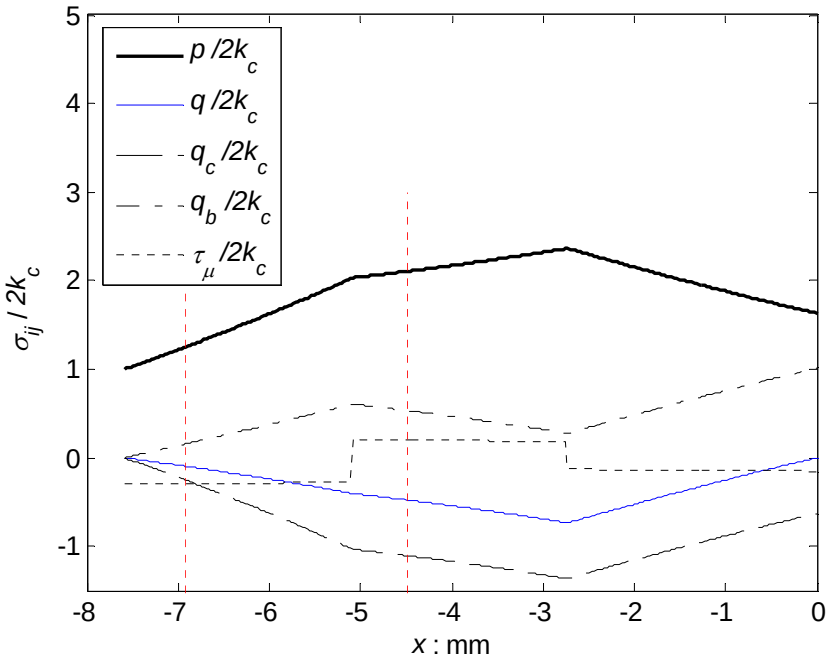

Figure 4.10 Slab stress state of Al/SST/Al sheet in bonding roll gap (overall thickness reduction r_t=30%)

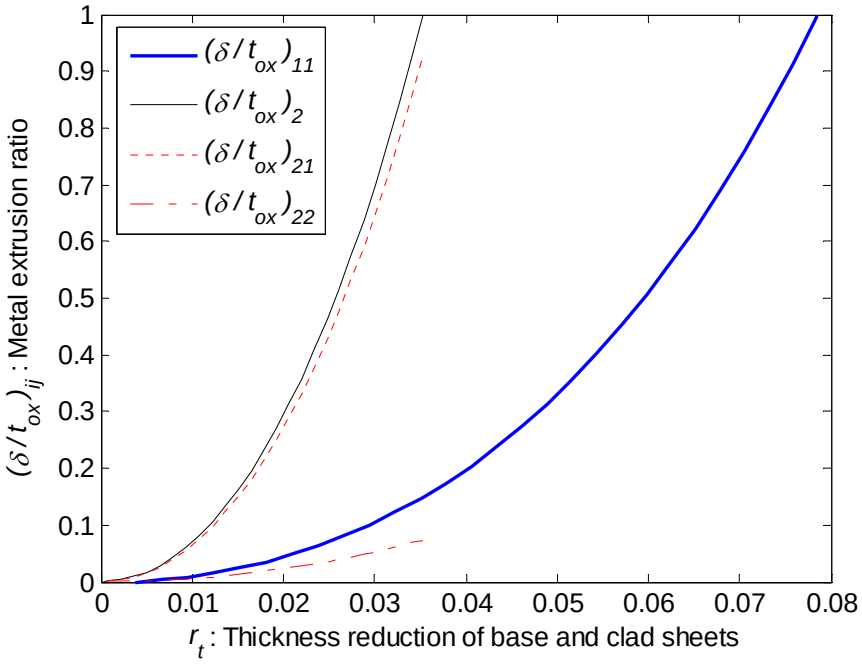

Figure 4.11 Exposed metal extrusion through the crevice between oxide film fragments

base metal (stainless steel) respectively. The computation result shows that the extruded aluminum contacts the extruded stainless steel when the thickness reduction of the stainless steel goes up to 3.54%. The overall thickness reduction is 19.57% respectively. This is a threshold thickness reduction for the extruded metals from component layers to contact and hence to bond to each other. Bay *et al.* [85] used experimentally determined threshold surface expansion (equivalent to the thickness reduction to describe the material deformation) as a constant for particular bonding couples in their numerical method. In our model, it shows that the threshold thickness reduction (or the surface expansion in Bay's model) for a particular bonding pair to contact each other through the cover layer cracks has dependency on the rolling thickness reduction, material properties, and friction conditions. The metal extrusion curves also demonstrate that the extruded stainless steel fills the 7.4% of the oxide crevice and the extruded aluminum fills the rest 92.6% of the oxide crevice. This result is reasonable considering the yield stress of aluminum is about one third of that of the stainless steel.

4.7 Discussions

In the proposed rolling mechanics model, the metal sheet sandwich in the roll gap is divided into four zones by the yielding of the hard base sheet, the contacting of the extruded metals, and the neutral point. In the analysis procedure, there is another characteristic point where the soft aluminum extrudes through the oxide fragment crevice and contacts the opposite surface. Those characteristic points actually divide the rolled metal sheet sandwich into five zones. The materials in different zones have

different interactive loadings due to different oxide film fracture conditions, metal extrusion state, harder metal yield state and the relative motion speed compared to the rolls. In order to understand the effect of the oxide film fracture state, the metal extrusion state, the harder metal yield state and the relative metal motion speed on the roll bonding state, relative extrusion-through length (RETL), relative yield length (RYL) for hard metal, relative contact length (RCL) for adjacent extruded metals, and relative reverse shear length (RRSL) are introduced. RETL is defined as the ratio of the distance from the point (where soft metal extrudes through its oxide fragment crevice and contact the opposite surface) to the exit over the contact length (L). By the similar definition, RYL=$|x_y|/L$; RCL=$|x_b|/L$; RRSL=$|x_n|/L$.

4.7.1 Effect of the overall thickness reduction ratio

The effect of the overall thickness reduction ratio on the stress state of the metal sheet sandwich during a steady roll bonding process is depicted in Figure 4.12. It is obvious that the contact length of the metal sheet sandwich with the rolls increases as the overall thickness reduction ratio increases. In Figure 4.12-(a), it can be seen that more thickness reduction ratio requires more rolling pressure to squeeze and bond the metal sheets. The shear stress (or the friction) between the base and cladding sheets is not significantly affected as the overall thickness reduction increases. In Figure 4.12-(b), it can be observed that more thickness reduction ratio causes less horizontal tensile stress on the base sheet but more compressive stress on the cladding sheet.

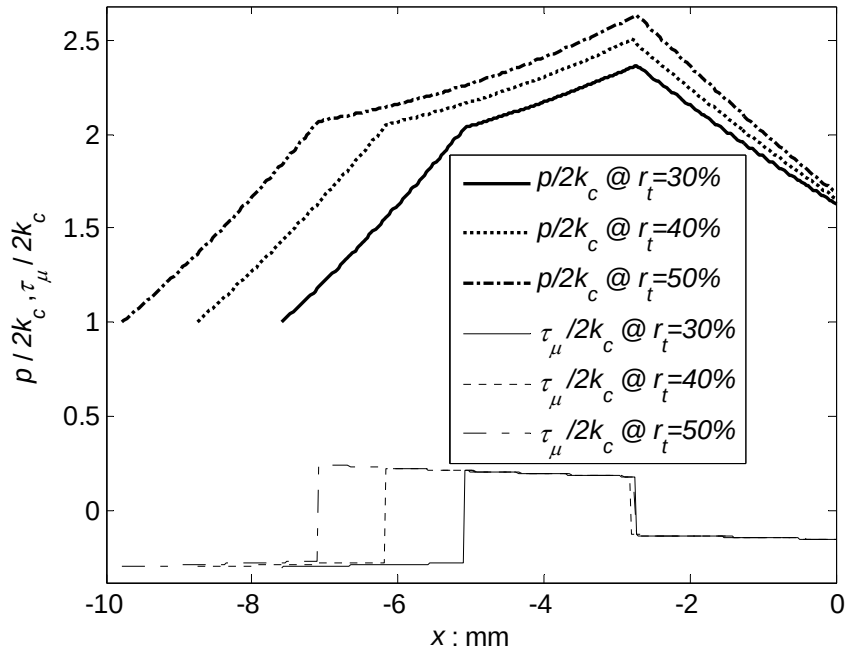

(a) Vertical pressure in metal sheet sandwich and shear stress between base and clad sheets

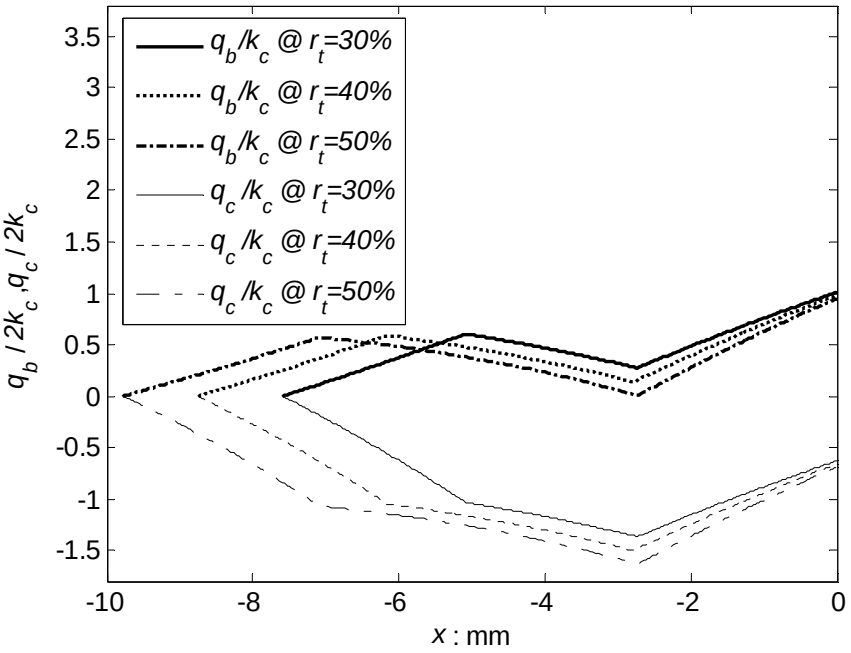

(b) Horizontal stress on base and clad sheets

Figure 4.12 Slab stress state of metal sheet sandwich in roll gap by overall thickness reductions 30%, 40%, and 50%

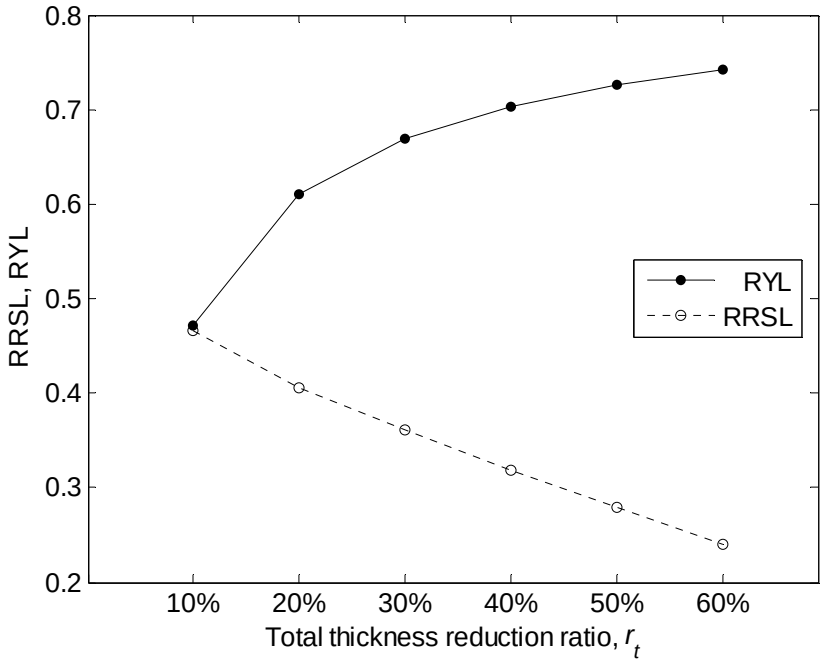

Figure 4.13 The dependence of RYL and RRSL on total thickness reduction

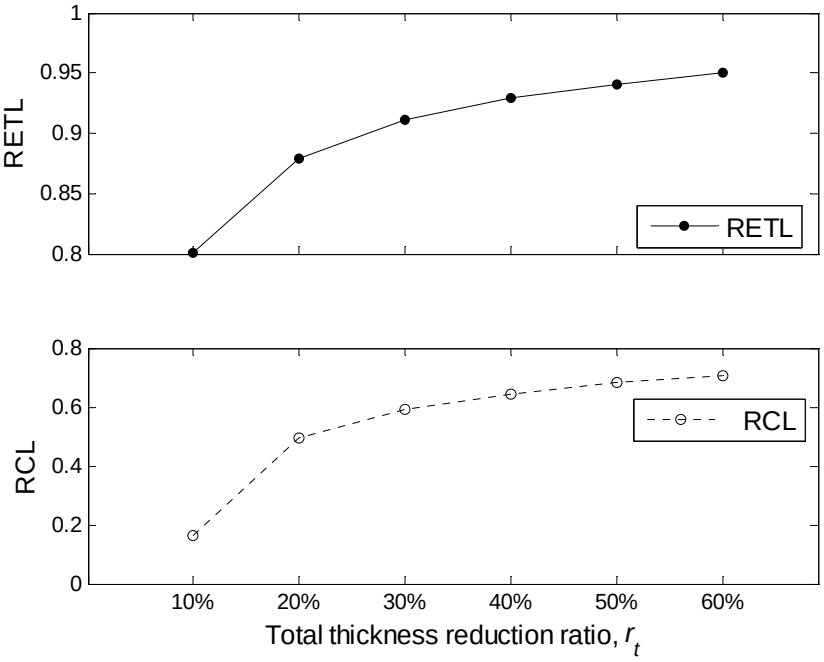

Figure 4.14 The dependence of RETL and RCL on total thickness reduction

The effect of the overall thickness reduction ratio on those characteristic relative lengths is illustrated in Figure 4.13 and Figure 4.14. It can be observed that RETL, RYL, and RCL increase and the increasing rate decreases as the rolling thickness reduction increases. RRSL decreases with the increase of the rolling thickness reduction. As shown in Figure 4.13, RYL curve and RRSL curve would intersect approximately at the overall thickness reduction 10% as the RYL decreases and RRSL increases with the decrease of the overall thickness reduction ratio. It indicates the harder metal sheet will not yield before the neutral point if the overall thickness reduction ratio is lower than 10%. Since the rolling pressure decreases after the neutral point, it indicates that the harder metal sheet does not yield during the rolling process and hence the atomic metal bond will not occur. Therefore, the intersection point of RYL and RRSL curves versus the overall thickness reduction actually identifies the minimum thickness reduction to provide necessary condition for the atomic metal bond. In Figure 4.14, it can be seen that RCL increases with more overall thickness reduction ratio. Since the atomic metal bonding occurs in RCL area, the larger RCL is preferred in the roll bonding process of the metal sheet sandwich.

4.7.2 Effect of the initial component sheets' thickness ratio

In practical applications, the component layers of the metal sheet sandwich could have various thicknesses upon their functionality and cost control. In a roll bonding process, the thickness ratio of a component layer to the total structure will influence the stress and bonding state of the metal sheet sandwich. The effect of the initial soft metal

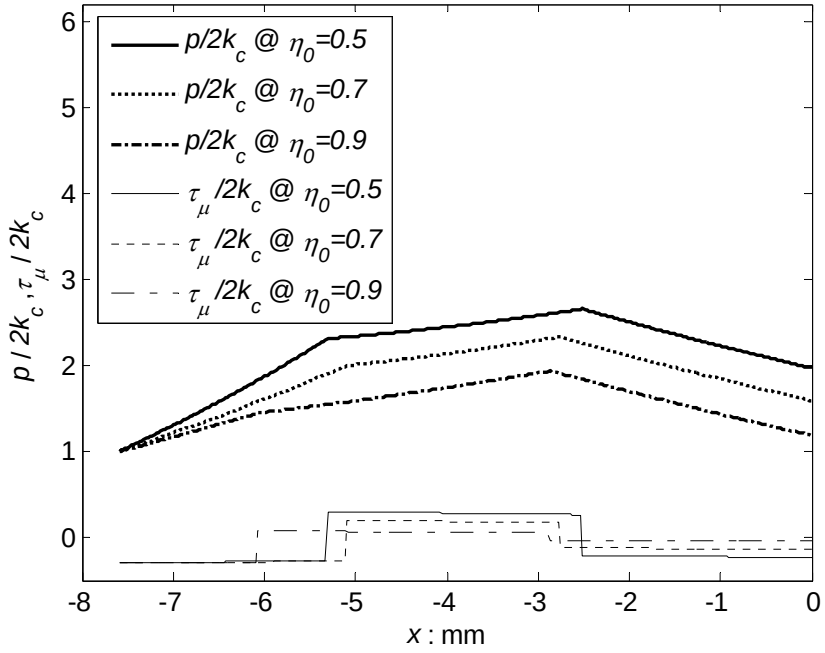

(a) Vertical pressure in metal sheets and shear stress between base and clad sheets

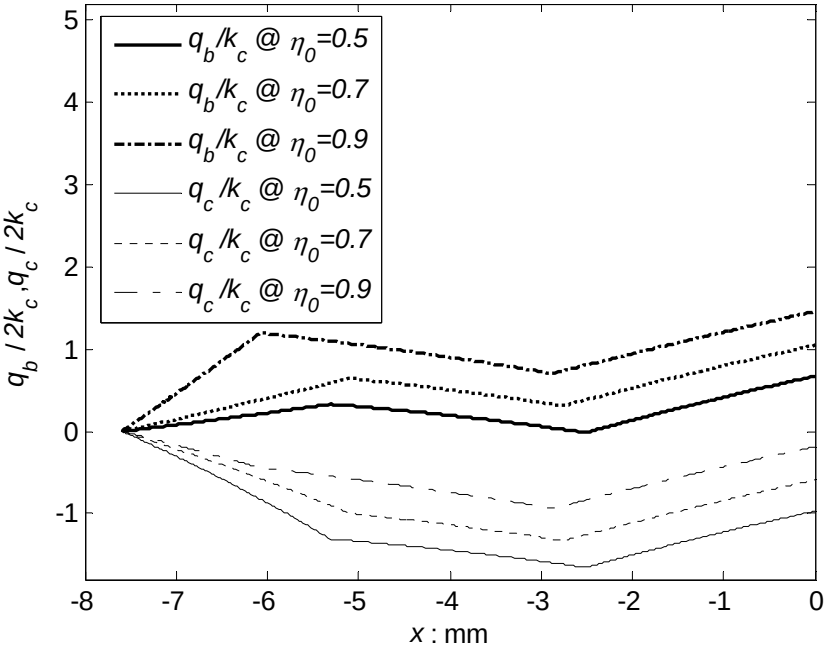

(b) Horizontal stress on base and clad sheets

Figure 4.15 Slab stress state of metal sheet sandwich in roll gap by clad metal thickness ratios 0.5, 0.7, and 0.9

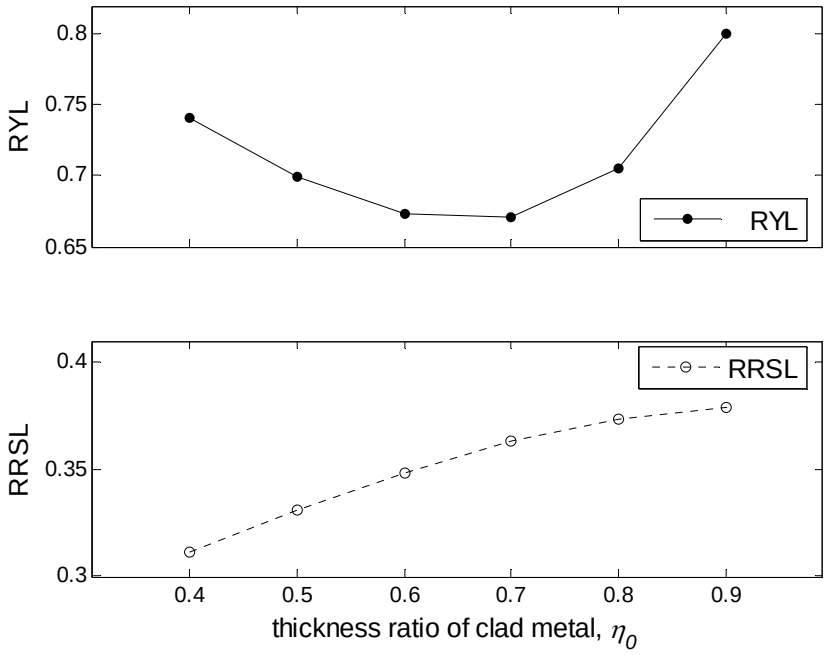

Figure 4.16 The dependence of RYL and RRSL on thickness ratio of clad metal

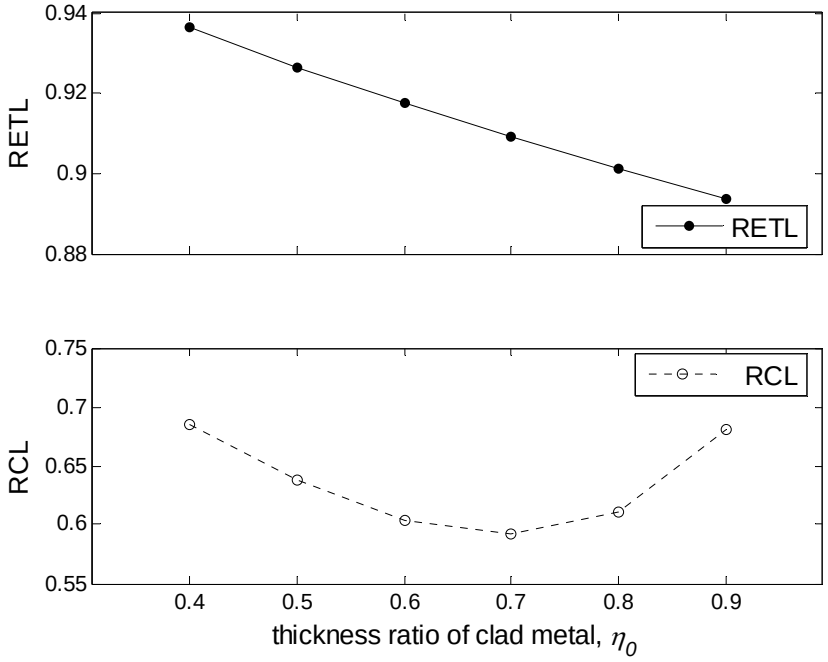

Figure 4.17 The dependence of RETL and RCL on thickness ratio of clad metal

thickness ratio on the slab stress state and the characteristic relative lengths is analyzed through the proposed model and is illustrated in Figure 4.15-Figure 4.17. It could be expected that more thickness ratio of the soft layer in the sandwich structure will cause less rolling force and hence less pressure on the rolling specimen. Figure 4.15-(a) quantitatively shows how the pressure on the component sheets and the shear stress at the interface are reduced by increasing the thickness of the soft layers. It can also be observed, in Figure 4.15-(a), that the horizontal stress on the component sheets is increased as the soft layer thickness ratio increases. Figure 4.16 shows that the yielding of the hard sheet occurs later in the rolling process until the soft layer thickness ratio goes up to 0.7. When the soft layer thickness ratio is greater than 0.7, the yielding position of the hard sheet gets closer to the entrance. The RRSL curve shows that the neutral point moves closer to the entrance as the soft layer thickness increases but the change is insignificant.

Figure 4.17 shows that the RETL almost linearly decreases as the soft layer thickness ratio increases. It means the position where the exposed soft aluminum contact the hard sheet surface becomes farther from the entrance with the higher thickness ratio of soft sheets. The reason is that the pressure driving exposed metal extrusion through oxide crevice is reduced as shown in Figure 4.15-(a). It can also be seen in Figure 4.17 that the RCL decreases first and then increases as the soft layer thickness ratio increases. The minimum RCL is achieved when soft layer thickness ratio is around 0.7.

4.7.3 Effect of the roll radius

With the constant initial thickness of metal sheets and thickness reduction in the roll bonding process, roll radius will determine the contact length. It can be expected that the contact length will increase with larger rolls. The stress state and hence the bonding state will also be influenced. The effect of the roll radius on the roll bonding of the metal sheet sandwich is analyzed by the proposed model using three rolls with different roll radii. Results are provided in Figure 4.18-Figure 4.20. It can be observed in Figure 4.18 that the pressure is increased by using larger rolls while the horizontal stresses on component sheets are decreased. Although the shear stress at interface does not change significantly, the yielding of the hard sheet occurs at different RYL and the neutral point changes position. As shown in Figure 4.19 and Figure 4.20, RYL, RRSL, RETL, and RCL are all increased by using larger rolls, and RETL is slightly changed. It indicates that, even though the larger roll radius-to-sandwich thickness ratio increases the rolling pressure (and hence rolling force), it promotes bonding state by increasing RYL and RCL. In addition, the increased contact length will make plastic deformation of the metal sheets smoother and hence prevent the rolled metals from cracking in the roll bonding process.

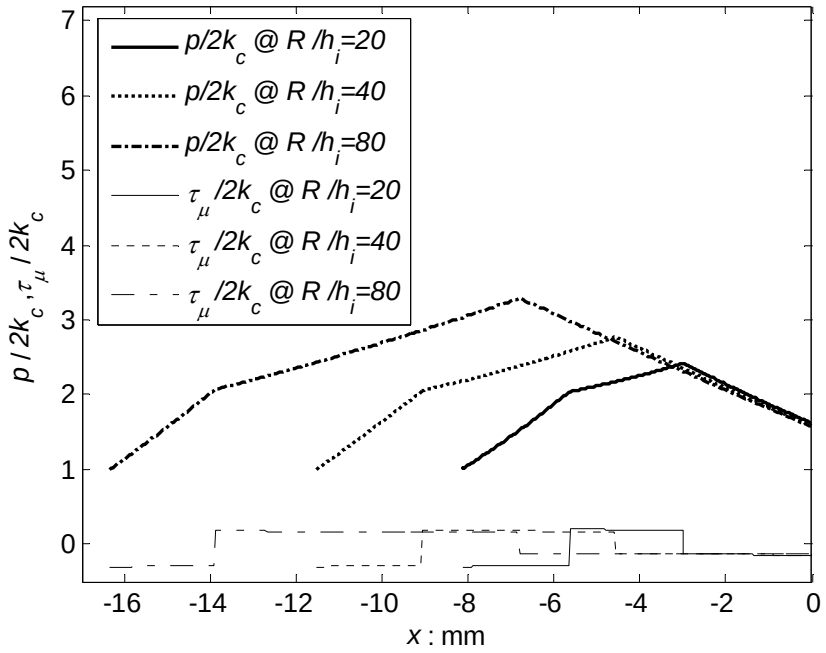

(a) Vertical pressure in metal sheets and shear stress between base and clad sheets

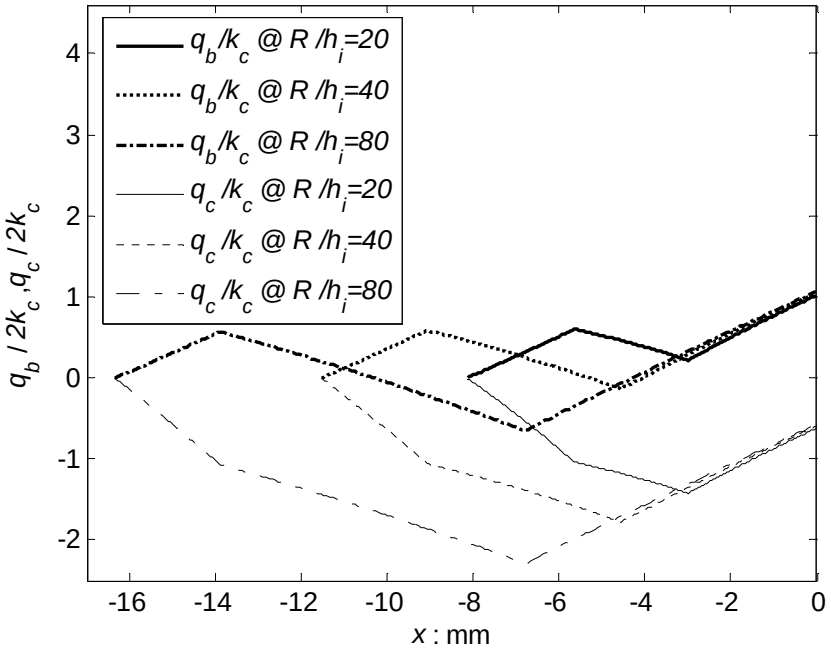

(b) Horizontal stress on base and clad sheets

Figure 4.18 Slab stress state of metal sheet sandwich in roll gap at R/h_i=20, 40, and 80

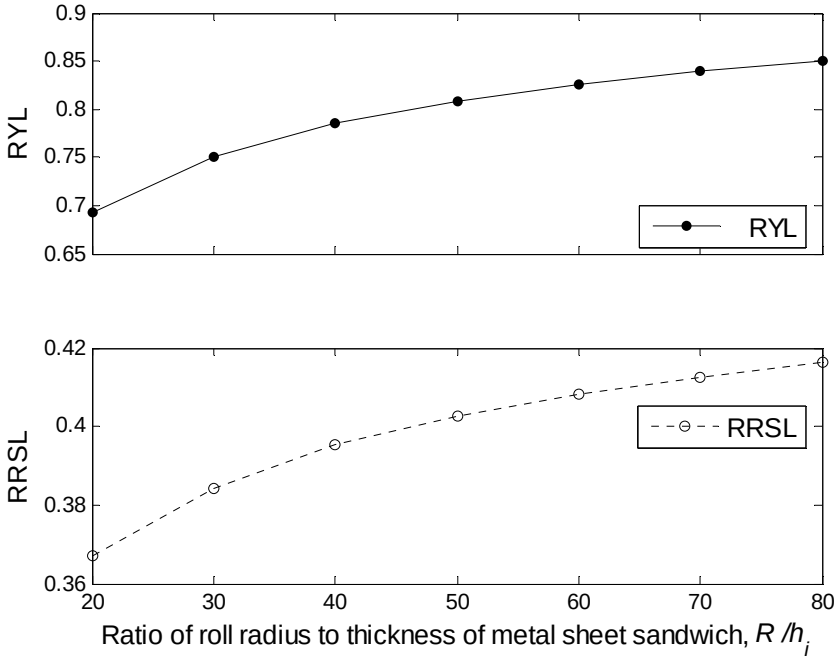

Figure 4.19 The dependence of RYL and RRSL on R/h_i

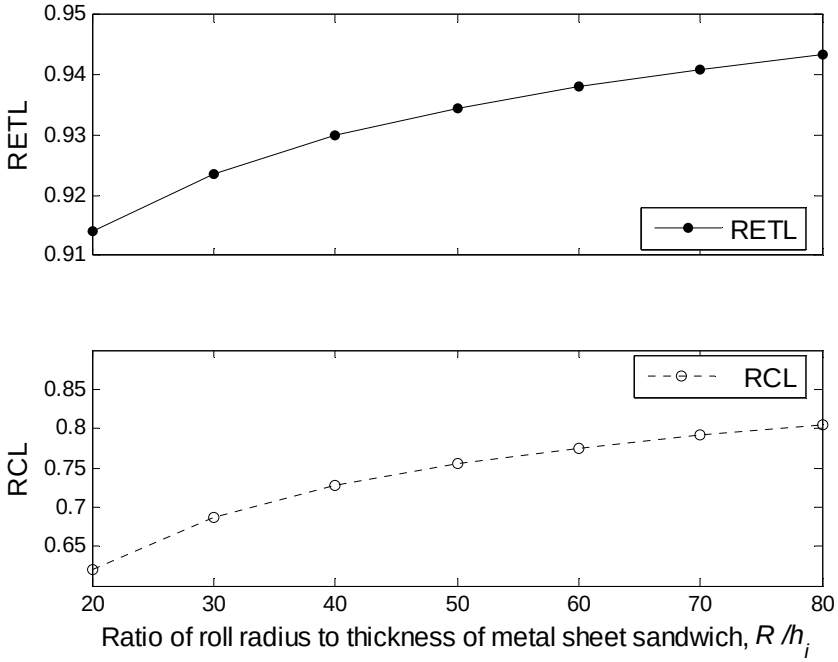

Figure 4.20 The dependence of RETL and RCL on R/h_i

4.7.4 Effect of flow stress mismatch of component layers

The flow stress mismatch of component layers in a metal sheet sandwich is characterized by the flow stress ratio of the hard metal to the soft metal. For example, in the previous sections, the hard metal layer is stainless steel and the soft metal layer is aluminum. The flow stress ratio is assumed to be constant 2.64 for analytical simplification. In order to analyze the feasibility of the roll bonding of various metal sheets, various flow stress ratio is considered in the analytical model. The effect of flow stress ratio on the slab stress state and the bonding state is depicted in Figure 4.21-Figure 4.23. Since the stress result is normalized by the soft sheet's flow stress, the higher flow stress ratio means the higher flow stress of the hard sheet. As shown in Figure 4.21, the rolling pressure increases as the flow stress ratio increases. The horizontal stress on the hard sheet becomes greater tensile stress while the horizontal stress on the soft sheets becomes larger compressive stress as the flow stress ratio increases. It can be seen in Figure 4.22 and Figure 4.23 that the RYL, RRSL and RCL are reduced by increasing flow stress ratio. This is because the increase of flow stress of the hard sheet will require more pressure to make hard sheet yield and extrude to contact the other metal. Since the soft metal usually extrudes through the crevice between its oxide film fragments and contacts the hard sheet surface before hard sheet yields, the increase of flow stress of hard sheet does not affect the RETL, as shown in Figure 4.23.

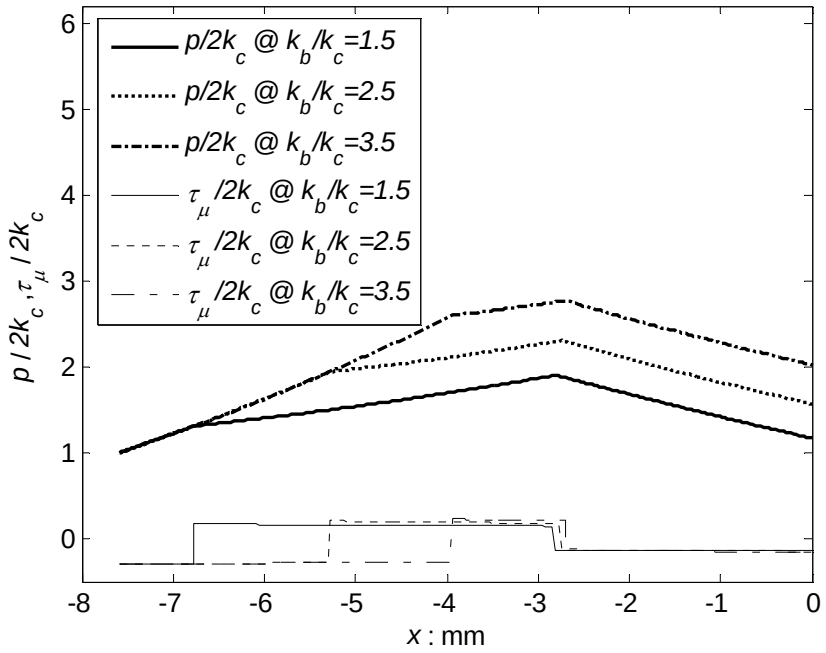

(a) Vertical pressure in metal sheets and shear stress between base and clad sheets

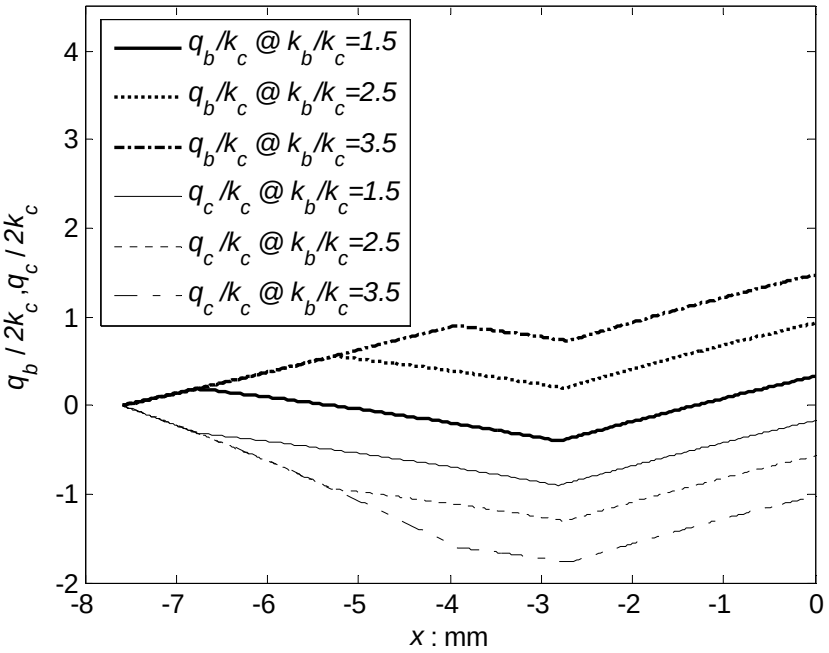

(b) Horizontal stress on base and clad sheets

Figure 4.21 Slab stress state of metal sheets in roll gap at k_b/k_c=1.5, 2.5, and 3.5

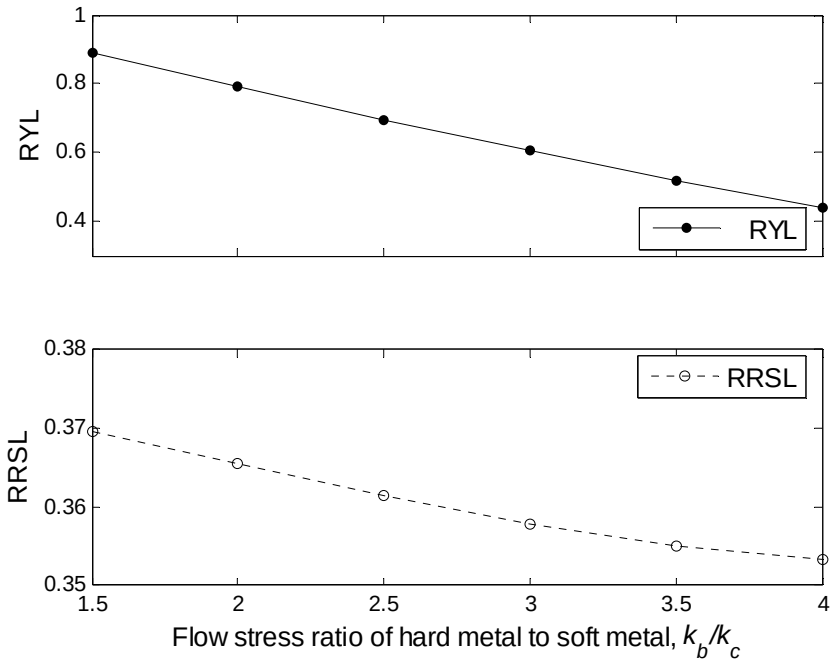

Figure 4.22 The dependence of RYL and RRSL on k_b/k_c

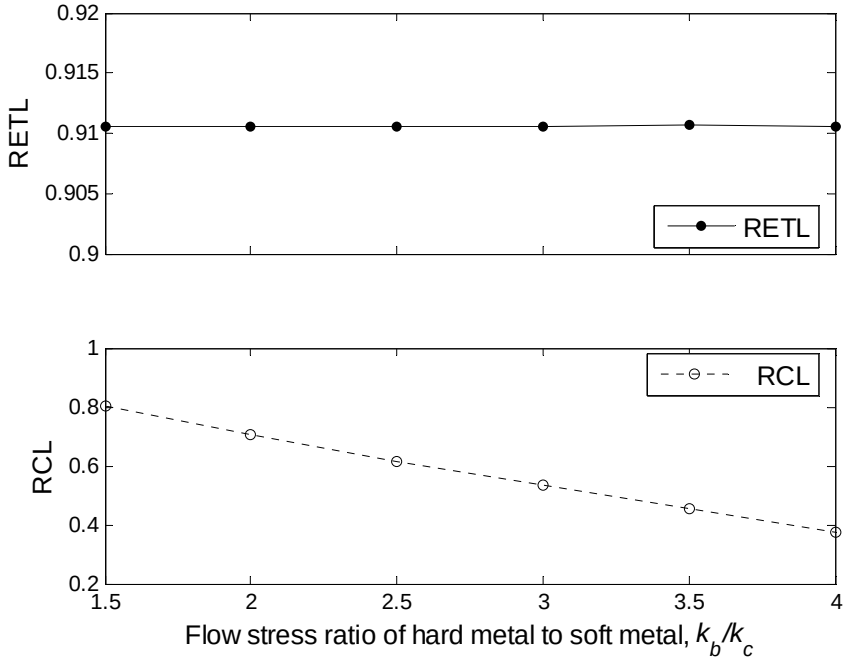

Figure 4.23 The dependence of RETL and RCL on k_b/k_c

4.7.5 Effect of the friction condition

Because the loading condition in a roll bonding process usually leads to the plastic deformation of the contacting surfaces, the frictions between the rolls and the cladding sheets as well as between the base and cladding sheets are defined by Eq. (4.30)-(4.33). It needs to be noted that the friction coefficients used in Eq. (4.32) and (4.33) are not coefficient of Coulomb friction. The coefficients of friction (COF) μ_{rc} and μ_{bc} used here relate the shear stress between contacting surfaces to the pure shear yielding stress of the softer material. The effect of the friction condition between the base and cladding sheets on the slab stress state and the bonding state of metal sheet sandwich is illustrated in Figure 4.24-Figure 4.26, when the COF μ_{rc} is fixed at constant 0.9. Similarly, the effect of the friction condition between the rolls and the cladding sheets is illustrated in Figure 4.27-Figure 4.29, when the COF μ_{bc} is fixed at constant 0.6.

In Figure 4.24, the results show that the COF between the base and cladding sheets seriously affects the slab stress before the yielding point of the hard metal sheet while slightly changes the stress after the yielding point of the hard metal sheet. Greater COF between the base and cladding sheets leads to higher rolling pressure on the specimen before the yielding point of the hard metal. It also causes higher horizontal tensile stress on the base sheet and higher compressive stress on the cladding sheets before the yielding point of the hard metal sheet. As the COF between the base and cladding sheets increases, the yielding point of hard metal sheet becomes obviously closer to the entrance while the neutral point does not change significantly. This effect can also be observed in Figure 4.25 and Figure 4.26. RYL and RCL are increased significantly with

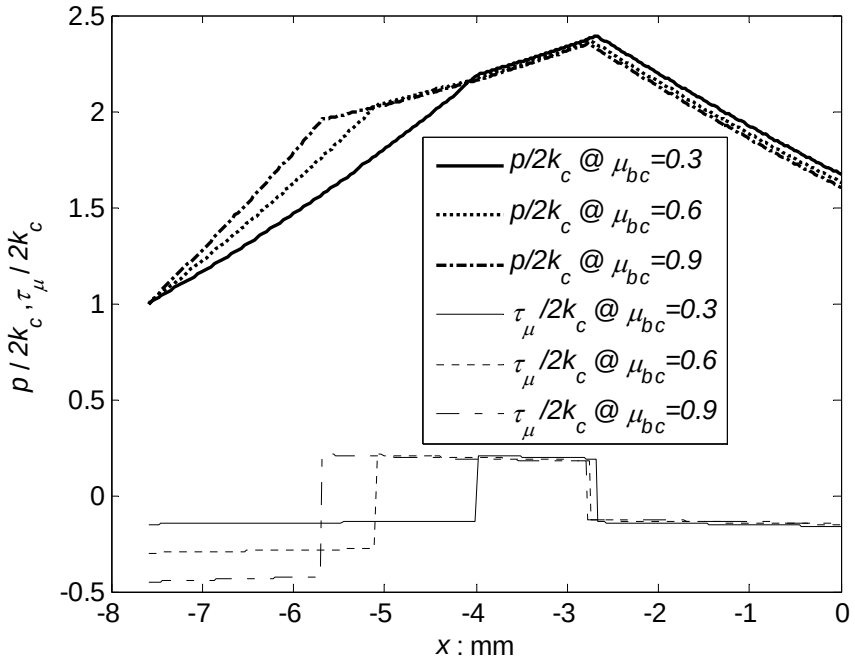

(a) Vertical pressure in metal sheets and shear stress between base and clad sheets

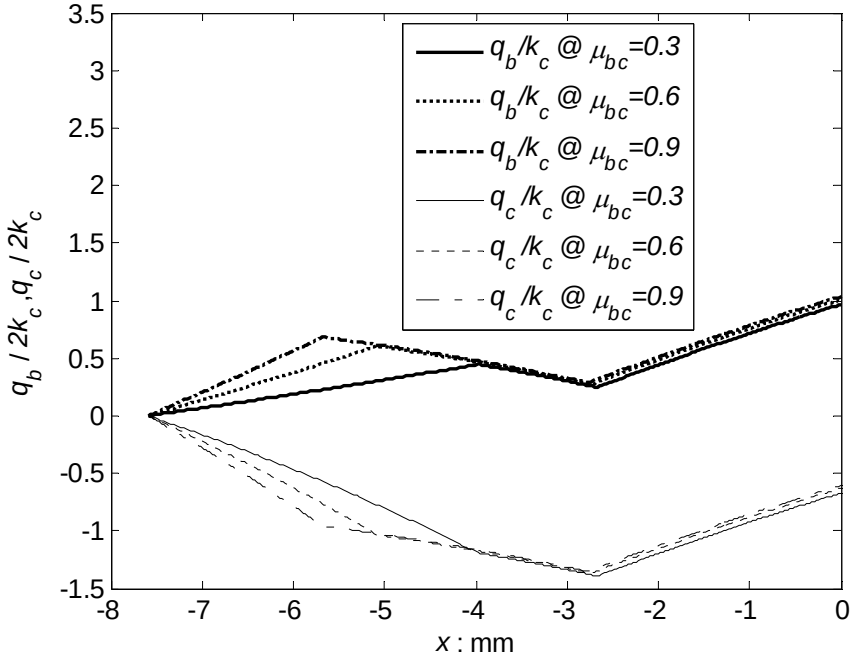

(b) Horizontal stress on base and clad sheets

Figure 4.24 Slab stress state of metal sheet sandwich in roll gap at μ_{bc}=0.3, 0.6, and 0.9 (μ_{rc}=0.9 is fixed)

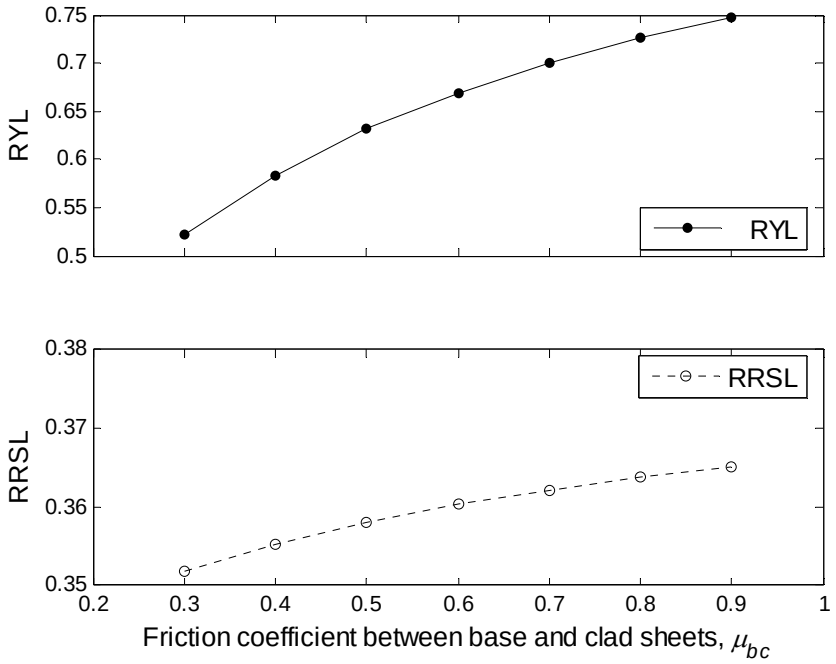

Figure 4.25 The dependence of RYL and RRSL on μ_{bc} (μ_{rc}=0.9 is fixed)

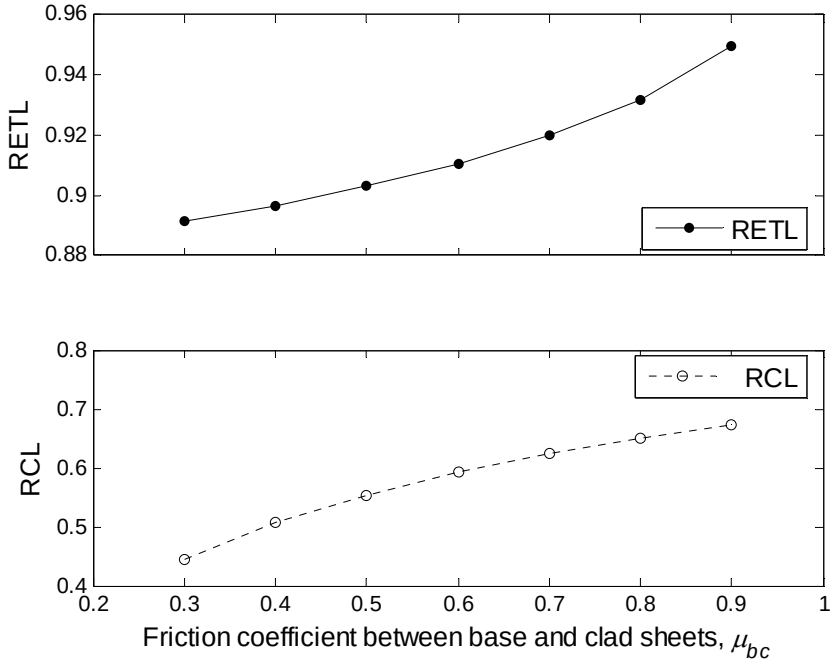

Figure 4.26 The dependence of RETL and RCL on μ_{bc} (μ_{rc}=0.9 is fixed)

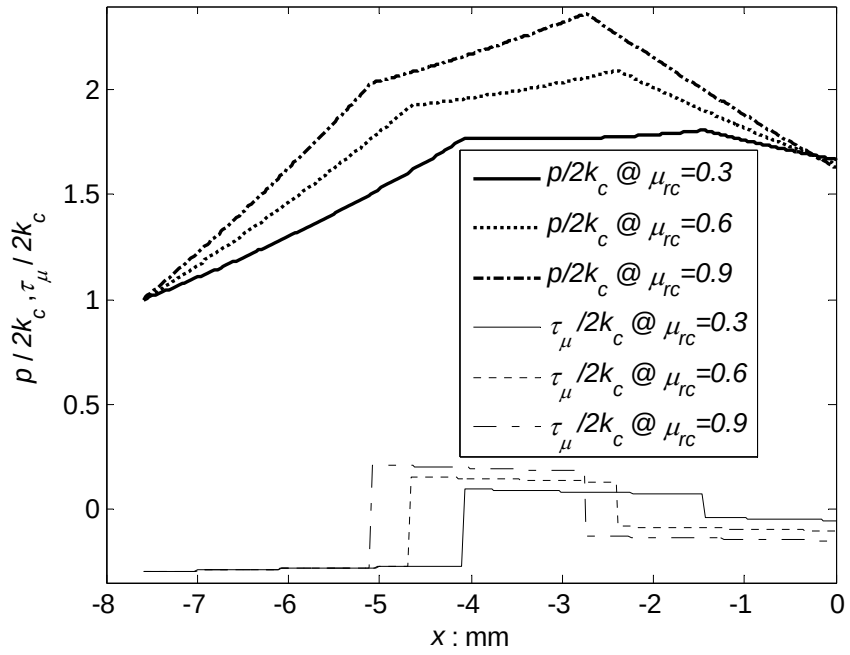

(a) Vertical pressure in metal sheets and shear stress between base and clad sheets

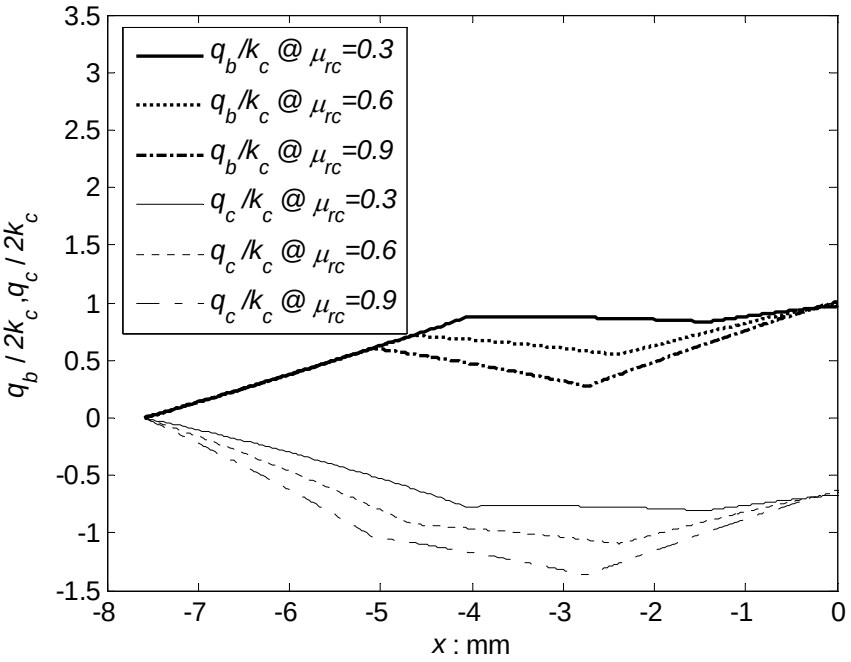

(b) Horizontal stress on base and clad sheets

Figure 4.27 Slab stress state of metal sheet sandwich in roll gap at μ_{rc}=0.3, 0.6, and 0.9 (μ_{bc}=0.6 is fixed)

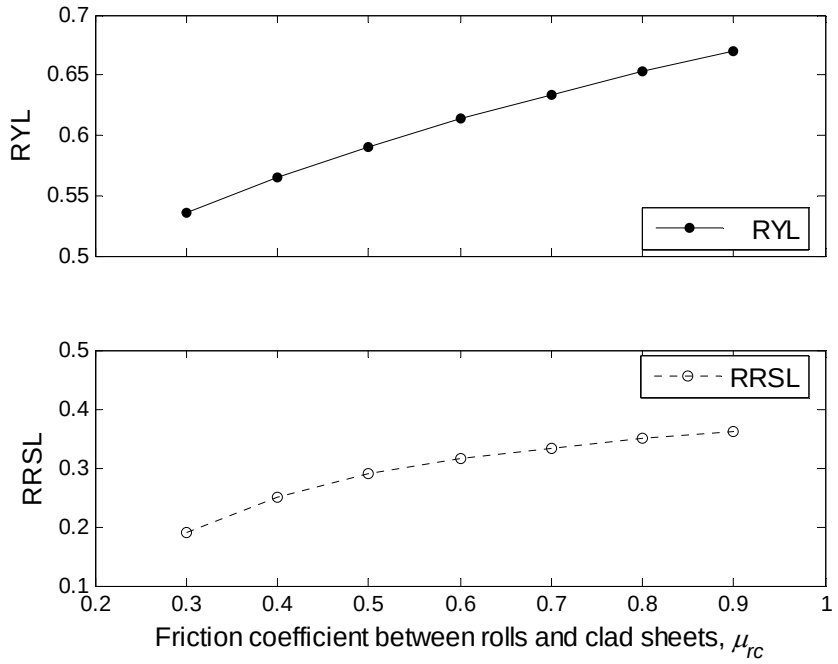

Figure 4.28 The dependence of RYL and RRSL on μ_{rc} (μ_{bc}=0.6 is fixed)

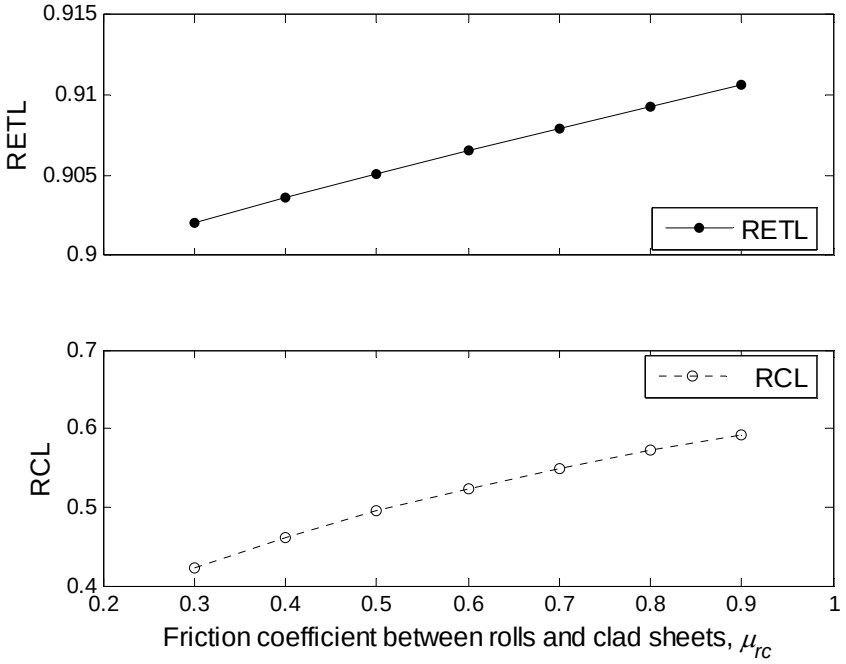

Figure 4.29 The dependence of RETL and RCL on μ_{rc} (μ_{bc}=0.6 is fixed)

greater COF between the base and cladding sheets while RRSL and RETL are only slightly increased. Those results can be easily understood since the COF only has effect on the interactive loading when the contacting pair of metal sheets has relative motion to each other before the hard metal yields.

As shown in Figure 4.27, the COF between the rolls and the cladding sheets influences the slab stress state of the metal sheet sandwich through all the contacting length. The rolling pressure on the specimen and the friction or shear stress at the interface are increased through higher COF between the rolls and cladding sheets, while the horizontal stress on the base and cladding sheets are decreased. It can be observed in Figure 4.28 and Figure 4.29 that RYL, RRSL, and RCL are increased by higher COF between the rolls and cladding sheets. Since the soft metal sheets always yield in the roll gap, the increase of COF between rolls and clad sheets don't have significant effect on RETL, as shown in Figure 4.29.

Considering the necessary plastic deformation to activate the roll bonding of metal sheets, the effect analysis of the friction conditions indicates that the increase of COF both between component layers and between the rolls and the cladding sheets will promote the roll bonding of metal sheet sandwich. The increase of COF between the base and cladding sheets slightly increases the rolling force while the increase of COF between rolls and clad sheets will significantly increase the requirement of the rolling force and hence the rolling power.

4.7.6 End tension effect

In the proposed model, the end-tensions are applied as q_{ic} and q_{ib} at the input end, as well as q_o at the exit end, as shown in Figure 4.1. The effect of the pull-back tension on the input end of the soft clad sheet is illustrated in Figure 4.30-Figure 4.32. It can be observed that, as q_{ic} increases, the vertical pressure on specimen is reduced before neutral point while the horizontal stresses on the base and cladding sheets are increased. The stress state after the neutral point is not affected significantly. From Figure 4.31 and Figure 4.32, it can be seen that all of the RYL, RRSL, RETL, and RCL are reduced with more end-tension on the soft cladding sheets at the entrance. The end-tension q_{ic} makes clad sheets yield more easily. Thus it actually has equivalent effect as the increase of the flow stress mismatch between the hard base sheet and the soft cladding sheets. Therefore, the end-tension q_{ic} on the soft cladding sheets makes the roll bonding more difficult, which is not recommended for the roll bonding of the metal sheet sandwich. On the other hand, the end-tension q_{ib} on the hard base sheet at the entrance helps the base sheet to yield, which is equivalent to decrease the flow stress mismatch between the base and cladding sheets. The effect of the end-tension on the hard base sheet at entrance is illustrated in Figure 4.33-Figure 4.35. It could be expected that the pressure on the specimen is decreased, as shown in Figure 4.33. The horizontal stresses on the base and cladding sheets increase due to the end-tension loading q_{ib}. The stress state of the specimen is affected insignificantly by the end-tension q_{ib} on the base sheet, just as by the end-tension q_{ic}. Figure 4.32 and Figure 4.33 show that the RYL and RCL are increased by the end-tension q_{ib}. So the end-tension on the hard base sheet is preferred

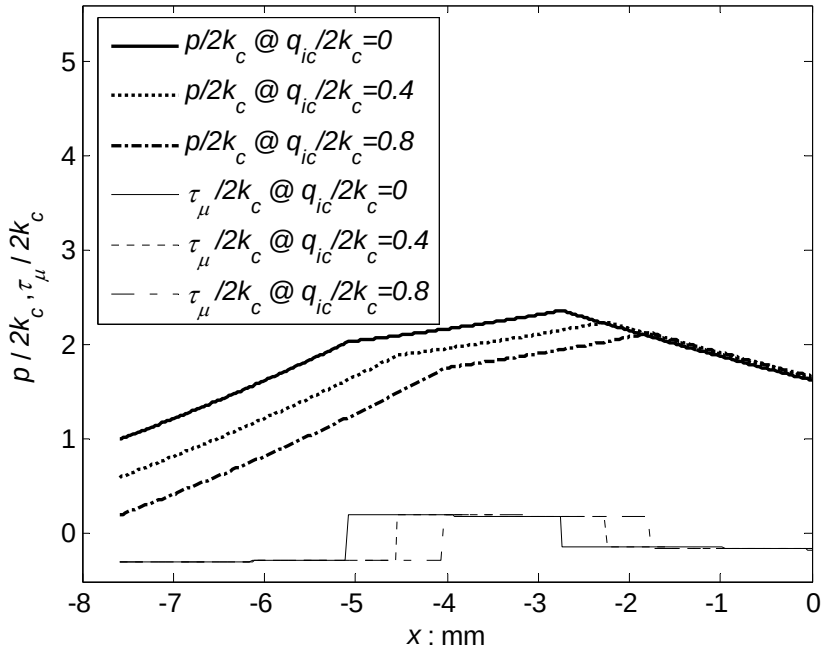

(a) Vertical pressure in metal sheets and shear stress between base and clad sheets

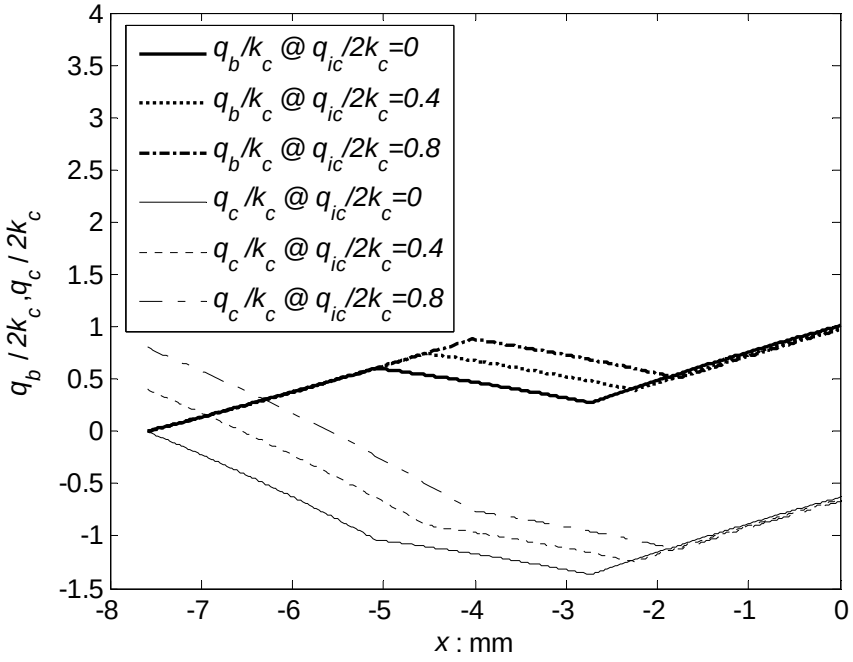

(b) Horizontal stress on base and clad sheets

Figure 4.30 Slab stress state of metal sheet sandwich in roll gap at $q_{ic}/2k_c$=0, 0.4, 0.8 ($q_{ib} = q_o = 0$)

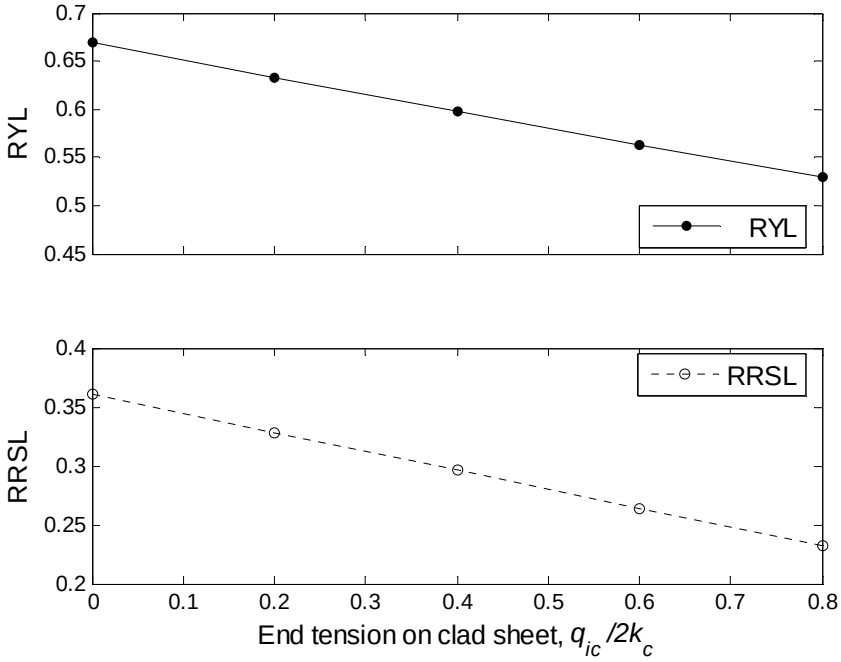

Figure 4.31 The dependence of RYL and RRSL on q_{ic} ($q_{ib} = q_o = 0$)

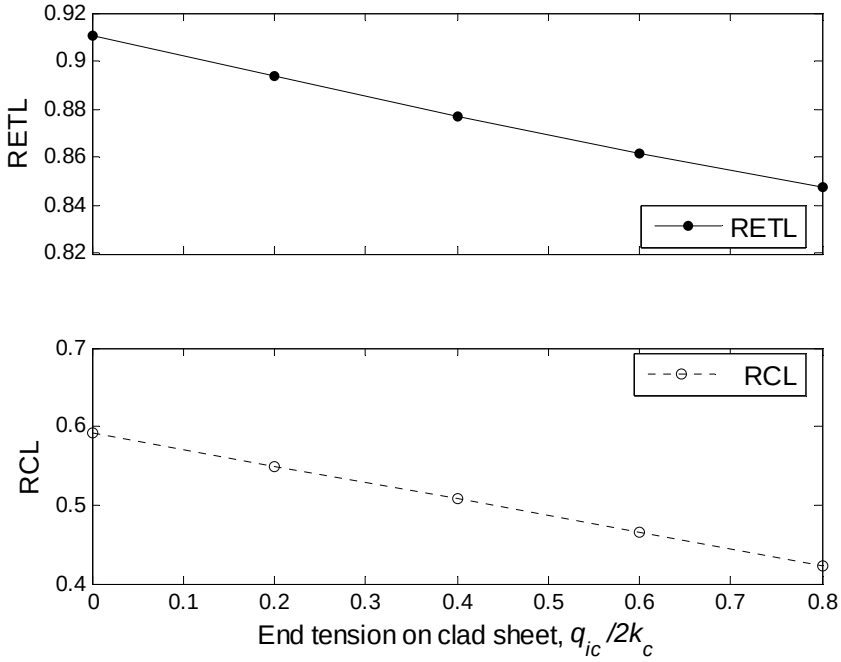

Figure 4.32 The dependence of RETL and RCL on q_{ic} ($q_{ib} = q_o = 0$)

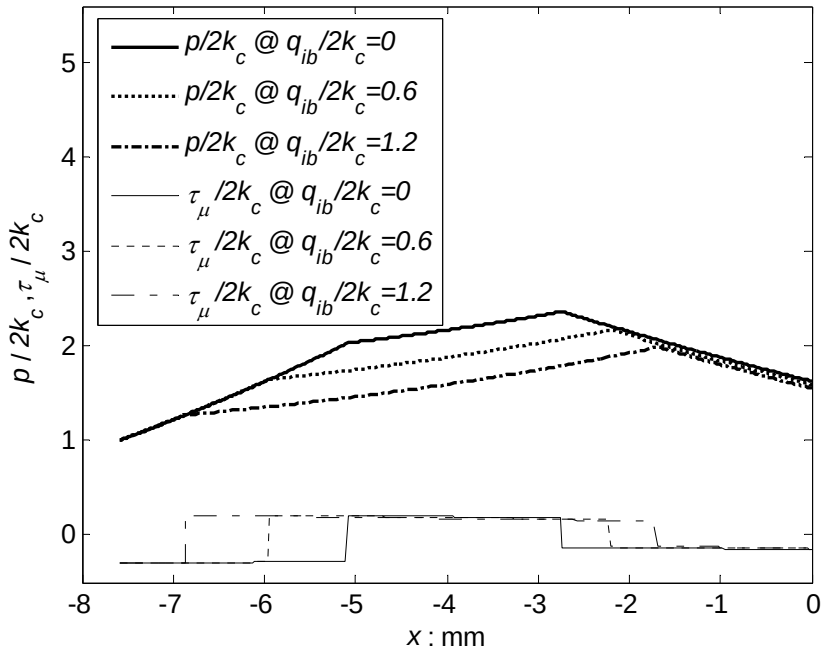

(a) Vertical pressure in metal sheets and shear stress between base and clad sheets

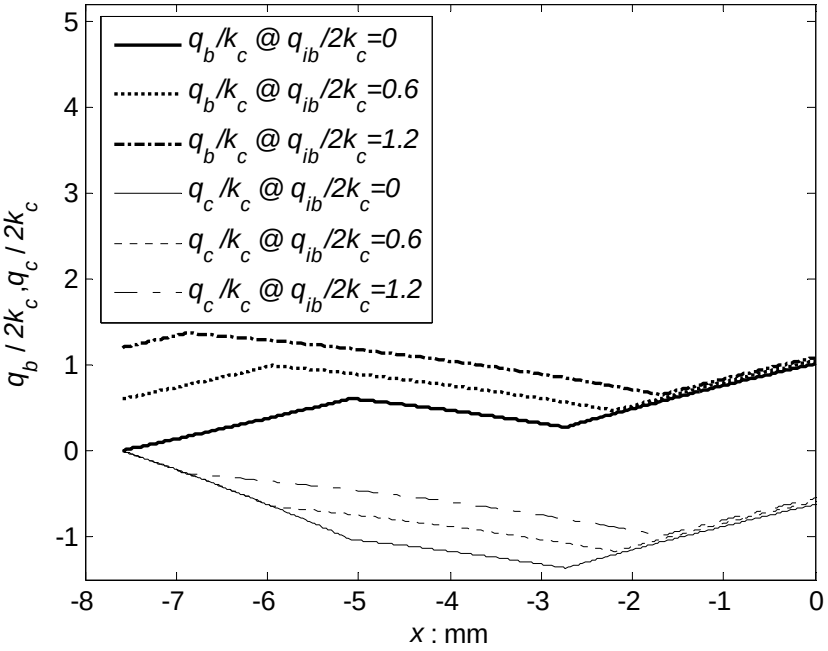

(b) Horizontal stress on base and clad sheets

Figure 4.33 Slab stress state of metal sheet sandwich in roll gap at $q_{ib}/2k_c$=0, 0.6, 1.2 ($q_{ic} = q_o = 0$)

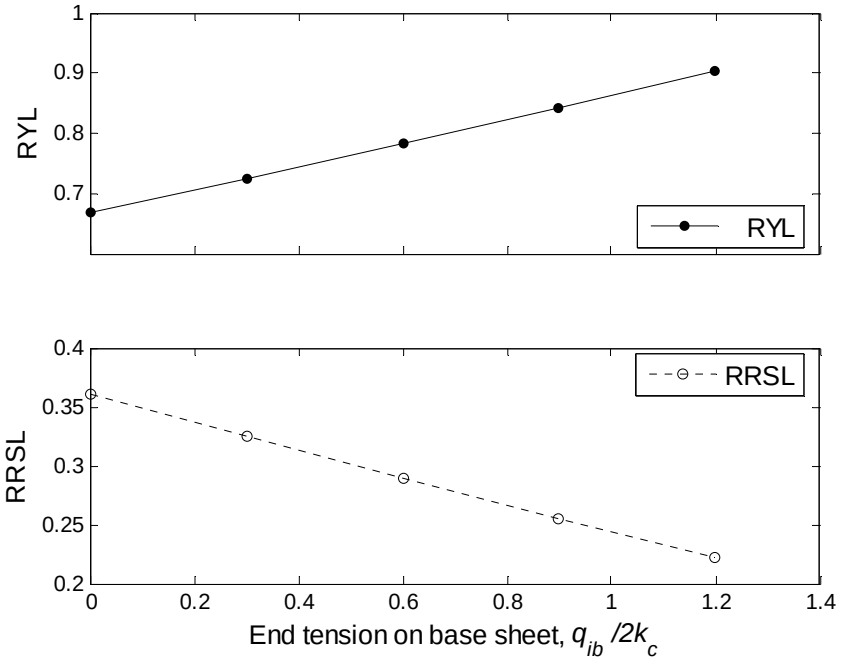

Figure 4.34 The dependence of RYL and RRSL on q_{ib} ($q_{ic} = q_o = 0$)

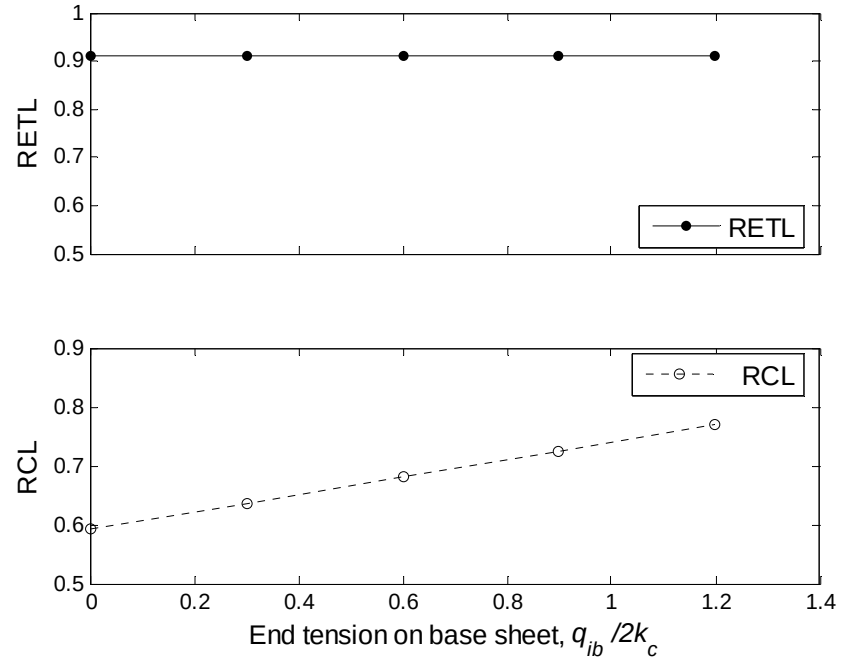

Figure 4.35 The dependence of RETL and RCL on q_{ib} ($q_{ic} = q_o = 0$)

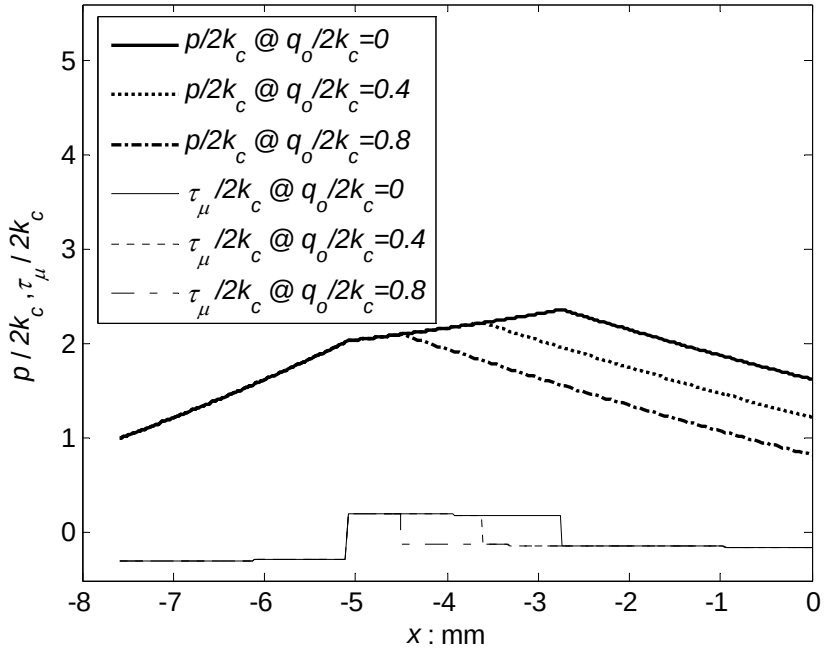

(a) Vertical pressure in metal sheets and shear stress between base and clad sheets

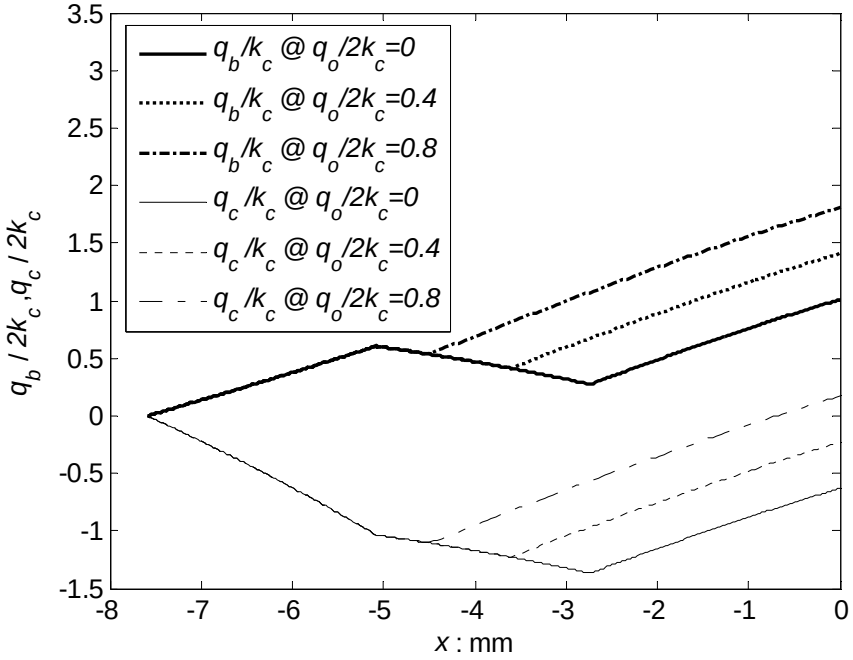

(b) Horizontal stress on base and clad sheets

Figure 4.36 Slab stress state of metal sheet sandwich in roll gap at $q_o /2k_c$=0, 0.4, 0.8 ($q_{ib} = q_{ic} = 0$)

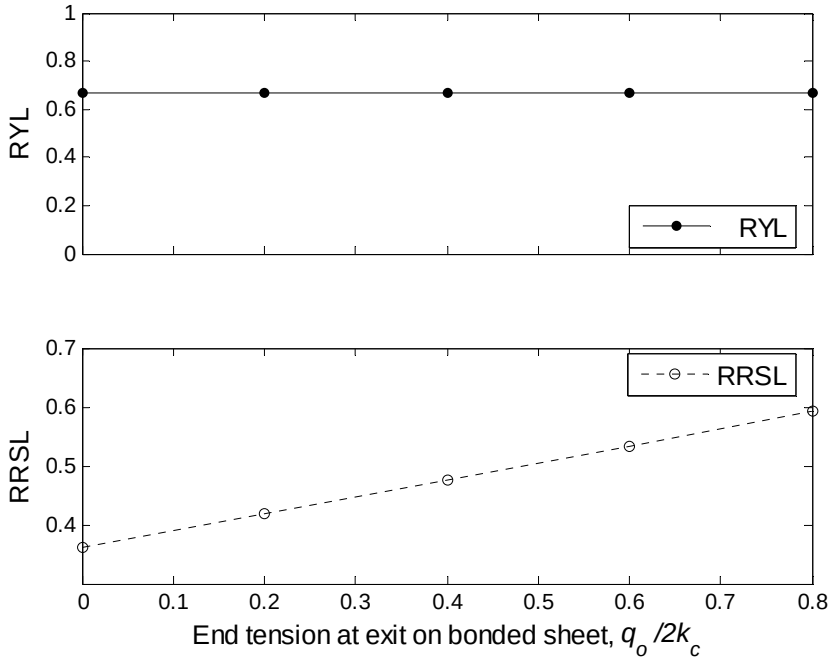

Figure 4.37 The dependence of RYL and RRSL on q_o ($q_{ib} = q_{ic} = 0$)

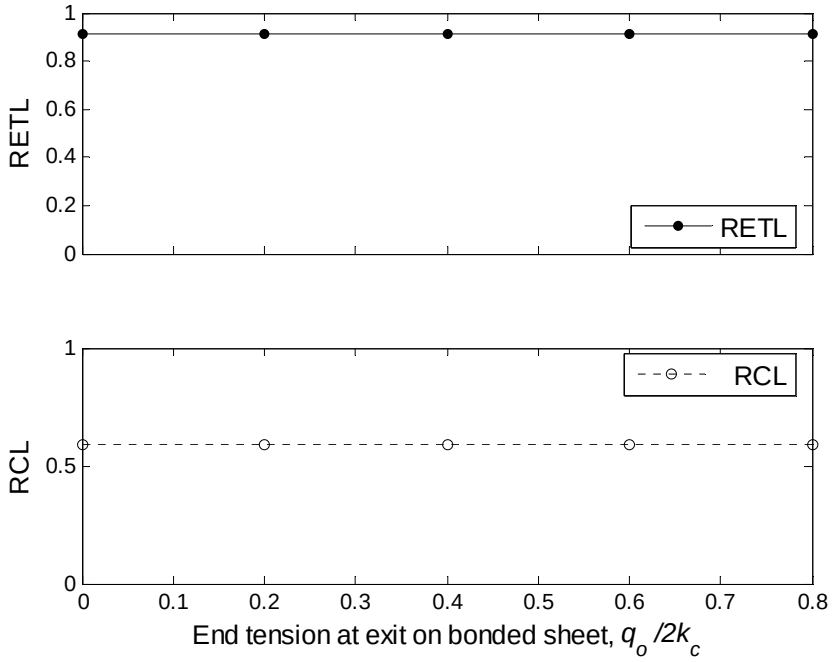

Figure 4.38 The dependence of RETL and RCL on q_o ($q_{ib} = q_{ic} = 0$)

for the roll bonding of the metal sheet sandwich.

The combined effect of the end-tensions on RYL can also be mathematically illustrated. Eq. (4.39) can be rearranged as:

$$2k_c f\left(x_y\right) = F\left(x_y\right) + \left(q_{ib} - q_{ic} - 2k_b\right) \tag{4.51}$$

where $F(x_y)$ is a function independent of q_{ib}, q_{ic}, and k_b.

It can be seen from Eq. (4.51) that the solution x_y of $f(x_y)$ =0 depends on the constant $\left(q_{ib} - q_{ic} - 2k_b\right)$. It indicates that the difference $\left(q_{ib} - q_{ic}\right)$ can counteract the increase of the flow stress of the hard base sheet k_b. Therefore, the end-tension can promote the roll bonding of dissimilar metal sheets as long as the end-tension on the hard base sheet is greater than those on the soft clad sheets.

The effect of the end-tension at the exit on the stress and bonding state of the metal sheet sandwich is illustrated in Figure 4.36-Figure 4.38. The results show that the end-tension at the exit only influences the stress state of metal sheets after the neutral point. The end-tension q_o at the exit reduces the rolling pressure on the specimen after the neutral point. It is obvious that the end-tension loading at the exit will increase the horizontal stress of metal sheets but the effect only occurs after the neutral point as shown in Figure 4.36. From Figure 4.37, it can be observed that the RRSL increases as the end-tension at the exit increases. It means the neutral point is moving farther from the exit. Since the soft metal extrusion through crevices, the yielding of the hard metal

sheet and the contacting of the extruded metals in this analysis occur before the neutral point, the end-tension at the exit does not affect RYL, RETL and RCL as shown in Figure 4.37 and Figure 4.38. However, the end-tension at the exit can be applied if the rolling power is limited when the roll bonding of dissimilar metal sheets is performed. In industrial, the end-tension either at the entrance or the exit to promote the roll bonding of metal sheets can be achieved by changing the input or output coiling velocity relative to the rolling velocity.

4.8 Summary

The fracture of the oxide film on the metal sheet's surface and the exposed metal extrusion through the crevice between oxide fragments in a rolling process were quantitatively evaluated. With the integration of the oxide film fracture and the exposed metal extrusion, a model based on the slab method was developed to describe the stress and bonding state of the metal sheet sandwich. The proposed analytical model was solidified by FEA of the metal sheet sandwich rolling. The analytical approach can quickly provide the stress and bonding information to help understand the roll bonding mechanism of clad metals. The effect of various rolling conditions, such as, thickness reduction ratio, the ratio of initial sheets' thickness, roll radius, the flow stress mismatch of component metal sheets, the friction coefficients between the rolls and the cladding sheets as well as between the base and cladding sheets, and the end-tensions on the stress state and bonding state of the metal sheet sandwich was investigated. Based on the analytical results, the following conclusions were reached.

Higher thickness reduction increases the relative bonding length and hence promote the roll bonding of metal sheets; The thicker soft cladding sheets are preferred to make more relative bonding length and less shear stress between the bonded base and cladding sheets; The larger rolls are also a positive factor to the roll bonding of a soft-hard-soft sheet sandwich. Flow stress mismatch of component layers increases the difficulty in the roll bonding of a metal sheet sandwich. Friction between the base and cladding sheets promotes the increase of the relative bonding length while the friction between the rolls and the cladding sheets reduces the relative bonding length and increase the shear stress between the bonded base and cladding sheets; Application of the end-tension on the hard base sheet can release the flow stress mismatch of the base and cladding sheets, therefore it is necessary to bond the base and cladding sheets, especially when the flow stress mismatch of the component layers is serious.

CHAPTER V

EXPERIMENTAL ESTIMATION OF DIFFUSIVITY

In the roll bonding process of clad metals, the mechanical loading is applied to create the intimate contact of dissimilar metals for diffusion bonding and the thermal loading is considered to be the drive of solid diffusion. In this chapter, a diffusion model is developed based on Fick's laws to describe the diffusion process during the roll bonding process and a diffusivity model is established to extract the diffusion coefficients from the experimental measurement of roll bonded specimens. The corresponding experimental measurement will be described in this chapter.

5.1 Theoretical Diffusion & Diffusivity Model Based on Fick's Law

Fick's law can be applied to characterize the diffusion process during the roll bonding process. Fick's second law gives the diffusion equation [66]:

$$\frac{\partial c}{\partial t} = \nabla \cdot \left(D \nabla c \right) \tag{5.1}$$

where c is the concentration of chemical composition, t is time and D is the diffusion coefficient. If D depends on c, Eq. (5.1) is a non-linear second-order partial differential equation which usually cannot be solved analytically. The concentration dependent diffusivity is usually denoted as the inter-diffusion coefficient. If D is independent of c, Eq. (5.1) can be simplified to

$$\frac{\partial c}{\partial t} = D\Delta c \tag{5.2}$$

where, Δ denotes the *Laplace operator*. This diffusion equation becomes a linear equation. For many cases with specified boundary and initial conditions, analytical solutions are available.

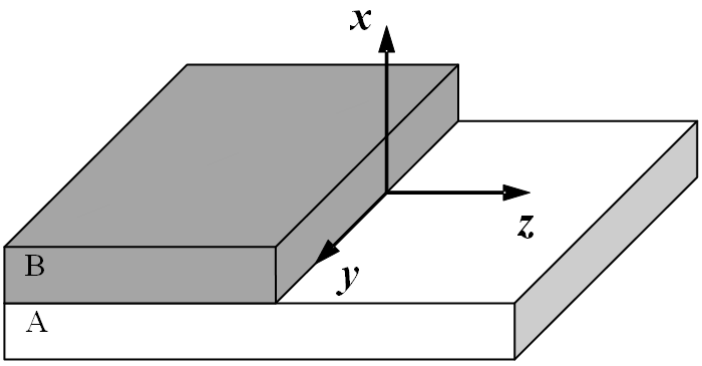

Figure 5.1 The diffusion pairs of sheet metals for roll bonding

For a roll bonding process, the diffusion occurs between two sheet metals as shown in Figure 5.1. The boundary and initial condition of the element B can be illustrated by Figure 5.2 and described by Eq.(5.3). The boundary and initial condition of the element A is complementary to those of the element B.

$$\begin{aligned} c &= c^{-} \quad \text{for } x < 0, \text{ at } t = 0 \\ c &= c^{+} \quad \text{for } x > 0, \text{ at } t = 0 \end{aligned} \tag{5.3}$$

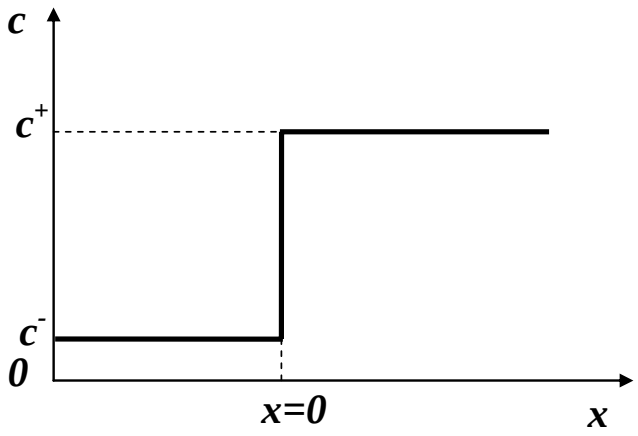

Figure 5.2 The boundary condition for element B at t =0

Theoretically, it can be predicted that the concentrations of the elements A and B do not change with respect to the direction of the axis z or the axis x. If the diffusivity is independent of concentration, Eq. (5.2) becomes one dimensional linear diffusion equation

$$\frac{\partial c}{\partial t} = D\frac{\partial^2 c}{\partial x^2} \tag{5.4}$$

with the introduction of error function

$$erf(z) = \frac{2}{\sqrt{\pi}}\int_0^z \exp(-\eta^2)d\eta \tag{5.5}$$

The solution of Eq. (5.4) is Eq. (5.6) and it can be illustrated in Figure 5.3.

$$c(x,t) = \frac{c^+ + c^-}{2} + \frac{c^+ - c^-}{2} erf\left(\frac{x}{2\sqrt{Dt}}\right) = c^+ - \frac{c^+ - c^-}{2} erfc\left(\frac{x}{2\sqrt{Dt}}\right) \tag{5.6}$$

The error function has the property:

$$erf(-z) = -erf(z) \text{ and } erf(z) \in [-1,1] \text{ for } z \in (-\infty, +\infty) \tag{5.7}$$

The complementary error function is defined as:

$$erfc(z) = 1 - erf(z) \tag{5.8}$$

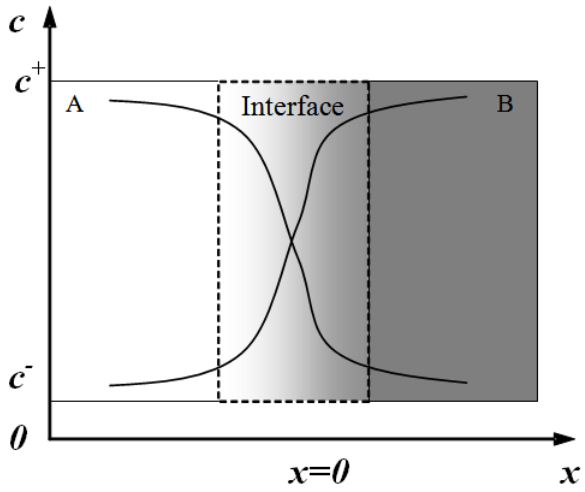

Figure 5.3 The solution of 1-D linear diffusion equation for a rolling boundary condition

From the solution Eq.(5.6), it can be derived that:

$$D = \frac{1}{t}\left(\frac{x}{2erfc^{-1}\left(2\frac{c^{+} - c(x,t)}{c^{+} - c^{-}} \right)} \right)^{2} \tag{5.9}$$

This derivation can only be applied while $t \neq 0, x \neq 0$ and $c(x,t) \neq \frac{c^{+} + c^{-}}{2}$. In a diffusion process, time *t* is always positive. The application of this formula only needs to avoid *x=0,* where theoretically $c(x,t) = \frac{c^{+} + c^{-}}{2}$. Therefore, given any concentration profile of an element in a diffusion process, the diffusivity *D* can be derived by applying Eq. (5.9) at any point *x* with concentration $c(x,t)$ in the diffusion path except the point *x=0*. Moreover, the diffusivity *D(x)* is theoretically constant along the entire diffusion path. However, in reality, the concentration distribution of diffusion elements can never be measured with absolute accuracy and neither the practical diffusion process occurs perfectly according to Fick's law. Therefore, the oscillation of diffusivity *D* with respect to *x* is expected when Eq. (5.9) is applied to determine the diffusivity of a diffusion process. Then, a statistical analysis of the oscillation is required to obtain a reasonable *D*.

Boltzmann studied the effect of the temperature on increasing the energies of gas molecules [130]. His statistical analysis shows that the probability *P* of finding a molecule or atom at an energy level E^{*} greater than the average energy $\overline{E}$ of all the molecules or atoms in a system at a particular temperature *T* in Kelvin was

$$P \propto e^{-\left(E^* - \bar{E}\right)/kT} \tag{5.10}$$

where $k = 1.38 \times 10\text{-}23\ J/(atom \cdot K)$ is Boltzmann's constant.

Svante August Arrhenius (1859-1927) experimentally found that the rate of many chemical reactions as a function of temperature could be expressed as following [130]:

$$V = V_0 e^{-Q/RT} \tag{5.11}$$

where V = *rate of reaction*

Q = *activation energy, J/mol or cal/mol*

$R = 8.314\ J/(mol \cdot K)$ *or* $1.987\ cal/(mol \cdot K)$ *is universal gas constant*

T = *absolute temperature (K)*

V_0 = *rate constant, independent of temperature*

Both the Boltzmann equation and the Arrhenius equation imply that the reaction rate among atoms or molecules in many cases depends on the number of reacting atoms or molecules that have activation energies of E^* or greater. The rates of many solid-state reactions obey the Arrhenius rate law, and hence the Arrhenius Eq.(5.11) is often used to analyze experimental solid-state diffusion rate data.

According to the Arrhenius equation, it can be seen that the diffusivity D depends on the material properties including the diffusion activation energy Q and the diffusion rate constant D_0, and the thermal loading condition T. Given a diffusion process, the diffusion pair is selected and hence the Q and D_0 are determined but the values are

unknown. In order to characterize the diffusion property of a pair of diffusants, at least two temperatures T_1, T_2 need to be applied and then two independent Arrhenius equations can be obtained.

$$\left.\begin{aligned} D_1 &= D_0 e^{-Q/RT_1} \\ D_2 &= D_0 e^{-Q/RT_2} \end{aligned}\right\} \tag{5.12}$$

The diffusion properties Q and D_0 can be derived by solving the Eq. (5.12):

$$D_0 = D_1^{\frac{1}{1-T_2/T_1}} D_2^{\frac{1}{1-T_1/T_2}} \tag{5.13}$$

$$\frac{Q}{R} = T_1 T_2 \frac{\ln D_1 - \ln D_2}{T_1 - T_2} \tag{5.14}$$

Given the diffusion property D, Eq.(5.1) to Eq.(5.6) can describe the diffusion process. The diffusion coefficients D_0 and Q can be determined by Eq.(5.9) to Eq.(5.14) if the diffusion process is a perfectly linear diffusion. In reality, a roll bonding process is not a perfectly linear diffusion and the temperature cannot keep perfectly constant due to the strain energy generated by severe deformation and the environment variation including the heat transfer from rollers and the working atmosphere. Therefore, some modification is required such that the diffusivity could be obtained via experiments and the diffusion model could be applied in a practical diffusion process.

5.2 Modified Diffusivity Model for Roll Bonding Process

The solutions of the diffusion Eq.(5.4) with the boundary and initial condition Eq.(5.3) are shown in Eq.(5.6) and Eq.(5.9). The boundary and initial condition are ideally assumed that the diffusion starts just when the two diffusion components contact each other and that the temperature T is kept constant during the entire diffusion process. While the initiation of the diffusion occurs during rolling, the major diffusion occurs during the reheating after rolling. Considering the factor of the severe plastic deformation and the oscillation of temperature during rolling, the diffusion model (5.4) cannot accurately describe the diffusion process during rolling. Furthermore, although the reheating provides a better temperature control, the initial condition of reheating is not the initial condition of Eq.(5.3) and hence the solution Eq.(5.6) and Eq.(5.9) are not directly applicable to describe the diffusion process during the reheating process.

It can be seen that the characteristic parameter of the solution Eq.(5.6) to the diffusion model Eq.(5.9) is the product of the diffusion coefficient D and the diffusion time t. In other words, the diffusion result will be the same if the product of D and t are kept the same. One diffusion state can be achieved through different approaches. For example, with different diffusion coefficients $D(T_1)$ and $D(T_2)$, the same diffusion state can be achieved by controlling the diffusion time such that $c(x,t_1)=c(x,t_2)$, as long as $D(T_1)\times t_1= D(T_2)\times t_2$. Therefore, even though the temperature varies in a rolling process, the diffusion state after rolling can be expressed by a diffusion coefficient D^* at a constant temperature and the corresponding time t^*.

If the factor of the temperature oscillation and the plastic deformation during rolling are considered, the diffusion result is determined by the product of diffusivity $D_{rolling}$ and rolling time $t_{rolling}$. On the other hand, the same diffusion result can also be achieved by a heating process with the diffusivity $D_{heating}$ and the heating time $t_{heating}$ as long as the product $D_{rolling}t_{rolling}$ and product $D_{heating}t_{heating}$ have the same value. This heating characteristic (product of diffusivity and diffusing time) is defined as the effective characteristic parameter $\left(Dt\right)_{heating}^{eff}$ and the heating time is defined as effective heating time t^{eff}.

Because the temperature in the heating process is easier to control than that in the rolling process, the effective heating characteristic parameter $\left(Dt\right)_{heating}^{eff}$ will be used to describe the initial diffusion process in rolling. To distinguish the *c(x,t)* at different temperatures, *c(x,T,t)* is used here to describe the distribution of the concentration. When the rolling and subsequent reheating occurs at the same temperature T_1, the diffusion result after rolling can be expressed with effective heating parameters as following:

$$D\left(T_1\right)t_1^{eff} = \left(\frac{x}{2erfc^{-1}\left(2\frac{c^+ - c\left(x, T_1, t_1^{eff}\right)}{c^+ - c^-} \right)} \right)^2 \tag{5.15}$$

With the effective description of the rolling process by heating parameters, the diffusion result after reheating at the same temperature T_1 and reheating time t_1 can be

considered as a whole heating process within the heating time $\left(t_1 + t_1^{eff}\right)$. Then the solution (5.6) can be applied and the diffusion result is provided as following:

$$D\left(T_1\right)\left(t_1 + t_1^{eff}\right) = \left(\frac{x}{2erfc^{-1}\left(2\frac{c^+ - c\left(x, T_1, t_1 + t_1^{eff}\right)}{c^+ - c^-}\right)} \right)^2 \tag{5.16}$$

At the rolling and reheating temperature T_1, the diffusivity $D_1 = D\left(T_1\right)$ can be determined by Eq. (5.15) and (5.16) as following:

$$\begin{aligned} D_1 &= D\left(T_1\right) \\ &= \frac{1}{t_1}\left(\left(\frac{x}{2erfc^{-1}\left(2\frac{c^+ - c\left(x, T_1, t_1 + t_1^{eff}\right)}{c^+ - c^-}\right)} \right)^2 - \left(\frac{x}{2erfc^{-1}\left(2\frac{c^+ - c\left(x, T_1, t_1^{eff}\right)}{c^+ - c^-}\right)} \right)^2 \right) \end{aligned} \tag{5.17}$$

In an experiment including the rolling and the reheating process, the distribution of the concentration $c_{rolling}\left(x, T_1\right)$ of a diffusing element after rolling and $c_{reheating}\left(x, T_1\right)$ after reheating can be measured by X-ray microanalysis. Applying the Eq. (5.17), the diffusion coefficient D_1 can be determined by the experimental data $c_{rolling}\left(x, T_1\right)$ and $c_{reheating}\left(x, T_1\right)$:

$$D_1 = \frac{1}{t_1}\left(\left(\frac{x}{2erfc^{-1}\left(2\frac{c^+ - c_{reheating}\left(x,T_1\right)}{c^+ - c^-}\right)}\right)^2 - \left(\frac{x}{2erfc^{-1}\left(2\frac{c^+ - c_{rolling}\left(x,T_1\right)}{c^+ - c^-}\right)}\right)^2\right) \quad (5.18)$$

Similarly, another experiment at a different temperature T_2 in the same procedure can determine the diffusion coefficient D_2:

$$D_2 = \frac{1}{t_2}\left(\left(\frac{x}{2erfc^{-1}\left(2\frac{c^+ - c_{reheating}\left(x,T_2\right)}{c^+ - c^-}\right)}\right)^2 - \left(\frac{x}{2erfc^{-1}\left(2\frac{c^+ - c_{rolling}\left(x,T_2\right)}{c^+ - c^-}\right)}\right)^2\right) \quad (5.19)$$

Substituting Eq. (5.18) and Eq. (5.19) into Eq. (5.13) and Eq. (5.14), the diffusion rate constant D_0 and the diffusion activation energy Q can be determined.

It is worth noting that the $c_{rolling}\left(x,T_1\right)$ and $c_{reheating}\left(x,T_1\right)$ have to be defined in the same coordinate system. So the location of the coordinate origins plays an important role in the application of this diffusivity model. The detailed discussion of the location of the initial contact plan of a diffusion couple can be found in [131]. From the modeling procedure, it can be seen that the initial diffusion bonded condition is not limited to the rolling initiation of the diffusion bonding. Any diffusion bonded sample can be tested before heating treatment and then be put into a heating diffusion process. As long as the diffusion state before and after the heating treatment at (at least) two temperature T_1 and

T_2 can be measured, the diffusivity constant D_0 and the diffusion activation energy Q can be determined.

5.3 Experimental Estimation of Diffusivity

In practice, the experimentally measured element distribution across the diffusion zone is fluctuating, as shown in Figure 5.4. Obviously, the fluctuation of the element distribution results from the testing noise. In this case, it is proposed to determine the diffusivity by measuring the diffusion length-L_D (the thickness of diffusion zone across the interface) with certain tolerance, as illustrated in Figure 5.5.

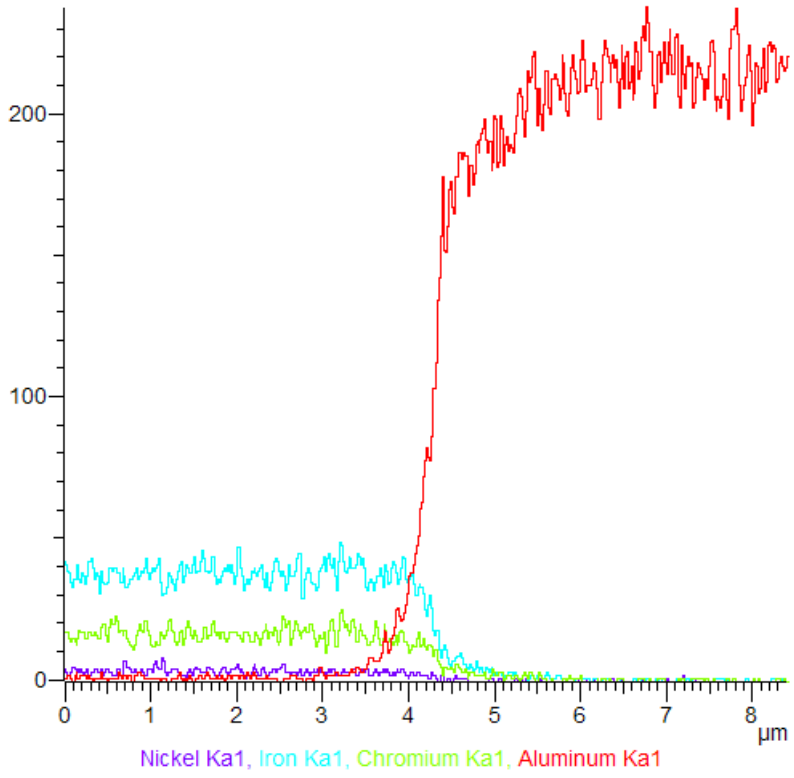

Figure 5.4 X-ray microanalysis of elements across diffusion zone of a bonding interface

Table 5.1 Tabulation of error function values

z	*erf(z)*	*z*	*erf(z)*
0	0	1.4	0.9523
0.1	0.1125	1.5	0.9661
0.2	0.2227	1.6	0.9763
0.3	0.3286	1.7	0.9838
0.4	0.4284	1.8	0.9891
0.5	0.5205	1.9	0.9928
0.6	0.6039	2.0	0.9953
0.7	0.6778	2.1	0.9970
0.8	0.7421	2.2	0.9981
0.9	0.7969	2.3	0.9989
1.0	0.8427	2.4	0.9993
1.1	0.8802	2.5	0.9996
1.2	0.9103	2.6	0.9998
1.3	0.9340	2.7	0.9999

The tabulation of error function-*erf(z)* values is provided in Table 5.1. Considering the fluctuating amplitude in experimental results as shown in Figure 5.4, a tolerance ϕ needs to be specified in order to measure the diffusion length L_D. According to Eq. (5.6) and Table 5.1, then the relationship between the diffusion length and the diffusion coefficient can be determined by:

$$c(x,t)\Big|_{x=\frac{L_D}{2}} = 1-\phi = \frac{1}{2}\left(1+erf\left(\frac{L_D}{4\sqrt{Dt}}\right)\right) \tag{5.20}$$

The diffusion coefficient D can be solved by Eq.(5.20):

$$D = \frac{{L_D}^2}{16\left(erf^{-1}(1-2\phi)\right)^2 t} \tag{5.21}$$

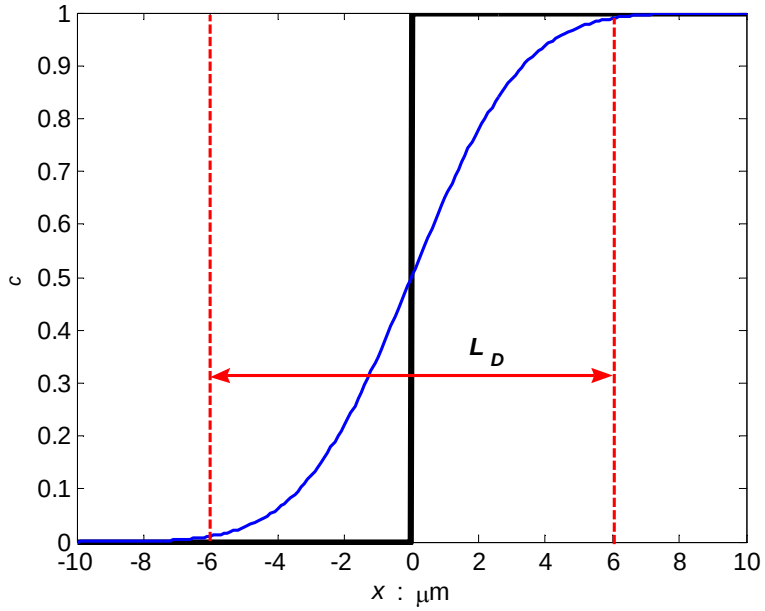

Figure 5.5 Illustration of an element concentration distribution across a diffusion interface

Similarly, the diffusion coefficient *D(T)* can also be determined by the diffusion length at the same temperature-*T* with different heat treatment time t_1 and t_2.

$$D(T)=\frac{L_D^{\,2}(T,t_1)-L_D^{\,2}(T,t_2)}{16\left(erf^{-1}(1-2\phi)\right)^2(t_1-t_2)} \tag{5.22}$$

When the tolerance is set to be 8%, Eq. (5.21) is specified as:

$$D(T)=\frac{L_D^{\,2}(T,t_1)-L_D^{\,2}(T,t_2)}{16(t_1-t_2)} \tag{5.23}$$

Considering the effect of X-ray interaction volume within the target sample, Eq. (5.21) is used instead of Eq. (5.20). This method applies different diffusion time at the

same temperature to characterize the diffusion coefficient. Thus the estimation method of the diffusion coefficient is denoted as differential characterization method for diffusion coefficients. This method only needs the difference of diffusion times, but not the accurate absolute diffusion time. Therefore, the difficulty in experiment measurements is significantly reduced.

The apparent diffusion lengths of Fe and Al reheated at the temperature 400^{o}C and 300^{o}C respectively were determined by EDS testing and it is provided in Table 5.2. Then the diffusion coefficients at the temperature of 400^{o}C and 300^{o}C can be calculated by Eq. (5.22). Substituting those values into Eq. (5.13) and Eq. (5.14), the diffusivity can be determined. The results are provided in Table 5.3.

Table 5.2 The apparent diffusion length of Fe and Al determined by EDS, unit: μm

Temperature: ^{o}C	400		320	
Time: min	30	480	30	120
Fe	1.95±0.09	3.68±0.23	1.80±0.29	2.24±0.28
Al	2.28±0.20	6.85±0.36	3.76±0.18	4.59±0.73

Table 5.3 The diffusion coefficients of elements in diffusion interface of Al-SST

Diffusant element	Matrix	$D(T=400^{o}C)$	$D(T=320^{o}C)$	D_0	Q/R
		μm^2/min	μm^2/min	μm^2/min	K
Fe (of SST304)	Al 1100	1.35E-03	1.21E-03	3.08E-03	553.34
Al	SST 304	5.79E-03	4.81E-03	2.26E-02	918.47

Since the D_0 and Q/R were determined by the experimental data at the temperature 400^{o}C and 320^{o}C, they could be used to predict the diffusion coefficient in the temperature range of 320^{o}C -400^{o}C. Since the temperature range is relatively small and the diffusion coefficients are not measurable in temperature range 240^{o}C-320^{o}C on available instruments, it is assumed that D_0 and Q/R are effective in the temperature range of 240^{o}C-400^{o}C. The diffusion coefficient predicted by D_0 and Q/R in the temperature range 240^{o}C-400^{o}C is hence called "effective diffusion coefficient".

5.4 Diffusion Boundary Analysis

In reality, the oxide film is not perfectly flat and thus the corner of the oxide film fragments could be round instead of sharp. Therefore the extruded metal around the round corner of oxide fragments has a fillet with certain fillet radius R_f. A finite element simulation of a 2-D diffusion example is performed to investigate the effect of the fillet radius R_f on the diffusion state. In this analysis, the temperature field is defined as uniform T=240^{o}C; the diffusion coefficient of SST 304 into Al 1100 is 1048 nm^2/min; the total thickness δ_{ox} of the oxide fragments is 10 nm; the aspect ratio of oxide fragments is 10; the contact area ratio is 10%; the diffusion is simulated in one minute. ABAQUS 6.91 is used to perform the FEA of the diffusion. The mass diffusion/heat transfer element is used. A non-dimensional variable fillet radius ratio $2R_f / \delta_{ox}$ is used for convenience. The result is tabulated in Table 5.4. The diffusion states for the diffusion pair of Al 1100 and SST 304 at 240^oC for one minute with sharp ($2R_f/ \delta_{ox}$= 0) and round corner boundaries ($2R_f/ \delta_{ox}$=40%) are shown in Figure 5.6 and Figure 5.7.

Table 5.4 Tabulation of FEA results of 2-D diffusion front growth

Fillet radius ratio: $2R_f / \delta_{ox}$	The ratio of the elliptical radius to the thickness of oxide fragment		Elliptical radius ratio ξ / η	The ratio diffusion front surface to the apparent interface
	Vertical η / δ_{ox}	Horizontal ξ / δ_{ox}		
0	2.77	2.72	0.9850	0.4311
20%	2.77	2.72	0.9850	0.4311
40%	2.84	2.80	0.9840	0.4426
60%	2.91	2.86	0.9818	0.4527
80%	3.00	2.96	0.9861	0.4679
98%	3.11	3.05	0.9794	0.4839

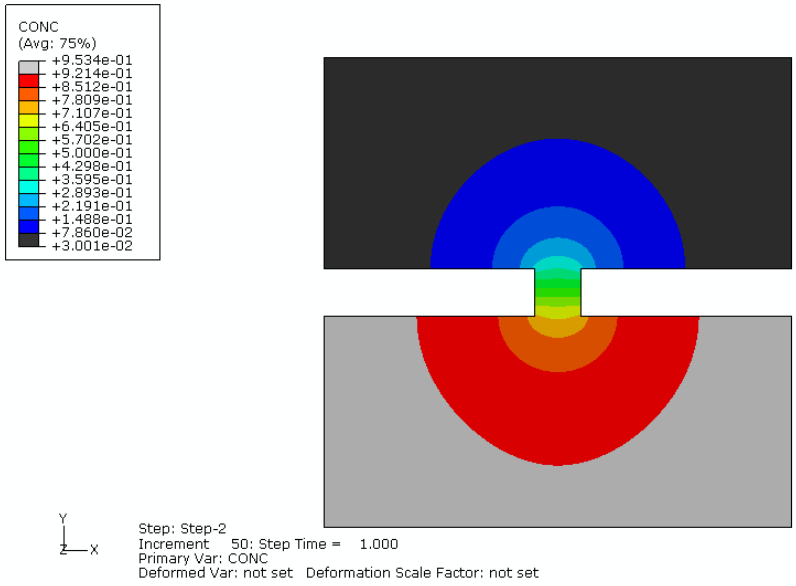

Figure 5.6 The diffusion state with sharp corner boundary

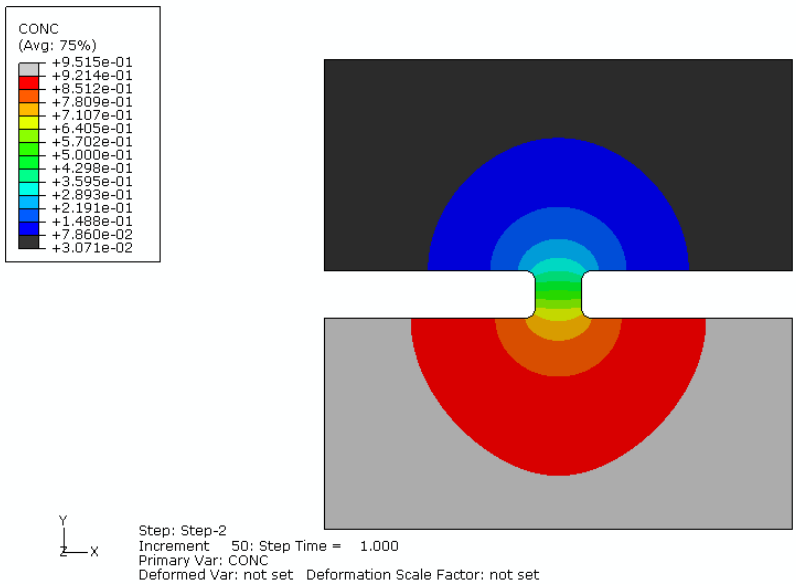

Figure 5.7 The diffusion state with round corner boundary, $2R_f / \delta_{ox}$=40%

The results show that the diffusion front surface ratio only increases by 0.05 (12%) as the fillet radius ratio ($2R_f / \delta_{ox}$) changes from 0 to 98%. It indicates that the fillet radius of the diffusion boundary around the corner of oxide fragments doesn't have significant effect on the diffusion front surface growth.

5.5 Summary

The diffusion zone at the bonding interface of clad metals was characterized by X-ray microanalysis. In order to reduce the effect of the interaction of incident electrons with the graded interface, a differential characterization method was developed to estimate the diffusion coefficient for the diffusion pair of aluminum 1100-O and stainless steel 304. Using this method, X-ray microanalysis yields the diffusivity of stainless steel 304 in aluminum 1100-O $D_0 = 3.08 \times 10^{-3}$ μm^2/min and $Q/R = 553.34$ K. The

finite element simulation of the diffusion evolution with varying boundary fillet radius ratios was performed to investigate the effect of the fillet radius ratio on the diffusion front surface growth. The simulation results show that the fillet radius have insignificant effect on the diffusion results.

CHAPTER VI

THE BONDING STRENGTH MODEL

In Chapter III, the thermo-mechanical bonding mechanism for roll cladding metals is introduced to qualitatively interpret the roll bonding properties based on experimental response data. In Chapter IV, the rolling plastic deformation of metal sheets, the fracture of oxide film and the exposed metal extrusion were analyzed by an analytical model. The effect of rolling thickness reduction, the flow stress mismatch of component sheets, and other rolling conditions on metal contact initiation was also quantitatively described. In Chapter V, the X-ray microanalysis of the diffusion bonding interface was performed. The effective diffusivity was extracted from EDS scanning data. The effective diffusivity can be used to simulate the diffusion front growth. In this chapter, the thermo-mechanical loading will be considered simultaneously. The relationship between the thermo-mechanical rolling conditions and the roll bonding property of dissimilar metal sheets will be established.

6.1 Rolling Mechanics in Roll Bonding Process

In the roll bonding mechanics model, it is illustrated that the contact area ratio of exposed metals is determined by the thickness reductions of both Al 1100 and SST 304 and that the thickness reductions of Al 1100 and SST304 are different from the overall thickness reduction. Considering the contacting probability of exposed Al 1100 and SST 304, the contact area ratio of exposed metals is defined as following

$$a = a_{Al} \cdot a_{SST} \tag{6.1}$$

where a_{Al} is the exposed Al 1100 area ratio and a_{SST} is the exposed SST 304 area ratio. The rolled metal sheets are considered as incompressible materials. According to the volume conversation law, the metal exposure ratio is equal to the thickness reduction ratio of the metal. Thus the Eq. (6.1) can be expressed as:

$$a = r_{t,Al} \cdot r_{t,SST} \tag{6.2}$$

Here $r_{t,\,Al}$ and $r_{t,\,SST}$ are the thickness reductions of component layers Al 1100 and SST 304 and they are function of rolling conditions involving the overall thickness reduction, the flow stress of component layers, the friction condition of the component layers' surfaces and the rollers' surfaces, the thickness ratio of the component layers, the thickness ratio of the radius to that of stacked metal sheets, as discussed in Chapter IV.

6.2 Diffusion Evolution in Roll Bonding Process

In the previous chapters, the diffusion process at the interface between contacting metals was described. In order to solve the diffusion evolution more efficiently, certain approximations are applied. The diffusion satisfies the diffusion governing Eq. (4.2). Since the total thickness of the metal sheets is small relative to the width and the length, the following condition is also satisfied:

$$\frac{\partial^2 c}{\partial^2 z} = 0 \tag{6.3}$$

Therefore, the diffusion field can be considered as a 2-D problem.

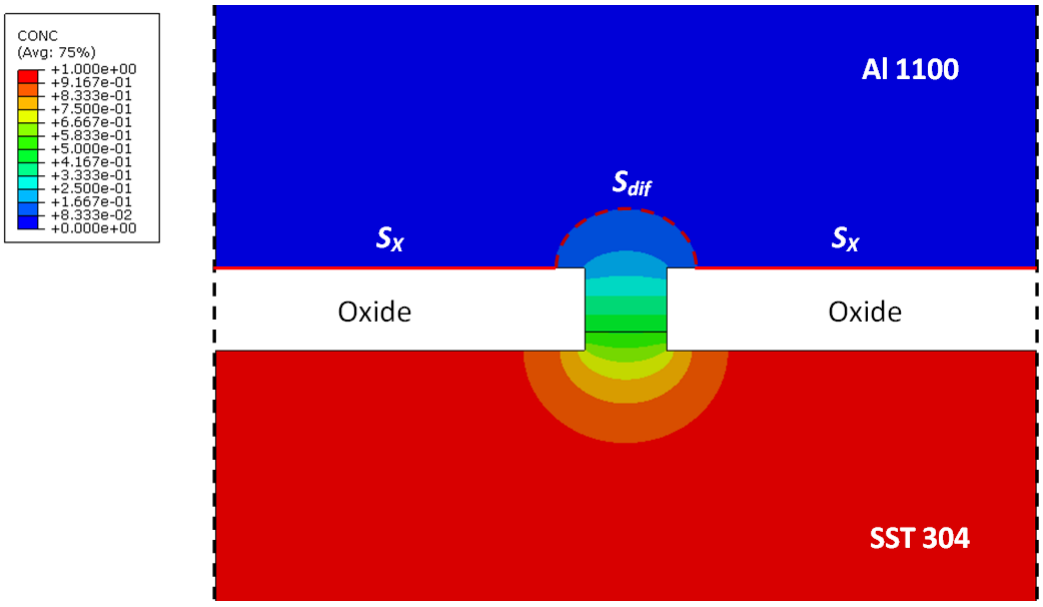

Figure 6.1 A diffusion state at a bonding interface between Al 1100 and SST 304

Figure 6.1 shows a symmetrical representative volume element for the diffusion between the dissimilar metals. The half plane of the representative volume element is shown in Figure 6.2. The symmetrical plane is defined as *x*-plane. The *y*-axis is in the vertical direction and $y=0$ is the initial contact surface of the extruded Al 1100 and SST 304. The diffusion state is illustrated by the normalized concentration of SST 304-$c(x,y,t)$. S_X is the contact length of the Al 1100 and its oxide film, S_{dif} is the contour length for a particular concentration, λ is the average spacing length of oxide fragments (*i.e.* the length of the representative volume element in Figure 6.1), δ_1 is the distance between the initial contact surface and the Al 1100-alumina interface, w is the width of the crevice between the oxide fragments, ξ is the maximum distance of the contour to the

axis-y (thus $\chi = \xi - w/2$) and η is the maximum height of the contour above the Al 1100-alumina interface. According to the mixture rule, the theoretical peel strength field $G_{dif}(x,y,t)$ in the diffusion zone can be expressed as:

$$G_{dif}(x,y,t) = G_{Al} + (G_{SST} - G_{Al}) \cdot c(x,y,t) \tag{6.4}$$

where G_{Al} is the peel strength of Al 1100 and G_{SST} is the peel strength of SST 304.

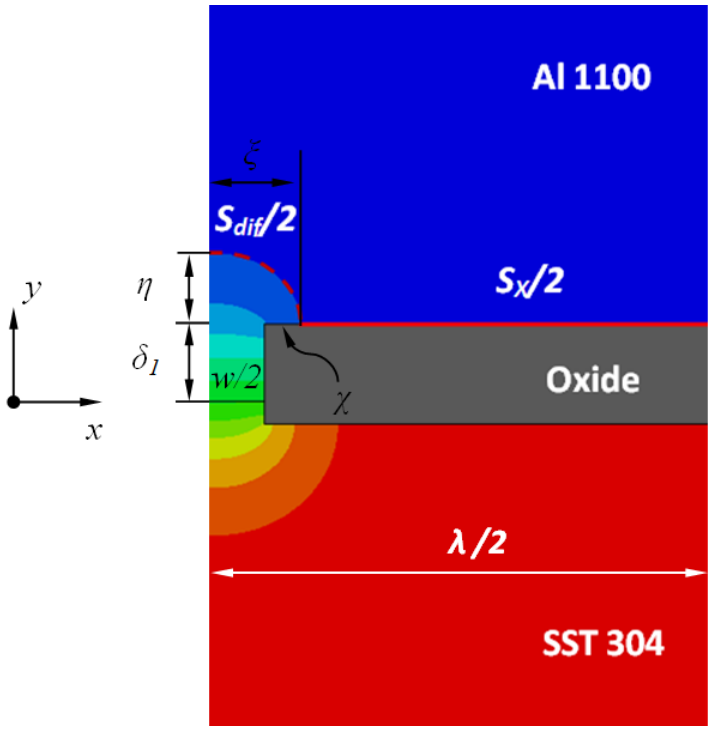

Figure 6.2 Diffusion front growth in roll bonding of Al 1100 and SST 304

It can be expected, from Eq. (6.4), that the material strength decreases to the strength of Al 1100 at the diffusion front of SST 304 where $c(x,y,t)=0$. As shown in Figure 6.2, the corresponding contour of the diffusion front has $\xi=\xi_0$ and $\eta=\eta_0$ and

S_{dif}=S^0_{dif}. Since the peel strength reaches the minimum value at the diffusion front, it is believed that the peeling path between Al 1100 and SST 304 in peel test will go along the diffusion front as shown by the red dash line in Figure 6.1. Since the alumina film and Al 1100 substrate have relatively sliding by extension in the rolling process, the peeling path would go along the interface (as shown in red solid line) between alumina and Al 1100 besides the diffusion front. This deduction is supported by the observation of the surface of SST 304 after the Al 1100 sheet is peeled off, as discussed in Chapter III.

According to the conservation of energy along peeling path, the overall peel strength G of the representative volume element can be derived:

$$G\lambda = G_{dif} S_{dif} + G_X S_X \tag{6.5}$$

where G_X is the peel strength of the interface of Al 1100 and its oxide film.

Reformulating Eq. (6.5), the overall peel strength can be expressed as:

$$G = G_{dif} f + G_X \frac{S_X}{\lambda} \tag{6.6}$$

where the area ratio of the diffusion front surface to the overall Al 1100-SST 304 interface is defined as a function of the diffusion state (involving D_0, Q, T and t) and the metal contact area ratio a.

$$f = \frac{S_{dif}}{\lambda} = f\left(a, T, t\right) \tag{6.7}$$

The function of diffusion front ratio can be determined by the finite element simulation of a 2-D diffusion between Al 1100 and SST 304. Obviously, the function of diffusion front ratio is a monotonically increasing function of the diffusion temperature and time. In the perspective of diffusion front growth, the bonding strength in term of peel strength G will increase as the diffusion temperature or time increases. Meanwhile, the peel strength of Al 1100, G_{Al}, is also changing during the roll bonding process. Initially, the peel strength of Al 1100 is increased by strain hardening due to the extrusion through the crevice between oxide fragments. Then the annealing effect decreases the peel strength of Al 1100 in the reheating treatment. Considering the strain hardening and annealing effect, the peel strength of Al 1100 is a function of plastic strain ε_p, heating temperature T and time t.

$$G_{Al} = G_{Al}\left(\varepsilon_p, T, t\right) \tag{6.8}$$

Therefore, the peel strength Eq. (6.6) can be reformulated as

$$G = G_{dif}\left(\varepsilon_p, T, t\right) \cdot f\left(a, T, t\right) + G_X \cdot \frac{S_X}{\lambda} \tag{6.9}$$

As shown in Figure 6.2, it could be expected that, when $\eta<0$, the peeling failure surface follows the line along the interface between Al 1100 and its oxide film. The

diffusion front curve length $S_{dif} > w$ only if $\eta > 0$. Therefore, the diffusion front ratio is derived as following:

$$f(a,T,t) = \begin{cases} a, & \text{when } \eta < 0 \\ \dfrac{S_{dif}}{\lambda}, & \text{when } \eta > 0 \end{cases} \tag{6.10}$$

Based on the diffusion front growth simulation in Chapter V and the contact area ratio created through a rolling process in Chapter IV, the peel strength for the roll bonding can be estimated by Eq. (6.9) according to the minimum energy principle:

$$G_{test} = MIN(G) \tag{6.11}$$

Since the diffusion front profile is in elliptical shape, it is possible that

$$\frac{S_{dif}}{\lambda} > 1$$

It will lead to

$$G > G_{Al} \tag{6.12}$$

In this case, the failure will occur in Al 1100 sheets in a peel test.

As the diffusion continues, the adjacent diffusion zone will merge with each other, as shown in Figure 6.3. The G_{test} will be approaching G_{Al} as S_{dif} approaches λ. Finally, the failure will also occur in Al 1100 sheets in a peel test.

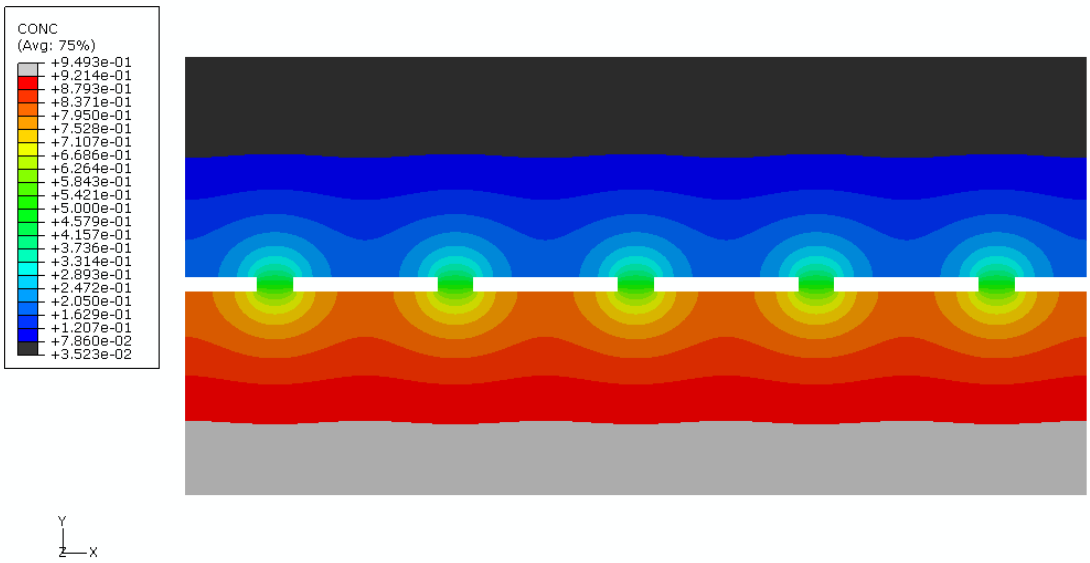

Figure 6.3 Mergence of adjacent diffusion bonding zones

6.3 Results and Validations for Roll Bonding Examples

For particular cases of the rolling bonding with the thickness reduction of 30%, 40%, and 50% at 240°C, the contact area ratio $a(r_t)$ can be solved in Chapter IV. Then the calculated contact area ratio specifies the boundary conditions for the 2-D diffusion problem as shown in Figure 6.2. With these boundary conditions, the 2-D diffusions were simulated through ABAQUS6.9. The numerical solutions of diffusion front dimensions for different contact area ratios are tabulated in Table 6.1~Table 6.3.

Here a non-dimensional quantity is introduced to analyze the bonding strength of dissimilar metals through a warm rolling process:

$$\frac{G}{G_{Al}} = \left(1+\left(k_G-1\right)\cdot c\left(0,y,t\right)\right)\cdot\frac{S_{dif}\big|_{c=c(0,y,t)}}{\lambda}+k_X\cdot\frac{S_X\big|_{c=c(0,y,t)}}{\lambda} \tag{6.13}$$

where $k_G = G_{SST} / G_{Al}$ and $k_X = G_X / G_{Al}$. Since the oxide film fragments have relative sliding to the substrate metal and hence no metal to oxide bond attributes to the metal bonding [76], it is considered that G_X=0.

Table 6.1 Tabulation of diffusion front dimensions for r_t =30% and T=240°C

w/2=3.1 nm, $S_X/2$=50 nm
(*a=5.9%, D=1048* nm^2/min)

t, min	ξ^0 , nm	η^0 , nm	S^0_{dif}, nm
0.027	3.1	0.9	3.4
0.048	5.3	4.4	7.7
0.068	6.5	5.6	9.5
0.088	7.4	6.8	11.1
0.108	8.3	7.7	12.5
0.128	8.9	8.6	13.7
0.148	9.4	9.2	14.6
0.248	12.1	12.1	19.0
0.348	14.2	14.2	22.3
0.448	15.9	15.9	25.0
0.548	17.4	17.4	27.4
0.648	18.6	18.6	29.2
0.748	20.1	20.1	31.5
0.848	21.3	21.0	33.1
0.948	22.7	22.4	35.5
1.048	24.2	23.3	37.3
1.168	25.7	24.8	39.6
1.248	26.9	25.7	41.3
1.348	28.3	26.6	43.1
1.448	30.1	28.0	45.7
1.548	31.6	28.9	47.5
1.648	33.4	30.1	49.9
1.748	35.1	31.0	52.0
1.848	37.2	31.9	54.3

Table 6.2 Tabulation of diffusion front dimensions for r_t =40% and T=240°C

$w/2$=6.6 nm, $S_X/2$=50 nm

(a=11.7%, D=1048 nm^2/min)

t, min	ξ^0 , nm	η^0 , nm	S^0_{dif}, nm
0.032	6.6	1.8	7.1
0.063	9.4	6.6	12.7
0.083	10.6	8.0	14.7
0.103	11.6	9.4	16.5
0.163	14.2	12.6	21.1
0.263	17.4	16.0	26.2
0.363	20.0	19.0	30.6
0.463	22.2	21.2	34.1
0.563	24.2	23.2	37.2
0.663	26.2	25.2	40.4
0.763	28.2	26.8	43.2
0.863	30.0	28.4	45.9
0.963	32.0	29.8	48.5
1.063	34.0	31.2	51.2
1.163	36.4	32.8	54.4
1.263	38.6	34.2	57.2

Table 6.3 Tabulation of diffusion front dimensions for r_t =50% and T=240°C

$w/2$=12.3 nm, $S_X/2$=50 nm
(a=19.7%, D=1048 nm^2/min)

t, min	ξ^0, nm	η^0, nm	S^0_{dif}, nm
0.042	12.3	3.6	13.4
0.085	15.0	9.2	18.6
0.105	16.3	11.0	21.0
0.125	17.0	12.8	22.8
0.145	17.9	13.9	24.4
0.165	19.0	15.2	26.3
0.185	19.9	16.1	27.7
0.205	20.8	17.5	29.4
0.225	21.5	18.4	30.6
0.285	23.7	20.8	34.3
0.385	26.6	24.2	39.2
0.485	29.3	27.3	43.7
0.585	31.8	29.8	47.6
0.685	34.0	32.0	51.1
0.785	36.7	34.3	55.0
0.885	38.9	36.0	58.2
0.985	41.4	37.8	61.5
1.085	44.3	39.8	65.4

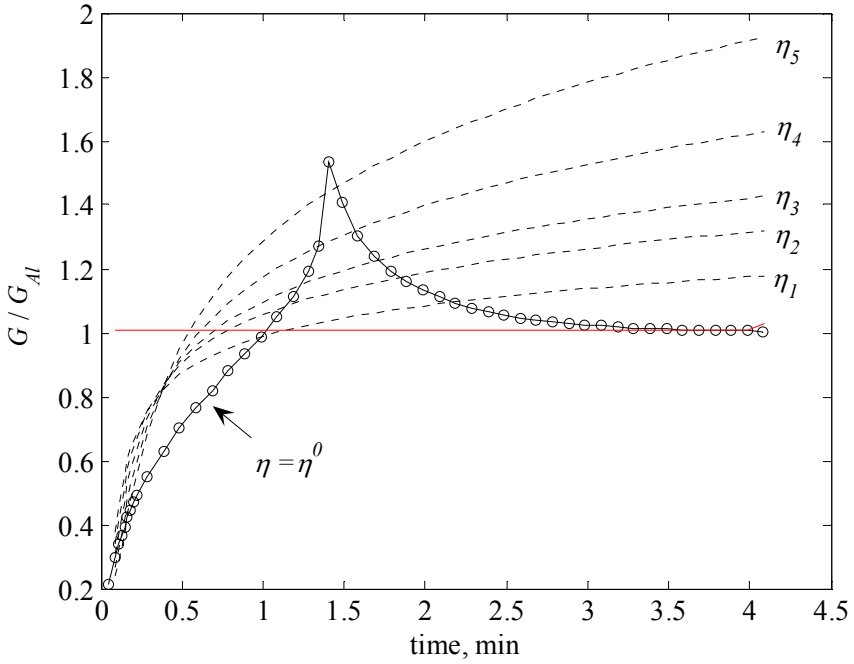

Figure 6.4 Non-dimensional peel strength growth along different contours on $\eta=\eta^0$and η_i (i=1, 2…5) with r_t =50%

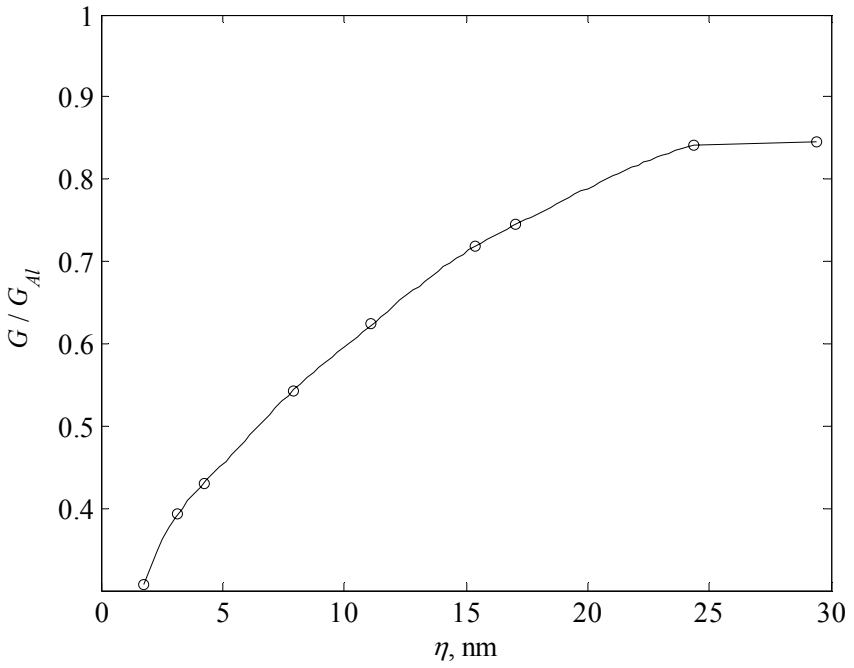

Figure 6.5 Non-dimensional peel strength along different contours on η with r_t =40%

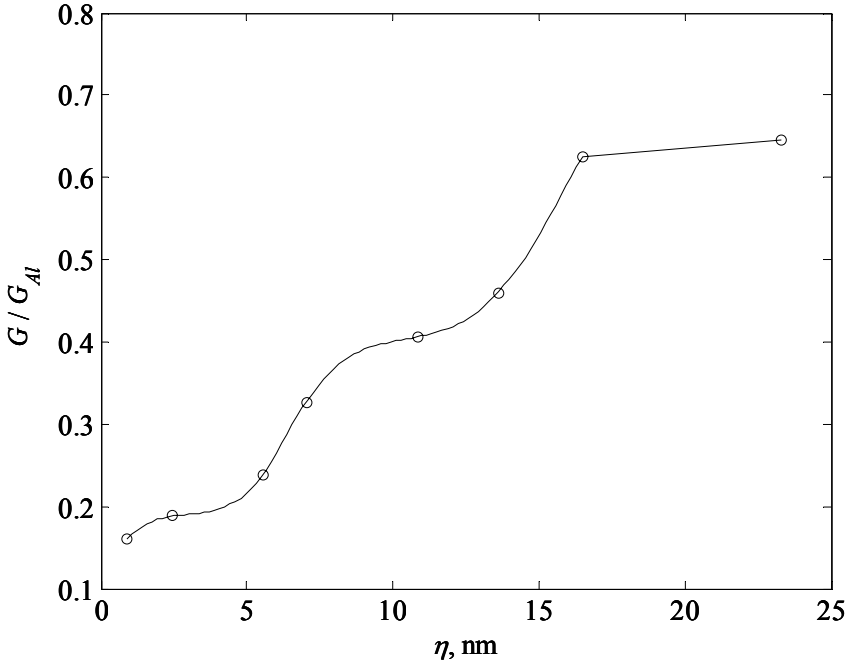

Figure 6.6 Non-dimensional peel strength along different contours on η with r_t =30%

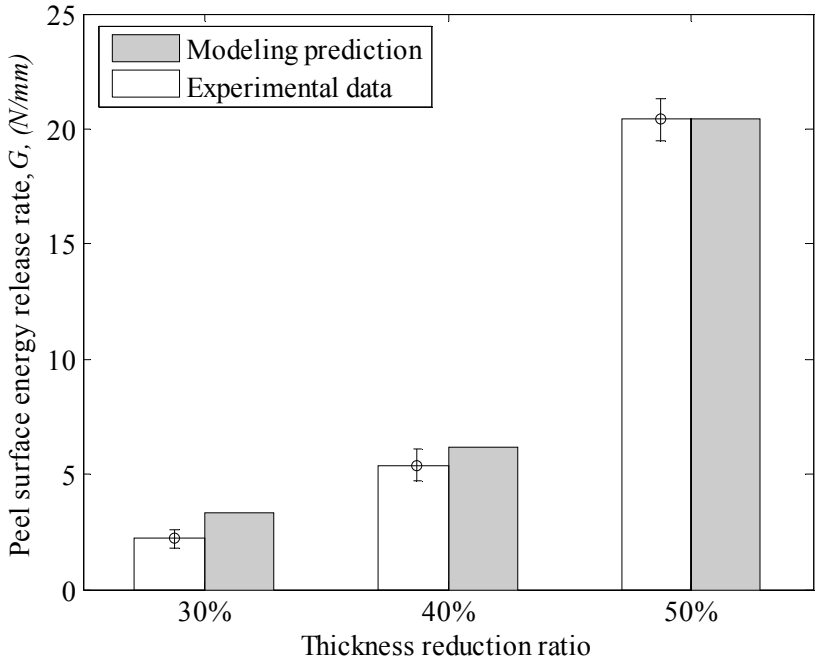

Figure 6.7 Comparison of modeling prediction with experimental data of peel strength under rolling condition T=240°C

For the diffusion with the boundary condition through the rolling at 50% thickness reduction ratio and 240°C entry temperature, the peel strengths along some particular contours on $\eta=\eta^0$ and η_i (i=1, 2…5, and $\eta_1< \eta_2< \eta_3< \eta_4< \eta_5$) were illustrated in Figure 6.4. It shows that the peel strength along the diffusion front (*i.e. the contour on* $\eta=\eta^0$) reaches the $G(\eta^0)=G_{Al}$ at the effective diffusion time t_{eff}=1.02 min. Before this time, the $G(\eta^0)$ is the minimum peel strength in the diffusion zone and it is less than G_{Al}. After this time, the peel strength in the diffusion zone is greater than the G_{Al}. This indicates that the peeling failure occurs along the diffusion front contour before t_{eff}=1.02 min and thereafter the Al 1100 will fail in the peel test. The experimental results from Chapter III show that the maximum peel strength at the entry temperature 240°C is 20.4±0.9 N/mm when the rolling thickness reduction is 50%. The Al sheet could fail in the peel test when the measured peel strength is slightly more than 20.4 N/mm. Thus, we consider the maximum peel strength 20.4 N/mm as the G_{Al}.

The effective diffusion times for the roll bonding at thickness reduction 40% and 30% are considered to be the same as that at 50% thickness reduction ratio. The peel strength along different SST concentration contours at the effective diffusion time t_{eff}=1.02 min for 40% and 30% thickness reduction rolling are provided in Figure 6.5 and Figure 6.6. The results indicate that the minimum peel strengths through the roll bonding processes at 40% and 30% thickness reduction ratio were obtained along the contours on $\eta=\eta^K$. The comparison between the modeling prediction and the experiment data of the peel strengths is provided in Figure 6.7. The modeling prediction of peel strength shows reasonable agreement with the experimental results. It indicates that the integrated

bonding strength model can effectively predict the peel strength of roll bonded clad metal Al1100-SST 304-Al 1100.

6.4 Discussions

As shown in Figure 6.2 for a particular diffusion state, as the Al concentration increases, the contour length for specified concentrations of SST and Al increases. On the other hand, the local peel strength along the contour with specified concentration of SST and Al decreases as the Al concentration increases. The minimum peel strength (i.e. the peel strength determined through peel testing) growth is determined by the combined effect of the local peel strength and the corresponding contour length. Depending on the diffusion state, the minimum peel strength can be reached either along the diffusion front contour on $\eta=\eta^0$, along the contour on $\eta=\eta^K$ (as shown in Figure 6.8), or along the contour on $\eta^K<\eta<\eta^0$. When the peel strengths along all the contours in the diffusion zone are greater than the peel strength of the soft metal(*i.e.* Al 1100 in the above case), the soft metal sheet will break in a peel test.

The results of the bonding strength model for the roll bonding of Al 1100 and SST 304 at entry temperature 240^{o}C indicates that the peel failure tends to occur along the diffusion front contour at high thickness reduction such as 50% in this case. In this peeling failure mode, more residual aluminum can be observed on the SST surface after peeling as shown in Figure 6.9-(a). At low thickness reduction such as 30% in this case, the peel failure tends to initiate at the corner *K* of the extruded metal on the soft metal side and to propagate along the contour $G_{dif}=G_K$, as shown in Figure 6.8. In this peeling

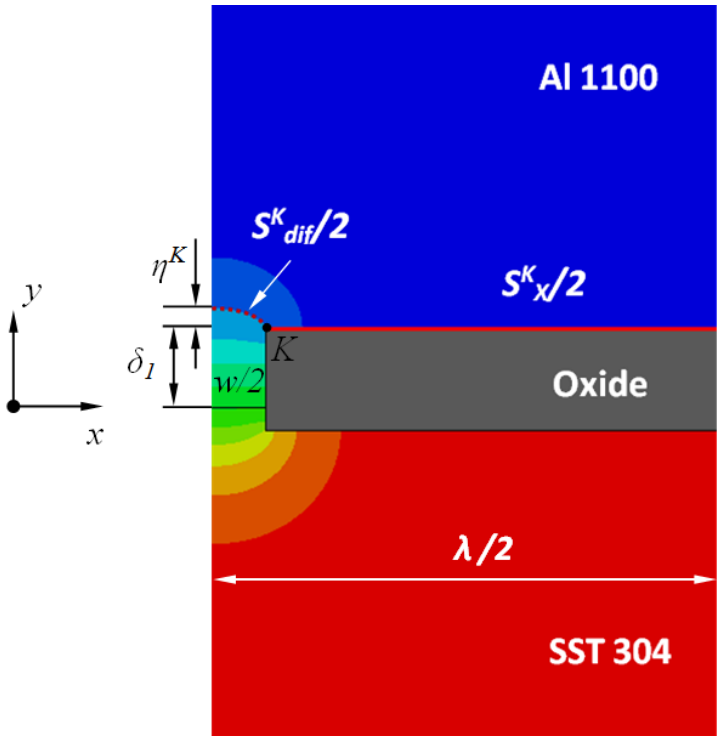

Figure 6.8 Peel failure contour in the diffusion zone between Al 1100 and SST 304 of roll bonded clad metals

(a) (b)

Figure 6.9 The residual aluminum left on stainless steel surface after aluminum sheet is peeled off: (a) r_t =50%; (b) r_t =30%

failure mode, little residual aluminum can be observed on the SST surface after peeling as shown in Figure 6.9-(b).

As the Eq. (6.3), (6.9) and (6.11) show, the roll bonding property of clad metals depends on the contact area ratio, the diffusion evolution and the strength of component metal sheets.

The contact area ratio generated in a rolling process is determined by rolling conditions and the material properties of component metal sheets and rolls. The rolling conditions include the rolling thickness reduction ratio, the end-tension loading, the roll radius, the thickness ratio of component metal sheets, and the friction condition between rolls and component layers as well as between component layers. The effect of those factors on the contact area ratio was discussed in Chapter IV.

The diffusion evolution results in the growth of the peel strength after the exposed metals contact with each other. The practical diffusion evolution depends on the diffusion property of materials and the boundary condition. The diffusion coefficient has significant dependence on temperature. The boundary condition is determined by the generation of contact area ratio. The combined effect of temperature and contact area ratio determines how fast the bonding strength grows, the adjacent diffusion zones merge with each other and the bonding strength reaches the weak component's strength.

In the roll bonding process, the strength of component metal sheets actually increases by rolling strain hardening and decreases by heating softening. That is the

reason why rolling at higher temperature makes stronger bonding but the reheating treatment for certain time decreases the bonding strength.

In a comprehensive view, the rolling thickness reduction and the rolling entry temperature are the major factor for the roll bonding strength of clad metals. High rolling thickness reduction creates more contact area of exposed metals and strengthens the component metal sheets by straining hardening. The roll bonding strength is hence increased. The high entry temperature provides high diffusion coefficient and thus the bonding strength increases faster before the roll bonded metal cools down. The high entry temperature could also soften the component metals such that the exposed metal extrudes more easily through the crevice between oxide film fragments. Thus the high entry temperature increases the roll bonding property of clad metals.

6.5 Summary

This chapter developed a bonding strength model that integrates the plastic deformation and the diffusion evolution into the roll bonding mechanism for the clad metal Al-SST-Al. The prediction of the peel strength by the integrated modeling and simulation agrees well with the experimental results. The roll bonding mechanism including the oxide film fracture, the exposed metal extrusion and the diffusion evolution was validated. It indicates that the rolling plastic deformation and the thermal diffusion evolution effectively explain the roll bonding mechanism of the clad metals with dissimilar component metal sheets. This model can quantitatively predict the peel strength of the roll bonded clad metals. It provides insights into the design and analysis of the roll cladding process.

CHAPTER VII

CONCLUSIONS AND FUTURE WORK

This dissertation presents both experimental investigation of the roll cladding process and thermo-mechanical modeling of the roll bonding mechanism of clad metals. The experimental observation and the quantitative analysis of the roll bonding process through the proposed models provides fundamental understanding of the bonding mechanism of dissimilar metals in a warm rolling process and hence could enhance our capability in designing and analyzing the roll bonding process for multifunctional clad metals.

The roll bonding process of aluminum 1100-O and stainless steel 304 was conducted based on the design of experiment. The bonding property was characterized by the 180^{o} peel test. A peeling mechanics model was developed to address the plastic dissipation of an aluminum sheet in the peel test. The accuracy of the evaluation of the peel strength was significantly improved by integrating the peeling mechanics model. The experimental investigation of the bonding property of roll cladding metals shows significant dependence of the peel strength on the thickness reduction and the entry temperature. The dependence is convexly non-linear. The experimental results also indicate that the peel strength is a non-monotonic function of reheating time. During reheating, the peel strength decreases first and increases afterwards.

The diffusion state at the bonding interface was characterized through microscopic imaging and X-ray microanalysis. The effect of the interaction volume of incident electrons with the target specimen on the diffusion interpretation was addressed. The differential diffusion characterization method was introduced to reduce the interaction volume effect. The effective diffusion coefficient was determined by the differential diffusion characterization method. The diffusivity of stainless steel 304 into aluminum1100 at the temperature range between 240°C and 400°C is D_0=3.08×10^{-3} μm^2/min and Q/R=553.34K.

Based on the experimental observation, this dissertation presents a roll bonding mechanism of clad metals involving rolling plastic deformation, oxide film fracture, exposed metal extrusion, and diffusion evolution. A roll bonding mechanics model and a bonding strength model for the roll bonding mechanism were developed. The effectiveness of the thermo-mechanical models was validated by the experiment of roll cladding of stainless steel 304 with aluminum 1100-O. The integrated roll bonding model is capable of predicting the peel strength of clad metals by a particular rolling process and of analyzing the effect of various rolling parameters on the bonding property of clad metals. The rolling parameters include the rolling thickness reduction, the friction coefficients between rolls and surface metal sheets as well as between component metal sheets, the thickness ratio of component layers, the size of rolls, the surface oxide property, the flow stress mismatch of component metal sheets, and the diffusivity of component metals.

Through the comprehensive investigations including the experiments, numerical simulations and the theoretical modeling, the following conclusions are reached:

- Dissimilar metals can be bonded through a warm rolling process and the different bonding strengths can be achieved by changing the warm rolling parameters such as the rolling thickness reduction ratio and the rolling temperature.
- The bonding strength can be increased by increasing the rolling thickness reduction or the entry temperature. A threshold rolling thickness reduction ratio at a particular entry temperature is required to bond dissimilar metal sheets through warm rolling and the threshold thickness reduction becomes lower as the entry temperature increases.
- The reheating treatment does not necessarily enhance the bonding strength. Only the reheating treatment in a sufficient heating time can enhance the bonding strength.
- The plastic dissipation must be considered when the 180^{o} peel test is used to evaluate the bonding property of the clad metals. Otherwise, the apparent peel strength from the measurement does not represent the true peel strength.
- The roll bonding mechanism for dissimilar metal sheets can be explained by the oxide film fracture, the exposed metal extrusion through the crevice between the oxide fragments and the diffusion at the bonding interface.

- The effect of various rolling parameters on the bonding process can be quantitatively analyzed through the proposed roll bonding mechanics model with the incorporation of the oxide film fracture and the exposed metal extrusion. The dissimilar metal sheets have different thickness reduction after the roll bonding process. In a roll bonding process for a soft-hard-soft clad metal, high thickness reduction, high friction coefficient, high thickness ratio of the component layers, large roll radius and low flow stress ratio are preferred for the increase of the bonding property. The differential end-tension loading can reduce the negative effect of the flow stress ratio on the contact area ratio.
- The bonding strength of dissimilar metal sheets can be predicted through the proposed bonding strength model. The quantitative analysis of the bonding strength of dissimilar metal sheets through a warm rolling process can provide significant insights for the design and analysis of the roll bonding process of clad metals. It can also help optimize rolling parameters for varying bonding strength depending on the demands of the application.

Although significant efforts and carefulness have been invested into this research, there are a few aspects that can be improved for better understanding of the roll cladding process and for more accurate predictions of bonding property of clad metals. Thus, the following directions are suggested for future work:

- The bonding property of clad metal can be evaluated by direct strength tests such as tensile strength test and shear strength test. New testing methods need to be designed and performed for the bonding property characterization of roll cladding metals.
- In terms of different evaluation approaches for bonding property, the bonding strength model needs to be modified for the description of bonding mechanism and the prediction of bonding property.
- The annealing (materials softening) effect during the reheating treatment needs to be evaluated and modeled to extend the roll bonding model to analyze the bonding evolution during reheat treatment.
- The dissolution of the oxide fragments into the metal substrate and the increase of the bonding due to the dissolution need to be studied to explain the higher temperature effect on the increase of the bonding strength.

REFERENCES

[1] Chen, L., Yang, Z., Jha, B., Xia, G. and Stevenson, J. W., 2005, "Clad metals, roll bonding and their application for SOFC interconnects," Journal of Power Sources, **152**, pp. 40-45.

[2] Al composite panel made by cladding, 2010, http://www.alcopanel.co.kr/.

[3] Bumpers made of clad metals, 2011, http://www.cladit.com/examples/bumpers.html.

[4] Fuel cell plates made of clad metals, 2011, http://www.cladit.com/examples/fuel-cell.html.

[5] Lenard, J., June 2007, *Primer on Flat Rolling*, Elsevier, London, UK.

[6] Liu, H.W., Guo, C., Cheng, Y., Liu, X.F., and Shao, G.J., 2006, "Interfacial Strength and Structure of Stainless Steel–Semi-Solid Aluminum Alloy Clad Metal," Materials Letters, **60**, pp.180-184.

[7] Rybin, V. V., Greeenberg, B. A., Antonova, O.V., Kar'kina, L.E., inozemtsev, A.V., Semenov, V.A., and Patselov, A.M., July 2007, "Examining the Bimetallic Joint of Orthorhombic Titanium Aluminide and Titanium Alloy (Diffusion Welding) ," Welding Journal, **86**(7), pp.205-209.

[8] Pan, D., Gao, K., and Yu, J., 1989, "Cold Roll Bonding of Bimetallic Sheets and Strips," Materials Science and Technology, **5**, pp. 934-939.

[9] Nakasuji, K., Masuda, K., and Hayashi, C., 1997, "Development of Manufacturing Process of Clad Bar by Rotary Rolling," ISIJ International, **37**, pp. 899-905.

[10] Li, H. and Han, J., 2006, "Effect of Plastic Deformation on Diffusion-Rolling Bonding of Steel Sandwich Plates," Journal of University of Science and Technology Beijing, **13**, pp. 532-537.

[11] Lee, J.E., Bae, D.H., Chung, W.S., Kim, K.H., Lee, J.H. and Cho, Y.R., 2007, "Effect of Annealing on the Mechanical and Interface Properties of Stainless Steel/Aluminum/Copper Clad-Metal Sheets," Journal of Material Processing Technology, **187-188**, pp. 546-549.

[12] Goldstein, J. I., Newbury, D., Joy, D., Lyman, C., Echlin, P., Lifshin, E. Sawyer, L., and Michael, J., 2003, *Scanning Electron Microscopy and X-ray Microanalysis*, Kluwer Academic/Plenum Publishers, New York.

[13] Boessenkool, H.W. and Durst, G., 1954, US Patent: 2,691,815, "Solid Phase

Bonding of Metals," Metals and Controls Corporation, Attleboro, MA.

[14] Li, L., Nagai, K. and Yin, F., 2008, "Progress in Cold Roll Bonding of Metals," Sci. Technol. Adv. Mater. **9**, 023001, pp.1-11

[15] Ulam, J.B., Camp, W.C., 1967, US patent: 3,350,772, "Methods of Cladding Stainless Steel to Aluminum," Composite Metal Products, Inc., Canonsberg, PA.

[16] Ulam, J.B., 1978, US Patent: 4,103,076, "Clad Metal Product of Cu, Al and Stainless Steel," Clad Metals, Inc., Canonsburg, PA.

[17] Pandey, A.K. and Jha, B., 2000, US Patent: 6,096,145, "Method of Making Clad Materials using Lead Alloys and Composite Strips Made by Such Method," Texas Instruments, Inc., Dallas, TX.

[18] Dubuc, R.A., 1970, US Patent: 3,449,211, "Metal Inlay and Method for Making the Same," Texas Instruments, Inc., Dallas, TX.

[19] Nakamura, Y., Hashimoto, A., Fujita, T. and Kawakami, M., 1989, US Patent: 4,826,736, "Clad Sheets," Sumitomo Special Metals Co., Ltd., Osaka, Japan.

[20] Clarke, J.F., 1969, US Patent: 3,475,811, "Clad Metal," Texas Instruments, Inc., Dallas, TX.

[21] Sharp, W.F., 1974, US Patent: 3,798,011, "Multilayered Metal Composite," E. I. du Pont de Nemours and Company, Wilmington, DE.

[22] Ueda, F., 1986, US Patent: 4,612,259, "Titanium Clad Steel Plate," Asahi Kaser Kogyo Kabushiki Kaisha, Osak, Japan.

[23] Ouchi, C., NiiKura, M. and Suenaga, H., 1987, US Patent: 4,694,985, "Method of Producing Titanium Clad Steel Plate by Hot Rolling," Nippon Kokan Kabushiki Kaisha, Tokyo, Japan.

[24] Suenaga, H., Ishikawa, M. and Minakawa, K., 1991, US Patent: 5,060,845, "Method for Manufacture Titanium Clad Steel Plate", NKK Corporation, Tokyo, Japan.

[25] Yan, J.C., Zhao, D.S., Wang, C.W., Wang, L.Y., Wang, Y. and Yang, S.Q., 2009, "Vacuum Hot Roll Bonding of Titanium Alloy and Stainless Steel using Nickel Interlayer," Materials Science and Technology, **25**(7), pp.914-918

[26] Dion, T.A., and Thomson, A.J., 1969, US Patent: 3,444,603, "Manufacture of Clad Wire and the Llike," Texas Instruments Incorporated, Dallas, TX.

[27] Dion, T.A., and Thomson, A.J., 1971, US Patent: 3,600,790, "Manufacture of Clad Wire and the Like," Texas Instruments Incorporated, Dallas, TX.

[28] Frieling, G.H. and Barrington, J., 1971, US Patent: 3,580,706, "Metal Strand Having A Chromium Steel Core and Corrosion-Resistant Cladding," Texas Instruments Incorporated, Dallas, TX.

[29] Sexton, P., 1975, US Patent: "Copper-Clad Aluminum Wire and Method of Making," Texas Instruments Incorporated, Dallas, TX.

[30] Nakasuji, K., Masuda, K. and Hayashi, C., 1997, "Development of Manufacturing Process of Clad Bar by Rotary Rolling," ISIJ International, vol.37, No.9, pp.899-905

[31] Clark, K.B., 1965, US Patent: 3,220,107, "Manufacture of Clad Rods, Tubing and Clad Tubing," Texas Instruments Incorporated, Dallas, TX.

[32] Zhan, Z., He, Y., Wang, D. and Gao W., 2006, "Cladding Inner Surface of Steel Tubes with Al Foils by Ball Attrition and Heat Treatment," Surface and Coatings Technology, **201**, pp.2684-2689.

[33] Mohebbi, M.S. and Akbarzadeh, A., 2010, "A Novel Spin-Bonding Process for Manufacturing Multilayered Clad Tubes," Journal of Materials Processing Technology, **210**, pp.510-517.

[34] Davey, K. and Ward, M.J., 2002, "A Practical Method for Finite Element Ring Rolling Simulation using the ALE Flow Formulation," International Journal of Mechanical Sciences, **44**, pp.165-190.

[35] Manesh, H.D. and Taheri, A.K., 2003, "The Effect of Annealing Treatment on Mechanical Properties of Aluminum Clad Steel Sheet," Materials and Design, **24**, pp.617-622.

[36] ASTM D903: Standard test method for peel or stripping strength of adhesive bonds, 2004.

[37] Eizadjou, M, Manesh, H.D. and Janghorban, K., 2008, "Investigation of roll bonding between aluminum alloy steeps," Materials Design, vol.**29**, pp.909-913.

[38] Eizadjou, M, Manesh, H.D. and Janghorban, K., 2009, "Mechanism of Warm and Cold Roll Bonding of Aluminum Alloy Strips," Materials Design, **30**, pp.4156-4161.

[39] ASTM D1876: Standard Test Method for Peel Resistance of Adhesives (T-peel test), 2008.

[40] ASTM D3167: Standard Test Method for Floating Roller Peel Resistance of Adhesives, 2004.

[41] ASTM D1781: Standard Test Method for Climbing Drum Peel for Adhesives, 2004.

[42] Gent, A.N. and Hamed, G.R., 1977, "Peel Mechanics for an Elastic-Plastic Adherend," Journal of Applied Polymer Science, **21**, pp.2817-2831.

[43] Gent, A.N. and Hamed, G.R., 1977, "Peel Mechanics of Adhesive Joints," Polymer Engineering and Science, **17**(7), pp.462-466.

[44] Gent, A.N. and Hamed, G.R., 1975, "Peel Mechanics," Journal of Adhesion, **7**, pp.91-95.

[45] Williams, J.G., 1993, "A Review of the Determination of Energy Release Rates for Strips in Tension and Bending. Part I-Static Solutions," Journal of Strain Analysis, **28**(4), pp.237-246.

[46] Williams, J.G., 1993, "A Review of the Determination of Energy Release Rates for Strips in Tension and Bending. Part II-Dynamic Solutions," Journal of Strain Analysis, **28**(4), pp.247-256.

[47] Wei, Y. and Hutchinson, J.W., 1998, "Interface Strength, Work of Adhesion and Plasticity in the Peel Test," International Journal of Fracture, **93**, pp.315-333.

[48] Zhao, H. and Wei, Y., 2008, "Inverse Analysis Determining Interfacial Properties between Metal Film and Ceramic Substrate with an Adhesive Layer," Acta Mech Sin, **24**, pp.297-303.

[49] Hong, D.C. and Yue, S., 1995, "Deterministic Chaos in Failure Dynamics: Dynamics of Peeling of Adhesive Tape," Physical Review Letters, **74**, No.2, pp.254-257.

[50] Georgiou, I., Hadavinia, H., Ivankovic, A., Kinloch, A.J., Tropsa, V., and Williams, J.G., 2003, "Cohesive Zone Models and the Plastically Deforming Peel Test," The Journal of Adhesion, **79**, pp.239-265

[51] Cotterell, B., Hbaieb, K., Williams, J.G., Hadavinia, H., and Tropsa, V., 2006, "The Root Rotation in Double Cantilever Beam and Peel Tests," Mechanics of Materials, **38**, pp.571-584.

[52] ASTM A263: Standard Specification for Stainless Chromium Steel-Clad Plate, 2009.

[53] ASTM 264: Standard Specification for Stainless Chromium-Nickel Steel-Clad Plate, 2009.

[54] ASTM 265: Standard Specification for Nickel and Nickel-Base Alloy-Clad Steel plate, 2009.

[55] ASTM B432: Standard Specification for Copper and Copper Alloy Clad Steel Plate,

2009a.

[56] ASTM B898: Standard Specification for Reactive and Refractory Metal Clad Plate, 2005.

[57] Buchner, M., Buchner, B., Buchmayr, B., Kilian, H., and Riemelmoser, F., April 2008, "Investigation of Different Parameters on Roll Bonding Quality of Aluminum and Steel Sheets," 11th ESAFORM2008 Conference on Material Forming, Lyon, France.

[58] ASTM D1002: Standard Test Method for Apparent Shear Strength of Single-Lap-Joint Adhesively Bonded Metal Specimens by Tension Loading (Metal-to-Metal), 2005.

[59] ASTM D2339: Standard Test Method for Strength Properties of Adhesives in Two-Ply Wood Construction in Shear by Tension Loading, 2004.

[60] ASTM D3983: Standard Test Method for Measuring Strength and Shear Modulus of Nonrigid Adhesives by the Thick-Adherend Tensile-Lap Specimen, 2004.

[61] Sitterle, V.B., Sun, W., and Levenston, M.E., 2008, "A Modified Lap Test to More Accurately Estimate Interfacial Shear Strength for Bonded Tissues," Journal of Biomechanics, **41**, pp.3260-3264.

[62] Kundu, S., and Chatterjee, S., 2008, "Diffusion Bonding between Commercially Pure Titanium and Micro-Duplex Stainless Steel," Materials Science and Engineering A, **480**, pp.316-322.

[63] Oliver, W.C, Pharr, G.M., 1992, "An Improved Technique for Determining Hardness and Elastic Modulus using Load and Displacement Sensing Indentation Experiments," J. Mater. Res., **7**(6), pp.1564-1583.

[64] Li, X. and Bhusha, B., 2002, "A Review of Nanoindentation Continuous Stiffness Measurement Technique and Its Applications," Materials Characterization, **48**, pp.11-36.

[65] Venkatesh, T.A., Van Vliet, K.J., Giannakopoulos, A.E., and Suresh, S., 2000, "Determination of Elasto-Plastic Properties by Instrumented Sharp Indentation: Guidelines for Property Extraction," Scripta Mater., **42**, pp.833-839.

[66] Mehrer, H., 2007, *Diffusion in Solids: Fundamentals, Methods, Materials, Diffusion-Controlled Process*, Springer, New York.

[67] Movahedi, M., Kokabi, A.H., and Seyed Reihani, S.M., 2011, "Investigation on the Bond Strength of Al-1100/St-12 Roll Bonded Sheets, Optimization and

Characterization," Materials & Design, **32**(6), pp.3143-3149.

[68] Castaing, R., 1951, "Application of Electron Probes to Local Chemical and Crystallographic Analysis," Ph.D dissertation, University of Paris.

[69] Castaing, R., 1991, "Early Times of Electron Microprobe Analysis, Electron Probe Quantitation," Edited by Heinrich, K.F.J. and Newbury, D.E., Plenum Press, New York.

[70] Newbury, D.E., 2001, "Castaing's Electron Microprobe and Its Impact on Materials Science," Microscope and Microanalysis, **7**, pp.178-192.

[71] Newbury, D.E., 2004, "Energy Dispersive X-ray Spectrometry in the Scanning Electron Microscope," Microscope and Microanalysis, **10**(Suppl. 2), pp.126-127.

[72] Arnould, O., and Hild, F., 2003, "Specific Effects and Deconvolutoin in Submicrometre EPMA: Application to Binary Diffusion," X-ray Spectrom., **32**, pp.345-362.

[73] Yang, W., Wang, J., and Guillemette, 2011, "X-ray Microanalysis of the Graded Diffusion Interfce by Roll Bonding," manuscript.

[74] Vaidyanath, L.R., Nicholas, M.G., and Milner, D.R., Jan., 1959, "Pressure Welding by Rolling," British Welding Journal, **6**, pp.13-28.

[75] Vaidyanath, L.R., and Milner, D.R., 1960, "Significance of Surface Preparation in Cold Pressure Welding," British Welding Journal, **7**, pp.1-6.

[76] Mohamed, H.A., and Washburn, J., 1975, "Mechanism of Solid State Pressure Welding," Welding Research, Supplement to The Welding Journal, **54**(9), pp.302s-310s.

[77] Wright, P.K., Snow, D.A., and Tay, C.K., Jan., 1978, "Interfacial Conditions and Bond Strength in Cold Pressure Welding by Rolling," Metals Technology, **5**, pp.24-31.

[78] Conrad, H. and Rice, L., 1970, "The Cohesion of Previously Fractured FCC Metals in Ultrahigh Vacuum," Metallurgical Transactions, **1**(11), pp.3019-3028

[79] Bay, N., 1979, "Cold Pressure Welding-the Mechanism Governing Bonding," Journal of Engineering for Industry, **101**(5), pp.121-127.

[80] Bay, N., 1983, "Mechanisms Producing Metallic Bonds in Cold Welding," Welding Research Supplement, **62**(5), pp.137s-142s.

[81] Bay, N., 1986, "Cold Welding, Part 1 Characteristics, Bonding Mechanism, Bond

Strength," Metal Construction, **18**(6), pp.369-372.

[82] Bay, N., 1986, "Cold Welding, Part 2 Process Variants and Applications," Metal Construction, **18**(8), pp.486-490.

[83] Bay, N., 1986, "Cold Welding, Part 3 Influence of Surface Preparation on Bond Strength," Metal Construction, **18**(10), pp.625-629.

[84] Zhang, W. and Bay, N., 1992, "Influence of Hydrostatic Pressure in Cold-Pressure Welding," Annals of the CIRP, **41**(1), pp.293-297.

[85] Bay, N., Clemensen, C., Juelstorp, O. and Wanheim, T., 1985, "Bond Strength in Cold Roll Bonding," Annals of the CIRP, **34**, pp.221-224.

[86] Zhang, W. and Bay, N., 1996, "A Numerical Model for Cold Welding of Metals," Annals of the CIRP, **45**(1), pp.215-220.

[87] Zhang, W. and Bay, N., 1997, "Cold Welding-Fractographic Investigation of the Weld Formation," Welding Research Supplement, **76**(9), pp.361s-366s.

[88] Zhang, W. and Bay, N., 1997, "Cold Welding-Theoretical Modeling of the Weld Formation," Welding Research Supplement, **76**(10), pp.417s-420s.

[89] Yan, H. and Lenard, J.G., 2004, "A Study of Warm and Cold Roll-Bonding of an Aluminum Alloy," Materials Science and Engineering A, **385**, pp.419-428.

[90] Engineering Properties of Steel, ASM International, 1982, pp.273.

[91] Aluninum 1100, Data on Worldwide Metals and Alloys, Engineering Alloys Digest, Inc., 1956, New Jersey.

[92] Montgomery, D.C., 1991, *Design and Analysis of Experiments (3rd ed.)*, John Wiley & Sons, Inc., New York.

[93] Wu, C.F.J and Hamada, M., 2000, *Experiments: Planning, Analysis, and Parameter Design Optimization*, John Wiley & Sons, Inc., New York.

[94] Manesh, H.D. and Taheri, A.K., 2005, "An Investigation of Deformation Behavior and Bonding Strength of Bimetal Strip during Rolling," Mechanics of Materials, **37**, pp.531-542.

[95] Madaah-Hosseini, H.R. and Kokabi, A.H., 2002, "Cold Roll Bonding of 5754-Aluminum Strips," Materials Science and Engineering A, **335**, pp.186-190.

[96] Aluminum Standards and Data, 1968-1969, Aluminum Association.

[97] Le, H.R., Sutcliffe, M.P.F., Wang, P.Z., Burstein, G.T., 2004, "Surface Oxide Fracture in Cold Aluminum Rolling," Acta Materialia, **52**, pp.911-920.

[98] Sutcliffe, M.P.F., 1999, "Flattening of Random Rough Surfaces in Metal-Forming Process," Journal of Tribology, **121**, pp.433-440.

[99] Le, H.R., Sutcliffe, M.P.F., 2003, "A Friction Model for Cold Strip Rolling with Two-Wavelength Surface Roughness in the "Mixed" Lubrication Regime," Journal of Tribology, **125**, pp.670-677.

[100] Wilson, W.R.D., Sheu, S., 1988, "Real Area of Contact and Boundary Friction in Metal Forming," Int. J. Mech. Sci., **30**(7), pp.475-489.

[101] Korzekwa, D.A., Dawson, P.R., Wilson, W.R.D., 1992, "Surface Asperity Deformation during Sheet Forming," Int. J. Mech. Sci., **34**(7), pp.521-539.

[102] Hwang, Y.M. and Tzou, G.Y., 1996, "An Analytical Approach to Asymmetrical Cold- and Hot-Rolling of Clad Sheet using the Slab Method," Journal of Material Processing Technology, **62**, pp.249-259.

[103] Tzou, G.Y. and Huang, M.N., 2000, "Study on the Minimum Thickness for the Asymmetrical PV Cold Rolling of Sheet," Journal of Material Processing Technology, **105**, pp.344-351.

[104] Tzou, G.Y., Tieu, A.K., Huang, M.N., Lin, C.Y., Wu, E.Y., 2002, "Analytical Approach to the Cold-and-Hot Rolling of Sandwich Sheet with Outer Hard and Inner Soft Layers," Journal of Material Processing Technology **125-126**, pp.664-669.

[105] Tzou, G.Y., and Huang, M.N., 2003, "Analytical Modified Model of the Cold Bond Rolling of Unbounded Double-layer Sheet Considering Hybrid Friction," Journal of Material Processing Technology, **140**, pp.622-627.

[106] Pan, S.C., Huang, M.N., Tzou, G.Y., Syu, S.W., 2006, "Analysis of Asymmetrical Cold and Hot Bond Rolling of Unbounded Clad Sheet under Constant Shear Friction," Journal of Material Processing Technology, **177**, pp.114-120.

[107] Aluminum 1100-O, 2011, MatWeb Data Sheet, http://www.matweb.com/search/DataSheet.aspx?MatGUID=db0307742df14c8f817bd8d62207368e&ckck=1.

[108] 1100-O Aluminum Alloy, ASM International, 2002, pp.301.

[109] Stainless Steel 304, 2011, MatWeb Data Sheet, http://www.matweb.com/search/DataSheet.aspx?MatGUID=abc4415b0f8b490387e

3c922237098da.

[110] 304 Stainless Steel, ASM International, 2002, pp.183.

[111] ABAQUS v6.9 Analysis User's Manual.

[112] Peter, J.B., "Static and Kinetic Friction Coefficients for Selected Materials," ASM handbooks online, **18**, Oak Ridge National Laboratory.

[113] Milosev, I. and Strehblow, H. H., 2000, "The Behavior of Stainless Steels in Physiological Solution Containing Complexing Agent Studied by X-ray Photoelectron Spectroscopy," J. Biomed.Mater. Res., **52**(2), pp.404-412.

[114] Kocijan, A., Donik, C., Jenko, M., 2007, "Electrochemical and XPS Studies of the Passive Film Formed on Stainless Steels in Borate Buffer and Chloride Solutions," Corros. Sci., **49**(5), pp.2083-2098.

[115] Abreu, C. M., Cristobal, M. J., Novoa, X. R., Pena, G., and Perez, M. C., 2008, "Effect of Chromium and Nitrogen Co-implantation on the Characteristics of the Passive Layer Developed on Austenitic and Duplex Stainless Steels," Surf. Interface Anal., **40**, pp.294–298.

[116] Jussila, P., Lahtonen, K., Lampimaki, M., Hirsimaki, M., and Valden, M., 2008, "Influence of Minor Alloying Elements on the Initial Stages of Oxidation of Austenitic Stainless Steel Materials," Surf. Interface Anal., **40**, pp.1149–1156.

[117] DePoorter, G.L., Brog, T.K. and Readey, M.J., 1990, "Structural Ceramics, Properties and Selection: Nonferrous Alloys and Special-Purpose Materials," ASM Handbook, ASM International, **2**, pp.1019–1024.

[118] Tabor, D., 1951, *The Hardness of Metals*, Oxford University Press, New York.

[119] Cahoon, J. R., Broughton, W. H., Kutzak, A. R., 1971, "The Determination of Yield Strength From Hardness Measurements," Metallurgical Transanctions, **2**, pp.1979-1983.

[120] Pavlina, E.J. and Van Tyne, C.J., 2008, "Correlation of Yield Strength and Tensile Strength with Hardness for Steels," Journal of Materials Engineering and Performance, **17**, pp.888-893.

[121] Wood, G. C. and Hodgkiess, T., 1972, "The Hardness of Oxides at Ambient Temperatures," Werkst. Korros., **23**, pp.766-773.

[122] Tortorelli, P.F., 1993, "Mechanical Properties of Chromia Scales," JOURNAL DE PHYSIQUE IV, **3**, pp.943-949.

[123] Hones, P., Levy, F., Randall, N.X., 1999, "Influence of Deposition Parameters on Mechanical Properties of Sputter-Deposited Cr_2O_3 Thin Films," J. Mater. Res., **14**(9), pp.3623-3629.

[124] Venkataraman, S.K., Kohlstedt, D.L., Gerberich, W.W., 1993, "Continuous Microindentation of Passivating Surfaces," J. Mater. Res., **8**(4), pp.685-688.

[125] Textor, M. and Grauer , R., 1981, "A Photo-electron and Secondary Ion Mass Spectrometric Study of the Chemical Composition of Thermal Oxide Layers on Technically Pure Aluminum," Corrosion Science, **23**(1), pp.41-53.

[126] Hatch, J.E., 1984, *Aluminum properties and physical metallurgy*, the American Society for Metals, pp.17.

[127] Mandrino, D., Donik, C., Jenko, M., 2010, "AES of Thin Oxide Layers on a Duplex Stainless Steel Surface," Surf. Interface Anal., **42**, pp.762-765.

[128] Normura, K. and Ujihira, Y., 1990, "Analysis of Oxide Layers on Stainless Steel (304 and 316) by Conversion Electron Mossbauer Spectrometry," Journal of Materials Science, **25**, pp.1745-1750.

[129] Normura, K. and Ujihira, Y., 1990, "CEM Study of Oxide Layers Formed on Stainless Steel (SUS304 and SUS316)," Hyperfine Interactions, **57**, pp.2023-2028.

[130] Smith, W.F. and Hashemi, J., 2005, *Foundations of Materials Science and Engineering (4th ed.)*, McGraw-Hill, New York.

[131] Paul, A., 2004, "The Kirkendall Effect in Solid State Diffusion," Ph.D dissertation of Eindhoven University of Technology, The Netherlands.

VITA

Wei Yang received his Bachelor of Science degree in Engineering Mechanics from Harbin Institute of Technology in July 2004. He entered the graduate school at Harbin Institute of Technology in August 2004 and received his Master of Science degree in July 2006. His research interests focus on solid mechanics, composite materials and advanced materials manufacturing/processing.

Mr. Yang may be reached at (c/o Dr. Jyhwen Wang) Thompson Hall, BLDG 483, Ross St., College Station, TX 77843. His email is wy.science@gmail.com.